SKB

TECHNICAL REPORT 95-29

DECOVALEX I – Test Case 3:

Calculation of the Big Ben Experiment – Coupled modelling of the thermal, mechanical and hydraulic behaviour of water-unsaturated buffer material in a simulated deposition hole

Lennart Börgesson[1], Jan Hernelind[2]

1 Clay Technology AB, Lund, Sweden
2 FEM-Tech AB, Västerås, Sweden

December 1995

SVENSK KÄRNBRÄNSLEHANTERING AB
SWEDISH NUCLEAR FUEL AND WASTE MANAGEMENT CO

P.O.BOX 5864 S-102 40 STOCKHOLM SWEDEN
PHONE +46 8 665 28 00 TELEX 13108 SKB
FAX +46 8 661 57 19

DECOVALEX I - TEST CASE 3:

CALCULATION OF THE BIG BEN EXPERIMENT - COUPLED MODELLING OF THE THERMAL, MECHANICAL AND HYDRAULIC BEHAVIOUR OF WATER-UNSATURATED BUFFER MATERIAL IN A SIMULATED DEPOSITION HOLE

Lennart Börgesson[1], Jan Hernelind[2]

1 **Clay Technology AB, Lund, Sweden**
2 **Fem-Tech AB, Västerås, Sweden**

December 1995

DECOVALEX I - TEST CASE 3:

CALCULATION OF THE BIG-BEN EXPERIMENT-

Coupled modelling of the thermal, mechanical and hydraulic behaviour of water-unsaturated buffer material in a simulated deposition hole

Lennart Börgesson[1], *Jan Hernelind*[2]

1 Clay Technology AB, Lund, Sweden
2 Femtech, Västerås, Sweden

December 1995

FOREWORD

This report is an integral part of SKB's engagement in the first part of the DECOVALEX project (DECOVALEX I). The work, that was made 1992-1994, is compiled in four reports and two articles.

The following SKB Technical Reports have been printed:

Börgesson L. and Hernelind J. (1995) - DECOVALEX I - Test Case 2: Calculation of the Fanay-Augères THM Test - Thermo-mechanical modelling of a fractured rock volume. SKB Technical Report TR 95-28.

Börgesson L. and Hernelind J. (1995) - DECOVALEX I - Test Case 3: Calculation of the Big Ben Experiment - Coupled modelling of the thermal, mechanical, and hydraulic behaviour of water-unsaturated buffer material in a simulated deposition hole. SKB Technical Report TR 95-29.

Israelsson J. (1995) - DECOVALEX I - Bench-Mark Test 3: Thermo-Hydro-Mechanical Modelling. SKB Technical Report TR 95-30.

Rosengren L. and Christianson M. (1995) - DECOVALEX I - Test Case 1: Coupled stress-flow model. SKB Technical Report TR 95-31.

The following articles have been published:

Rehbinder G. (1995) - Analytical Solutions of Stationary Coupled Thermo-Hydro-Mechanical Problems. *Int. J. Rock Mech. Min. Sci. & Geomech. Abstr.* Vol. 32, No 5, pp 453-463, 1995.

Claesson J., Follin S., Hellström G., and Wallin N.-O. (1995) - On the use of the diffusion equation in test case 6 of DECOVALEX. *Int. J. Rock Mech. Min. Sci. & Geomech. Abstr.* Vol. 32, No 5, pp 525-528, 1995.

ABSTRACT

PNC:s large scale laboratory test with an artificial deposition hole, named BIG-BEN, has been simulated with finite element calculations with the code ABAQUS. The test comprised water uptake from an artificial rock and heating of a canister in a deposition hole with the diameter 1 m during 5 months. Water content, pore pressure, and total pressure in the buffer was measured during the test.

The given data of the material properties were supplemented with results from own laboratory tests in order to determine parameters required for the calculation. The vapour flow process, which is not included in ABAQUS, was implemented and added to the code. After calibration of the properties of the buffer material, a completely coupled thermo-hydro-mechanical calculation of the test was done. The calculated thermal and hydraulic results were in good agreement with measured values while the prediction of the mechanical response was less good.

SAMMANFATTNING

PNC:s storskaliga laboratorieförsök av ett deponeringshål, kallat BIG BEN, har simulerats med finita element beräkning med programmet ABAQUS. Försöket omfattade vattenupptagning från artificiellt berg och uppvärmning av kanister i ett deponeringshål med diametern 1 m under 5 månader. Under försökets gång mättes vattenkvot, portryck och totaltryck.

De data om materialegenskaper som gavs har kompletterats med resultat från egna laboratorieförsök, för att bestämma erforderliga parametrar till beräkningen. Vattentransport i ångfas kan inte beräknas med ABAQUS och var därför implementerad och anpassad till ABAQUS. Efter kalibrering av buffertmaterialets egenskaper, gjordes en kopplad termo-hydro-mekanisk beräkning av försöket. De beräknade temperaturerna och den hydrauliska responsen stämde bra överens med mätningarna medan resultaten från den mekaniska beräkningen stämde mindre bra.

TABLE OF CONTENTS

SUMMARY

A large laboratory test simulating a deposition hole has been made by PNC. Members of DECOVALEX have been asked to predict the processes in the deposition hole during the first 5 months of the test. SKB gave this task to Clay Technology.

The calculations described have been made with the finite element code ABAQUS. The process of vapour flow, which cannot be simulated using the standard version of the program, has been added to the code. Some laboratory tests have been made on the buffer material in order to evaluate parameters required for the calculation but not provided for in the specifications. The material models were calibrated and verified by comparing predicted and actual laboratory test results.

The final simulation of the Big-Ben test was made using a coupled thermo-hydro-mechanical calculation. The calculations resulted in a complete prediction of the temperature, void ratio, degree of water saturation, pore pressure, and effective stress in the buffer material.

Although no final conclusion has been drawn about the results, it seems that this way of simulating the complicated processes in buffer materials is useful. However, additional laboratory tests on the buffer material are required in order to determine the necessary parameters with higher accuracy. Some processes need to be better understood and some models, like the effective stress concept for unsaturated buffer materials, need to be refined.

1 INTRODUCTION

A number of large scale tests have been performed for the international project DECOVALEX (DEvelopment of COupled models and their VALidation against EXperiments) in order to get an experimental basis for developing and testing coupled models describing Thermo-Hydro-Mechanical (THM) processes. Phase 3 includes a full scale laboratory test of a deposition hole. The test, called Big Ben, has been conducted by PNC for testing the Japanese concept for nuclear waste disposal.

The test is described in the specifications provided by PNC /1-1/ and contains the experimental facility and conditions, fundamental properties and parameters, results and output specifications. The test will be briefly described in this report.

On behalf of SKB, Clay Technology AB has got the task to predict the performance of the buffer material in this test. This report describes the work and the final coupled THM calculation made with the finite element program ABAQUS. The results should be considered to represent the first step in the ongoing research for improving the understanding and modelling of these complex processes in water-unsaturated buffer materials. The following should be noted:

- The standard ABAQUS code does not provide the facility to calculate vapour flow and a routine that coupled this process to the water flow process was therefore coded and added to the program.

- All of the parameters given in the specifications were not needed for the material models in our calculation.

- Additional laboratory tests were made in order to evaluate some parameters required for the calculation.

- The properties of some materials and the detailed design of some parts of the test were not known. This resulted in tedious calibration calculations especially of the temperature. Some given parameters also had to be changed.

- The short time given for the task (four months which included laboratory testing, theory development, coding, parameter verifications, calculations and reporting) was not sufficient to make completely satisfying evaluations and adjustments.

In spite of these problems we consider the outcome of the study to be good. It should be noted that although the thermal properties of material adjacent to the buffer were adapted to the results by back-calculations of the heat-evolution, no such revision was made of the thermo-hydro-mechanical properties of the buffer material. The latter properties were solely derived from laboratory tests and from information derived from the literature.

2 BIG-BEN EXPERIMENT

The BIG-BEN experiment simulated a deposition hole in full scale. Figs 2-1 and 2-2 show the design of the experiment /1-1/. An electric heater embedded by glass beads was confined by a steel container, which simulated the waste canister (overpack). The deposition hole was made with a diameter of 1.7 m and a depth of about 4.5 m in a simulated rock made by concrete with the radius 3 m and the height 5 m ("man-made rock"). The deposition hole was filled with the Japanese main buffer material candidate (30% sand and 70% Kunigel bentonite) compacted to the dry density 1.6 t/m^3. The water ratio at the application was 16.5%.

The radial thickness of the buffer material around the canister was 30 cm. A 2 cm thick layer of dry quartz sand was applied at the interface between the canister and the buffer. A similar layer with 3 cm thickness was applied in the radial interface between the buffer material and the simulated rock. The latter layer was filled with water and a water pressure of 50 kPa was applied in order to simulate water inflow from the rock.

A constant power of 800 W was applied to the heater at the beginning of the test at the same time as the outer sand layer was filled with water. Several different types of measurements relevant to the DECOVALEX project were made during the test:

- Measurement of temperature
- Measurements of total pressure in the buffer material
- Measurements of water ratio

The water ratio was measured by use of sensors and after 5 months also by sampling. Results of pressure, water ratio and temperature measurements up to 5 months after start are presented in the test specification /1-1/. Calculated results of axial and radial pressure, temperature and water ratio at 9 spots in the buffer were requested for comparison with measured values.

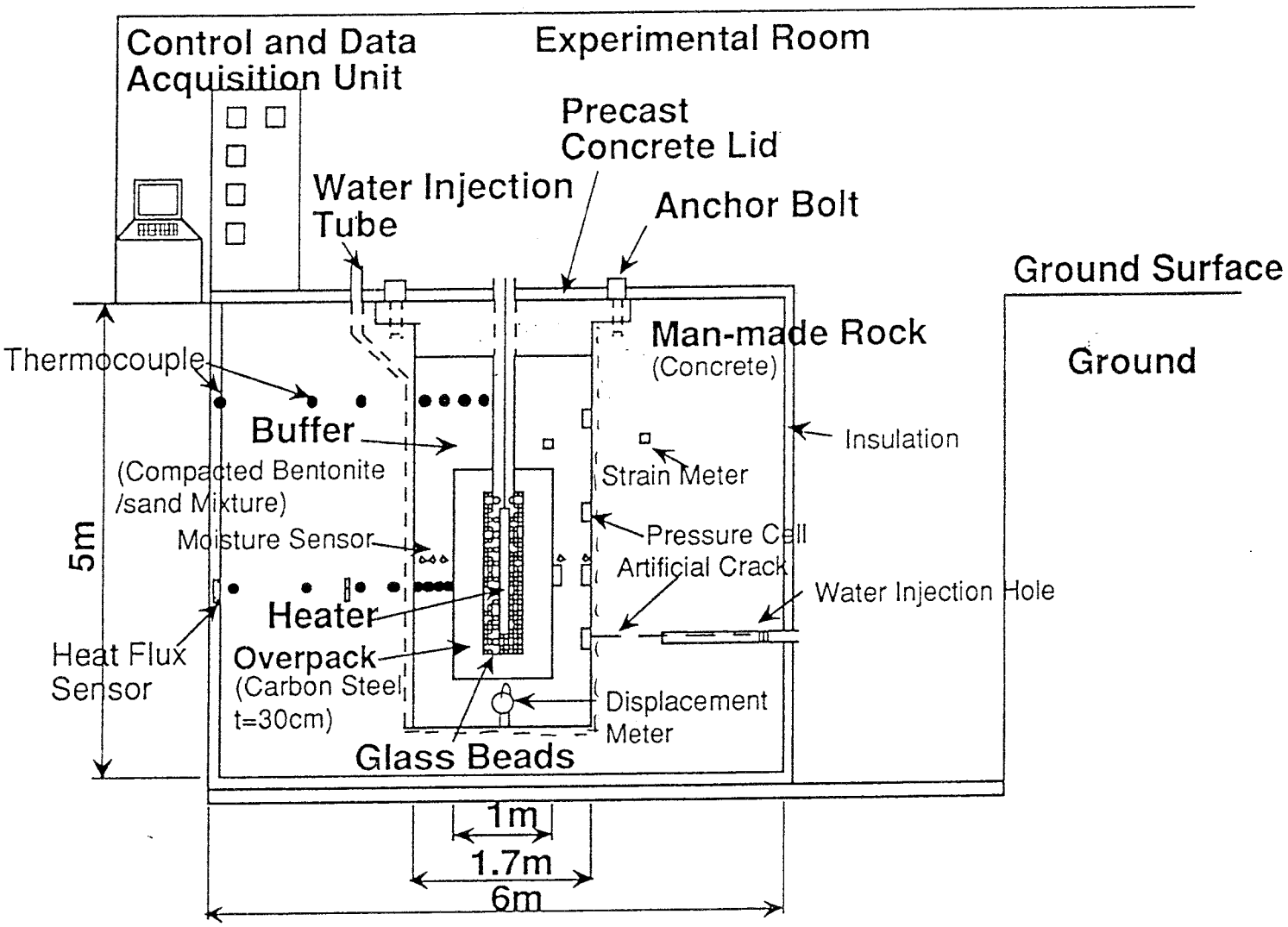

Figure 2-1. View of the Big-Ben experiment /1-1/.

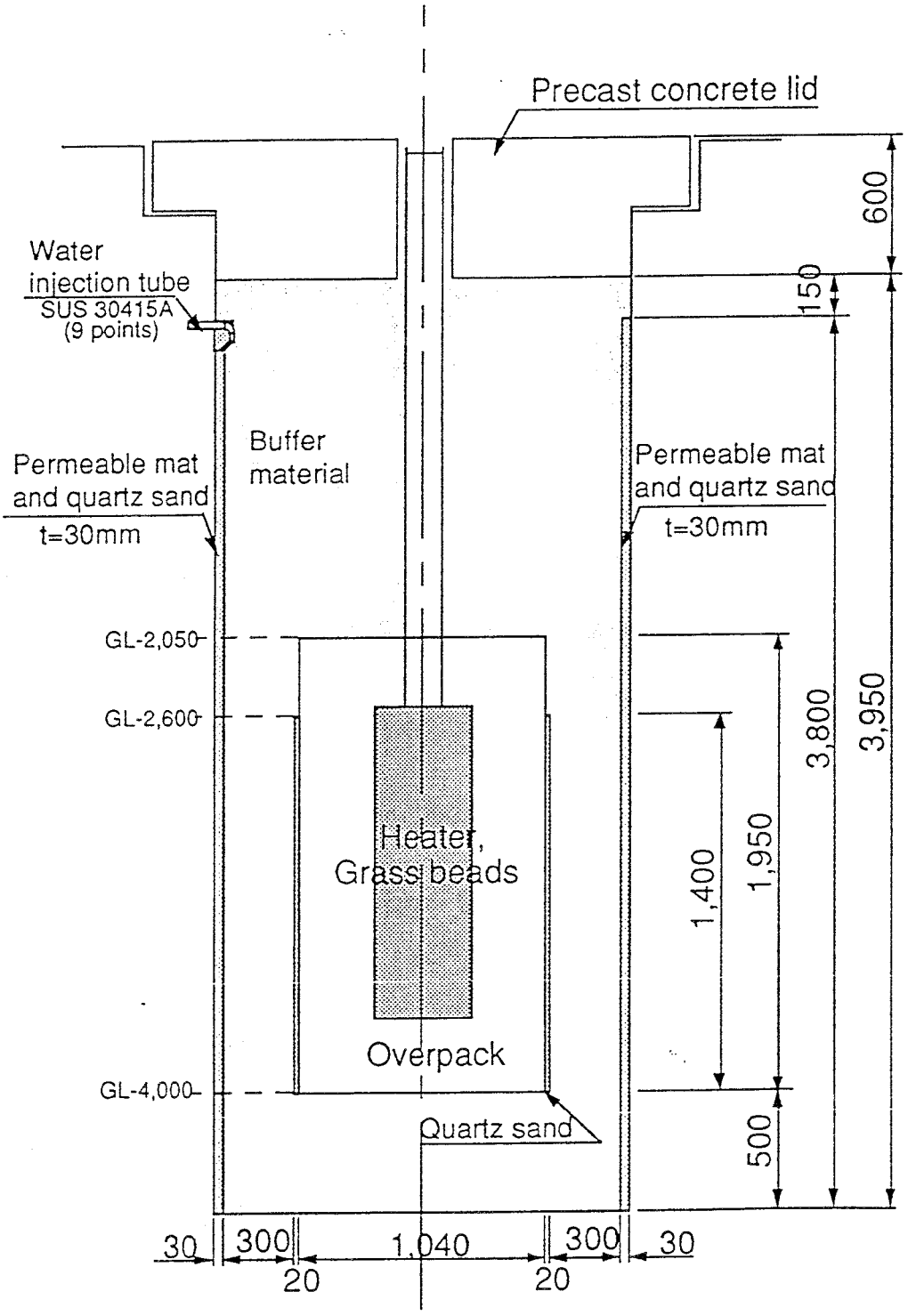

Figure 2-2. *Geometry and arrangements of the canister and the buffer material /1-1/.*

3 MODELLING OF PROCESSES

3.1 GENERAL

The calculations have been made by use of the finite element program ABAQUS, applying the techniques and material models developed for water saturated buffer materials /3-1, 3-2/. However, these models do not include water unsaturated materials and temperature-driven water vapour flow. The former process is included in the latest version of ABAQUS (version 5.3) /3-3/ but had to be adapted to the properties of bentonite based buffer materials. The water vapour flow process cannot be modelled in the present version of ABAQUS but a technique for such implementation was developed and coded.

The strategy applied to the present project has been to develop a technique for making completely coupled calculations. This was made in the following steps:

1. The mechanical model with the effective stress theory that is valid for water saturated buffer materials was used as a basis.

2. This model was applied to unsaturated conditions according to the existing ABAQUS models.

3. A number of hydro-mechanical laboratory tests were made on the same buffer material that was used in the Big-Ben test.

4. The parameters not given in the specifications but required for the hydro-mechanical modelling were determined.

5. A model for simulating the temperature-driven vapour flow was developed, coded and included into ABAQUS for the coupled hydro-thermo-mechanical modelling.

6. A number of thermo-hydro-mechanical laboratory tests were made on unsaturated buffer material samples with temperature gradients.

7. The parameters required for the thermo-hydro-mechanical modelling were determined.

8. The influence of the evaporation-condensation process on the thermal heat flux was estimated and included in the model.

9. Preliminary thermal calibration calculations of the Big-Ben test were made in order to estimate some thermal properties and boundary conditions that were not given in the specifications.

10. Coupled calculations of a simplified model of the Big-Ben test were made in order to investigate the influence of the thermo-mechanical behaviour of the canister and the rock on the function of the buffer material. The purpose of these calculations was to limit the size of the model to only include relevant parts.

11. Finally the coupled hydro-thermal-mechanical calculation of the Big-Ben test was made.

3.2 PROCESS THEORIES

The theories concerning the governing equations of the modelled processes are described in the theory manual of ABAQUS /3-3/ with the exception of the heat-driven vapour flow in the buffer material. The theories will be briefly described in this chapter.

Thermal flux

The only processes that have an effect on the temperature evolution and the thermal flux are heat conduction according to Fourier's law and (for the buffer material) the evaporation-condensation process. Convection and radiation are insignificant in clay /3-4/. The evaporation-condensation process is taken into account by changing the heat conductivity with temperature and degree of water saturation (see chapter 5).

Mechanical processes

Buffer material:

The mechanical function of the buffer material is simulated using the Porous Elasticity concept and a modified Drucker-Prager Plasticity. Porous Elasticity means that the stress-strain relation is modelled by the Porous Bulk Modulus κ according to Eqn 3-1.

$$\kappa = \frac{\Delta e}{\Delta \ln p} \qquad (3\text{-}1)$$

p =effective average stress (kPa)
e =void ratio

The Effective Stress Theory is applied meaning that the mechanical function is solely determined by the effective stresses in the material. The effective stress theory is generalised for unsaturated clays and is defined according to Eqn 3-2:

$$p = p_{tot} - \alpha s_w \tag{3-2}$$

p_{tot} =total average stress (kPa)
s_w =pore water pressure (kPa)
α =factor that determines what part of the pressure in the pore water that is distributed to an average pore pressure $u=\alpha s_w$ acting on the particles

If s_w is positive the material is water saturated and $s_w=u$. If the material is unsaturated, s_w is negative (suction) and the entire suction does not affect the effective stress. The factor α has been assumed to be equal to the degree of water saturation S_r:

$$\alpha=S_r \tag{3-3}$$

All other materials:

The rest of the materials are modelled as simple linear elastic models. Since the rest of the calculations show that the thermo-mechanical properties of the rock and the canister did not influence the results, these materials were excluded in the final mechanical calculation and the boundaries of the sand layers were considered as infinitely rigid boundaries.

Hydraulic processes

Only the buffer material is modelled hydraulically. The outer sand layer is assumed to be exposed to a constant hydrostatic pressure due to the high hydraulic conductivity, while the inner sand layer is taken to be impermeable due to the low suction potential of sand. No water would enter the inner sand layer until the bentonite is water saturated, which means that this layer does not need to be modelled in this short experiment.

The pore water and clay particles are thermo-mechanically modelled as separate elastic phases with the thermal expansion properties. In the water saturated state the water flux process is modelled according to Darcy's law with a hydraulic conductivity k that is a function of the temperature with the pore water pressure s_w as the driving force. In the water unsaturated state the water flux is also modelled by Darcy's law, the water flow only being driven by the negative pore pressure. It is also assumed that the water is only transported in the water-filled parts of the pores, which means that the cross section area available for water flow is smaller when the pores are unsaturated and that the hydraulic conductivity consequently smaller. The following simple relationship has been assumed to be valid /3-5/:

$$k_p = S_r^{\delta} k \tag{3-4}$$

where

k_p =hydraulic conductivity of partly saturated soil (m/s)
k =hydraulic conductivity of completely saturated soil (m/s)
δ =parameter ≈ 3-7 (assumed to be 3)

While the pore pressure in a saturated material can vary and depends on external factors, the pore pressure in unsaturated material is always negative and assumed to be a unique function of the degree of saturation. The relation between this suction and the degree of saturation must be defined for the material.

The redistribution of water in an unsaturated buffer material at isotropic temperature is thus entirely controlled by water flow in the water phase, driven by the suction. If water is available in some part of the buffer the degree of saturation will increase and the suction will be reduced there. The difference in pore pressure in the material will make water flow and increase the degree of saturation in other parts and, accordingly, even out pore pressure differences.

Moisture swelling

The mechanical coupling between the suction, the degree of saturation and the volume change of the buffer material is controlled by the porous bulk modulus. It will cause a change in volume when the material changes its degree of saturation for achieving stress equilibrium. This volume change must be adjusted to the real one, which is made through a procedure called moisture swelling.

Thermally driven water vapour flow

An increased temperature in one part of an unsaturated buffer will make water evaporate into the air phase of the pores. This will cause a locally increased vapour pressure and migration of the water vapour to where the vapour pressure and temperature are lower and where it may condense to water. There will thus be a water vapour transport in the air-filled passages of the pores from warmer parts to colder parts. This is a complicated process and the rate does not only depend on the temperature gradient but also on the presence and frequency of air-filled voids in the buffer, and also on the bonds between the clay particles and the water, both being functions of the degree of saturation.

In spite of the complexity it has been suggested that this process can be modelled as a diffusion process driven by the temperature gradient and the water vapour gradient /3-6/, /3-7/.

$$q_v = -D_{Tv}\nabla T - D_{pv}\nabla p_v \qquad (3\text{-}5)$$

where

q_v =vapour flow
D_{Tv} =thermal vapour flow diffusivity
T =temperature
D_{pv} =isothermal vapour flow diffusivity
p_v =vapour pressure

If the isothermal vapour flow is neglected Eqn, 3-5 will be simplified to Eqn 3-6.

$$q_v = -D_{Tv}\nabla T \qquad (3\text{-}6)$$

The process has been coded according to Eqn 3-6 and adapted to the ABAQUS code. It can be coupled to the other hydro-mechanical processes by introducing a superimposed element mesh that only models the vapour flow. The diffusion coefficient D_{Tv} can be made to vary with the degree of saturation as well as other variables, the former being necessary for taking into account the access to air-filled connections in the buffer and the difference in bonding between the clay particles and the water at different degrees of saturation

Coupled thermo-hydro-mechanical process

A completely coupled calculation of the changes with time in temperature, effective stress, pore pressure, void ratio (or dry density), and degree of saturation (or void ratio) in the entire buffer could be made using ABAQUS and derived models. The only incompletely coupled calculation was that of temperature derivation, which was made using the following semi-coupled technique:

1. The temperature was calculated as a function of time assuming that the initial values of void ratio and degree of saturation were constant during the test.

2. A coupled thermo-hydro-mechanical calculation was then made with the temperature data taken from the first temperature calculation.

3. The temperature calculation was repeated using the results from the thermo-hydro-mechanical calculation as input data at each time step.

4. Calculations 2) and 3) were repeated until there was no difference between the calculations.

The convergence of the results was rather fast and only a few iterations had to be made, probably because the change in thermal conductivity of the buffer material with degree of saturation was quite small when the thermal effect of the evaporation-condensation was taken into account at high temperatures.

4 FINITE ELEMENT CODE

ABAQUS is a finite element code originally designed for non-linear stress analyses. It has been extended significantly in the last 5 years and is now capable of modelling a large range of processes for many different materials, three-phase materials like unsaturated soils being most important for this project.

One, two, and three-dimensional elements are available. ABAQUS runs as a batch application. The main input is a file which indicates which options are required and gives the data associated with these options. There may also be many supplementary files, such as restart or result files from previous analyses, as well as auxiliary data files.

Detailed results from ABAQUS may be obtained via a post-processing code ABAQUS/Post. Detailed information on the available models, application of the code, and the theoretical background is given in the ABAQUS Manuals /3-3/.

5 MATERIAL MODELS

5.1 GENERAL

A large number of parameters are required for the material models of the different materials in the test. Most of these parameters are given in the specifications /1-1/. However, some of the parameters were changed because they were either not correct or did not yield logical results. Some parameters were not given and either had to be assumed or (for the buffer materials) determined. This chapter will briefly describe the material models and the parameters that have been used in the calculations. The changes and assumed parameters will be justified and the laboratory tests and the evaluation of the parameters described.

5.2 MATERIAL MODELS FOR ALL MATERIALS EXCEPT THE BUFFER

All materials except for the buffer have been modelled using the following parameters:

Thermally: Heat conductivity λ
Heat capacity c
Bulk density ρ
Coefficient of thermal expansion α

Mechanically: Modulus of elasticity E
Poisson's ratio ν

Hydraulically: Not modelled

The values of these parameters that were used in the calculations are shown in Table 5-1.

Table 5-1 Parameters of all materials except the buffer material

	λ W/m,K	c Ws/kg,K	ρ kg/m^3	α 1/K	E kPa	ν
Heater [1)]	10	1000	5000			
Glass beads	0.255	840	1600	1.0E-5	8.2E7	0.3
Steel canister	53	460	7800	1.64E-6	2.0E8	0.3
Steel shaft	53	460	7800	1.64E-6	2.0E8	0.3
Inner sand gap	0.3 [2)]	1000	1000	- [4)]	5.0E3 [3)]	0.45
Outer sand gap [5)]	1.5	1600	2000	-	5.0E3	0.3
Man-made rock	1.88	750	2300	1.0E-5	2.5E7	0.167

The footnotes in the table refer to the following explanations:

1) The properties of the heater were not given
2) The thermal conductivity given for the gap was 0.0729 W/m,K. It gave a too strong temperature drop and was therefore changed to 0.3 to agree better with the actually measured temperature drop
3) The given *E*-modulus was very low (86 kPa). It was changed to the same value as the outer sand gap
4) The given coefficient of thermal expansion was very high and could not be used together with the corrected high E-modulus
5) No properties of this layer was given

The sand layers caused some problems thermally as well as mechanically. It is unfortunate that the mechanical properties of these are unknown because they play a decisive role for the mechanical response of the buffer. The elasticity and thermal expansion of the canister and the rock are unimportant.

5.3 MATERIAL MODELS FOR THE BUFFER MATERIAL

5.3.1 General

Since the modelling of the processes in the buffer and the corresponding material models differ from those used by PNC in their modelling, the given data are insufficient. The required data had to be evaluated from additional laboratory tests made in the laboratory of Clay Technology. These laboratory tests were simulated with ABAQUS and could thus be used as calibration and verification tests for the models.

5.3.2 Additional laboratory tests

The tests were made on a mixture 70% of the same sodium bentonite (Kunigel-V1) that was used for the Big-Ben experiment and 30% quartz sand with the following grain size distribution:

Per cent finer by weight	10%	50%	90%
Grain size	0.14 mm	0.6 mm	1.5 mm

The following tests were made:

- Drying tests in order to determine the change in void ratio caused by a change in degree of saturation. These tests were made for evaluating the *moisture swelling* procedure.

- Moisture redistribution tests. These tests were made under different temperature gradients and at different temperature levels and were terminated at different times. The tests were made for evaluating the *thermal water diffusivity*.

- Water uptake tests. These tests were made to check that the rate of water uptake under isothermal conditions, which is controlled by the negative pore water pressure (suction) s_w and the hydraulic conductivity for partly saturated materials k_p.

Drying tests

For the "drying" tests a number of samples with identical void ratio and degree of water saturation were prepared. One of the samples was examined and the water ratio w and bulk density ρ determined. W was determined as the weight of water divided by the dry weight of the sample dried at 105°C. ρ was determined by use of the paraffin method /5-1/. The basic parameters S_r and e can be calculated according to Eqns. 5-1 and 5-2.

$$S_r = \frac{w \cdot \rho \cdot \rho_s}{\left[\rho_s \cdot [w+1] - \rho\right] \cdot \rho_w} \tag{5-1}$$

$$e = \frac{\rho_s - \rho}{\rho - \rho_w \cdot S_r} \tag{5-2}$$

where

S_r =degree of water saturation (volume of water)/(volume of pores)
e =void ratio (volume of pores)/(volume of solids)
ρ_s =particle density (=2750 kg/m^3)
ρ_w =density of water(=1000 kg/m^3)
ρ =bulk density
w =water ratio

The other samples were dried to different water ratios either in an oven or in the air, and then put in a plastic container for homogenisation for a day, after which ρ and w were determined. Fig 5-1 shows the results of three such test series with the void ratio plotted as a function of the water ratio and the degree of saturation.

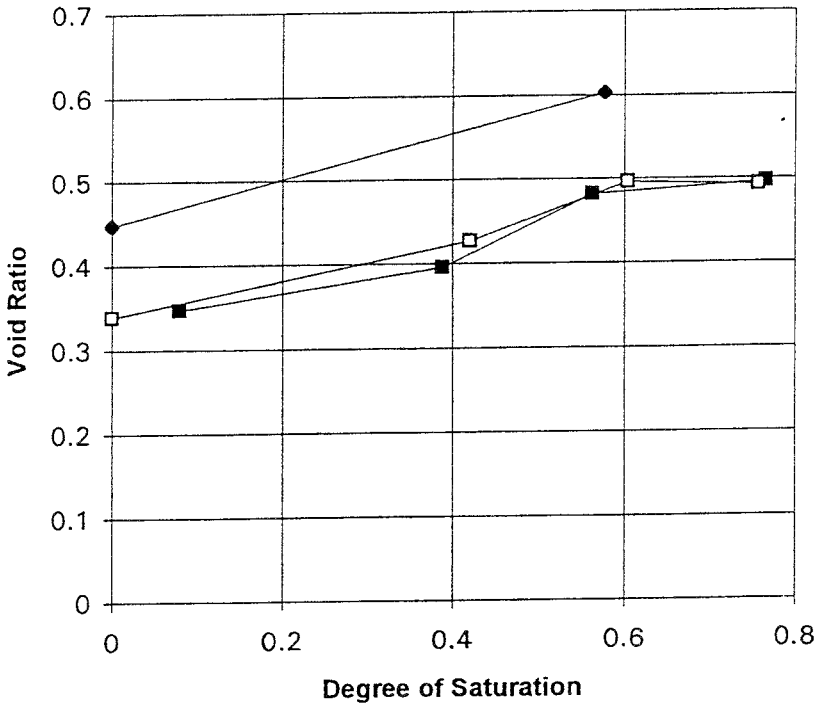

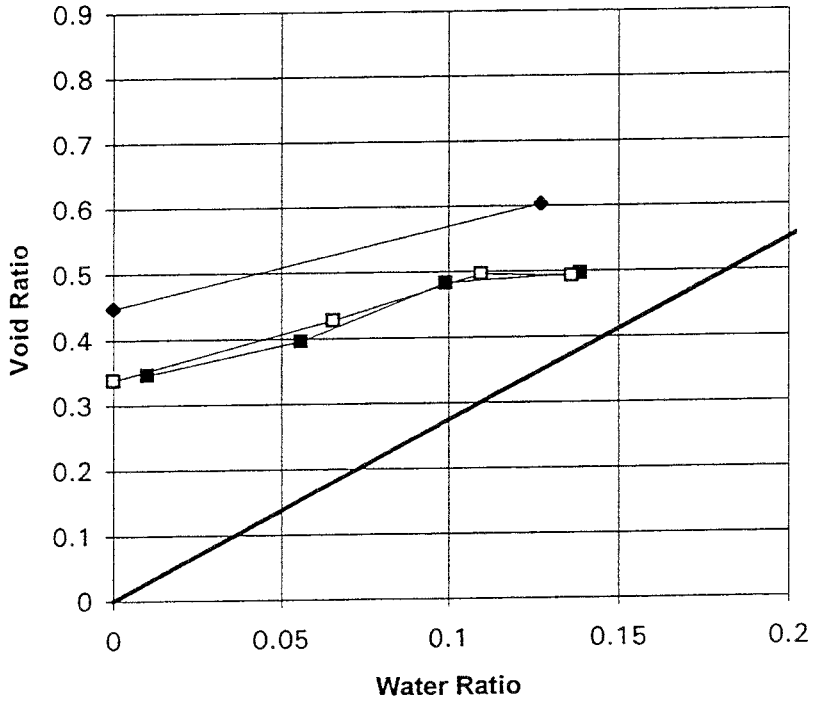

Figure 5-1. *Results of the drying tests. Three test series.*

Moisture redistribution tests

The experiments termed "moisture redistribution tests" were made in confined cells with 5 cm height and 5 cm diameter. A constant temperature gradient was applied in the axial direction of the sample. Three different series were performed of which one was performed at a temperature gradient of 13°C/cm and one at 2°C/cm. These tests were terminated after different periods of time and the samples were then cut in 10 slices for determining the density and water ratio. These tests made it possible to investigate the influence of time and temperature gradient. In the third series, three tests with the same temperature gradient but different average temperature were performed in order to study the influence of the temperature level. The tests are summarised in Table 5-2.

Table 5-2 Summary of the moisture redistribution tests

Test No	Max. temp. °C	Min. temp. °C	Temp. grad. °C/cm	w_0 %	e_0	S_{r0}	Time Days
1a	100	35	13	14.6	0.7	0.57	0.25
1b	100	35	13	18.2	0.7	0.64	1.00
1c	100	35	13	13.2	0.7	0.52	4.00
2a	35	25	2.0	16.7	0.67	0.69	1.00
2b	35	25	2.0	15.5	0.66	0.65	4.00
2c	35	25	2.0	15.7	0.67	0.64	16.00
3a	60	31	5.8	9.2	0.67	0.38	4.00
3b	75	47	5.6	9.6	0.66	0.40	4.00
3c	100	73	5.4	9.4	0.66	0.39	4.00

The results of the tests are shown in Figs 5-2 - 5-4. The aim was to prepare samples with e=0.7 and S_r=0.65 in series 1 and 2 but actual properties varied significantly. Furthermore, the values of the void ratio and thus also the degree of saturation are uncertain because of the difficulty in determining the density of slices of these samples. More accurate tests are required for studying the processes in more detail but the present results are sufficient for a rough estimate of the required parameters.

Test series 3 shows that the influence of the temperature level seems to be small. However, the difference in thermal conductivity at the different temperatures (see chapter 5.3.2) may cause a difference in the internal distribution of temperature and thermal flux. It has not been within the scope of this project to investigate these matters in detail. The calculations were made by assuming that there is no influence of temperature on any other parameters than the thermal conductivity and the hydraulic conductivity (see chapter 5.3.4).

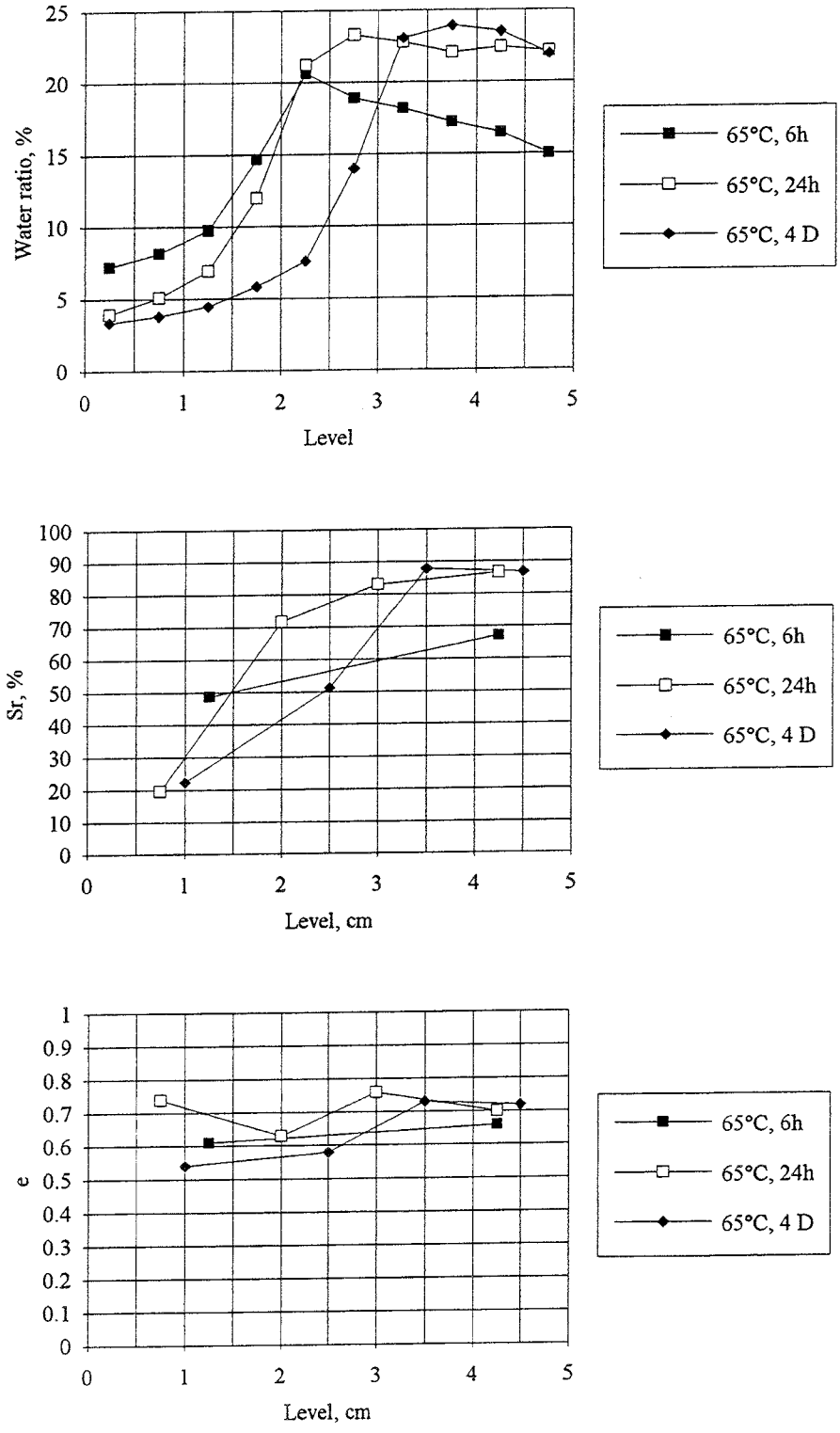

Figure 5-2. *Results from test series 1 of the moisture redistribution tests. The water ratio, degree of saturation and void ratio are plotted as a function of the distance from the cold end. ΔT=65°C over 5 cm during three different time periods.*

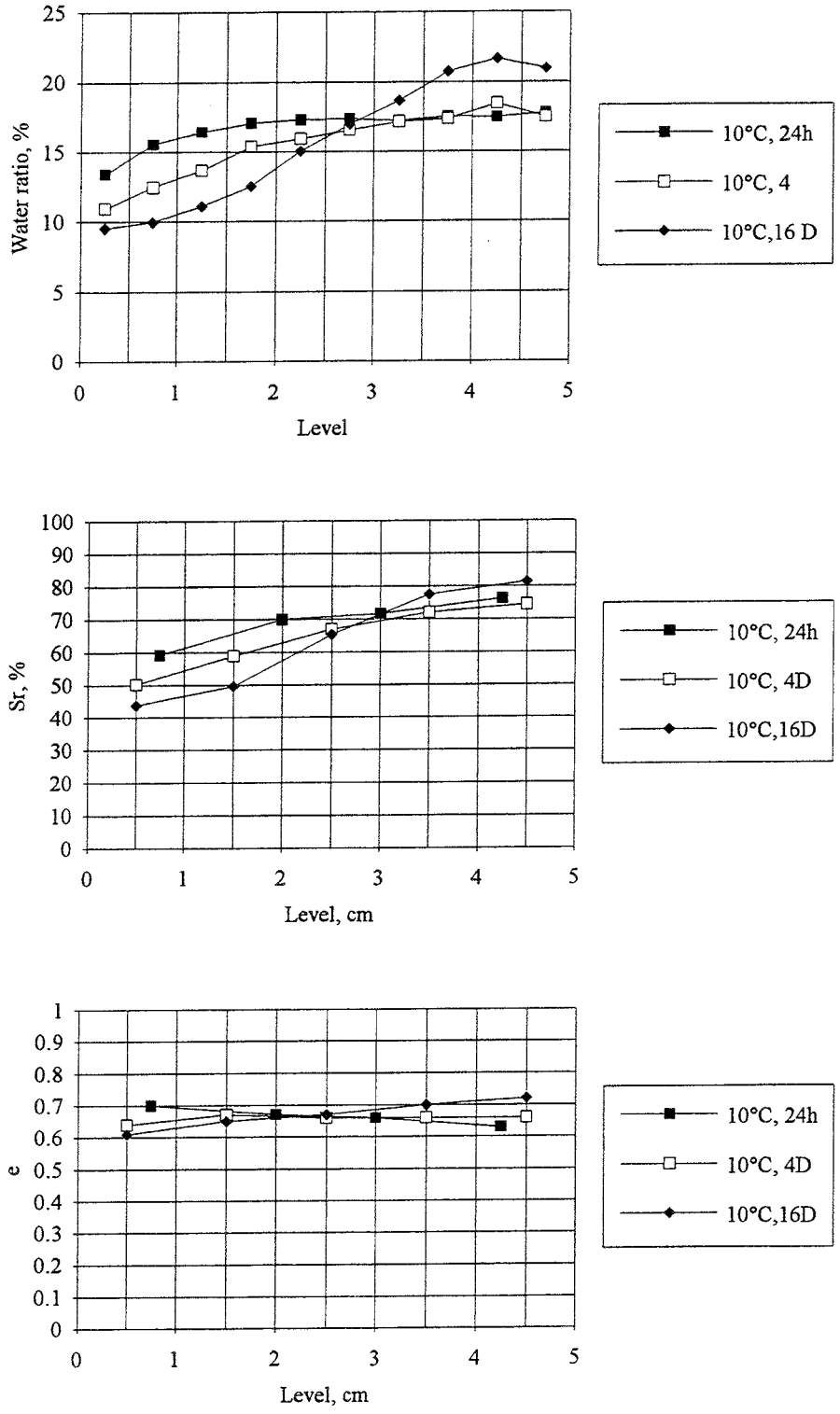

Figure 5-3. *Results from test series 2 of the moisture redistribution tests. The water ratio, degree of saturation and void ratio are plotted as a function of the distance from the cold end. ΔT=10°C over 5 cm during three different time periods.*

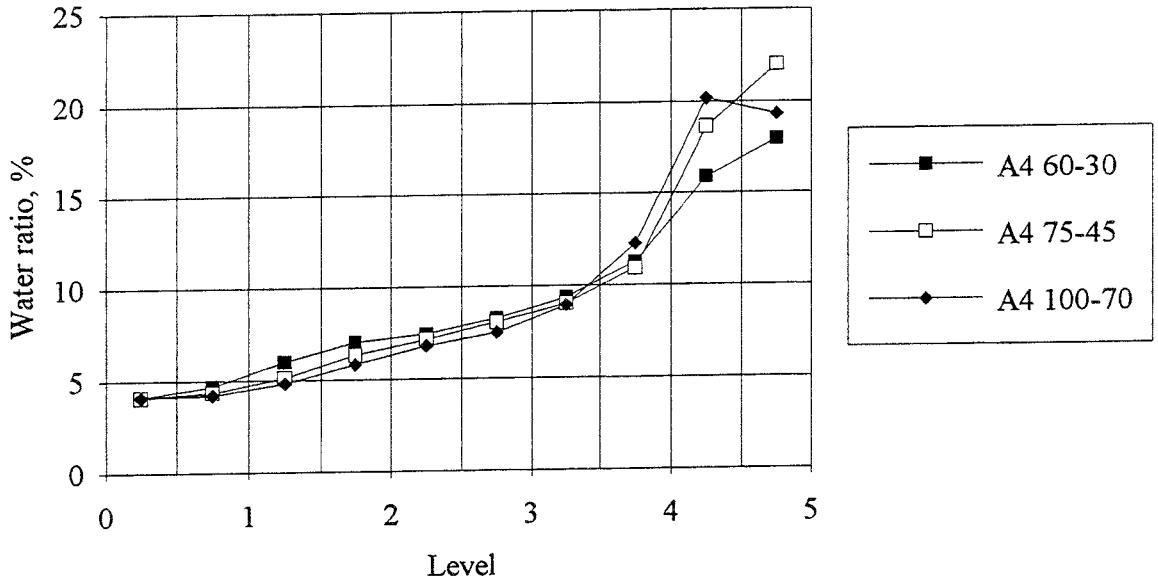

Figure 5-4. Results from tests series 3 of the moisture redistribution tests after 4 days. The water ratio is plotted as a function of the distance from the cold end. $\Delta T \approx 30°C$ over 5 cm at three different temperature levels with maximum temperatures 60°C, 75°C, and 100°C.

Water uptake tests

The two water uptake tests were made in a so-called swelling pressure oedometer /5-2/ with very stiff mechanical confinements on samples with 5 cm height. Water was applied in one end and the swelling pressure measured at the opposite end as a function of time. The tests were terminated after different periods of time and the samples cut and measured in the same way as in the moisture redistribution tests. Table 5-3 summarises the tests.

Table 5-3. Initial conditions for the water uptake tests

Test No	w_0 %	e_0	S_{r0}	Time Days
4a	15	0.74	56	5
4b	15	0.72	57	20

Figs 5-5 and 5-6 show the results of the tests. The pressure measurement only worked in the 20 days test.

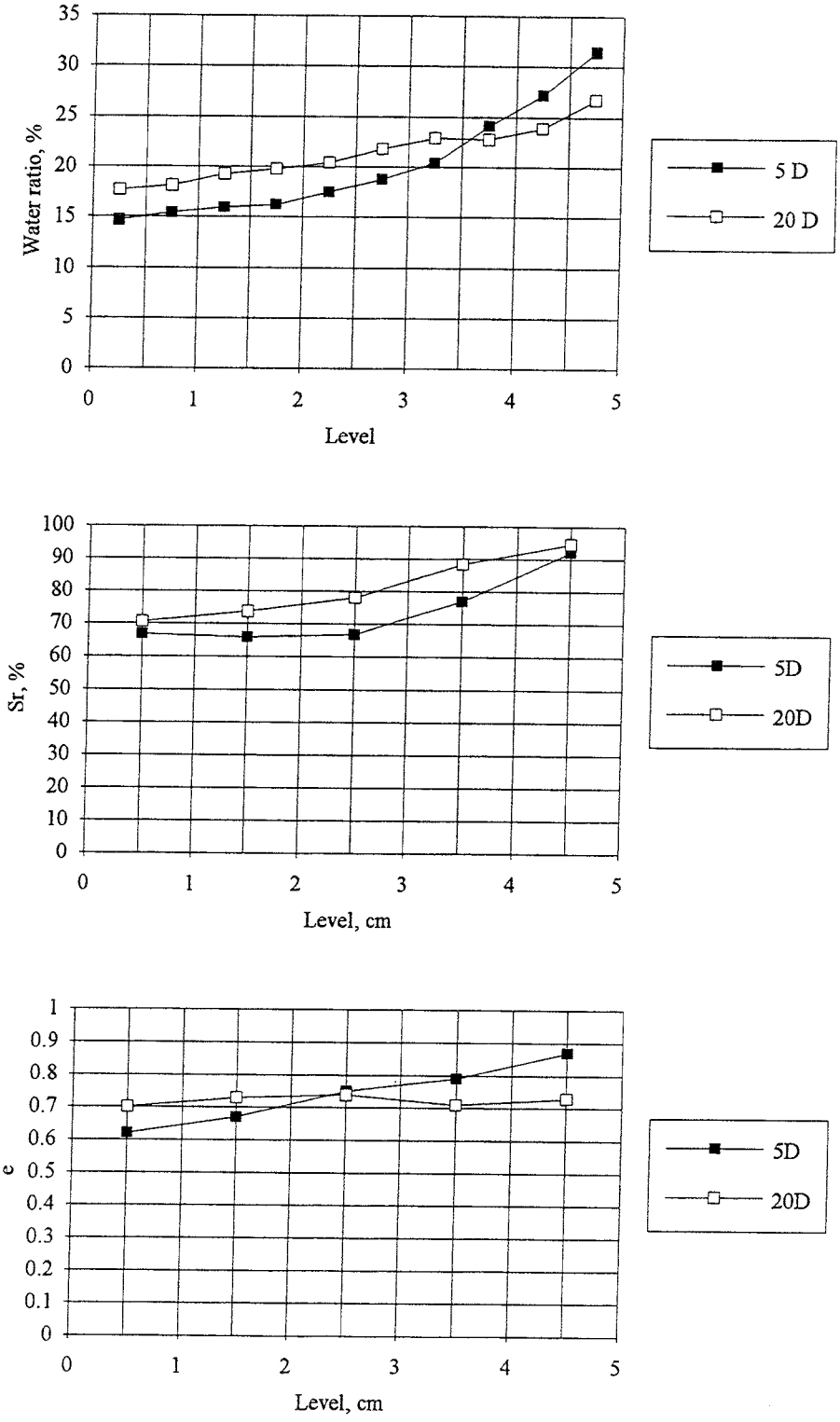

Figure 5-5. *Results from the water uptake tests. The water ratio, degree of saturation, and void ratio are plotted as a function of the distance from the hydraulically closed end after 5 and 20 days.*

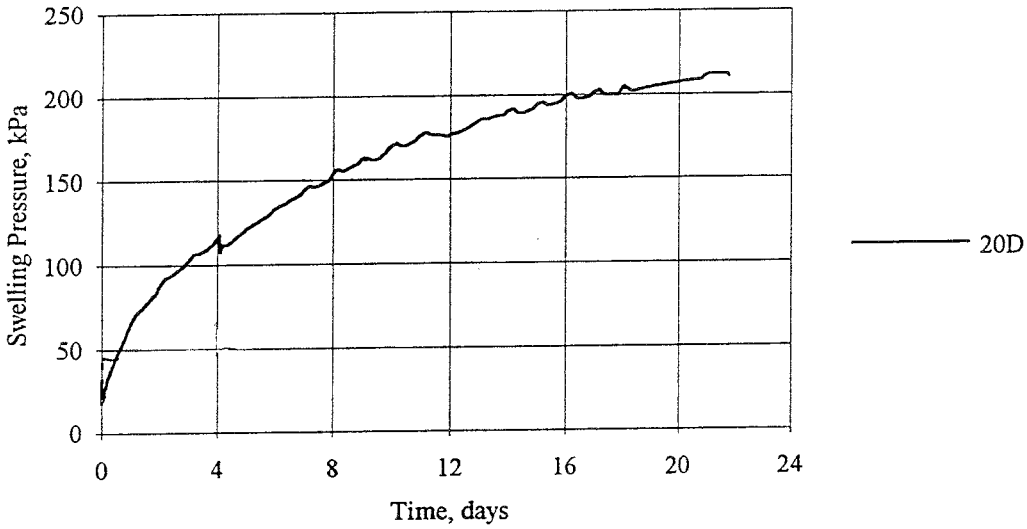

Figure 5-6. *Development of measured swelling pressure as a function of time for test 4b.*

5.3.3 Thermal material model

Eqn 5-3 was given for the thermal conductivity of the buffer material.

$\lambda=0.38+3.60\theta$ (W/m,K) (5-3)

where

θ= volumetric water content = $w\rho_d/\rho_w$

Eqn 5-3 can be reformulated to Eqn 5-4.

$\lambda=0.38+3.60S_r e/(1+e)$ (5-4)

However this relation is only valid at room temperature. The vapour flow that takes place in a temperature gradient will transport heat and increase the apparent heat conductivity under some conditions. According to De Vries /5-3/, the apparent heat conductivity of pore air increases with temperature due to the evaporation/condensation process. Fig 5-7 shows the change in apparent heat conductivity of the vapour k_{vs} with temperature. This can be taken into account if the geometric mean model for porous media /5-4/ according to Eqn 5-5 is applied.

$$\lambda = \lambda_s^{1-n} \cdot \lambda_w^{n \cdot S_r} \cdot \lambda_a^{n \cdot (1-S_r)} \quad (5\text{-}5)$$

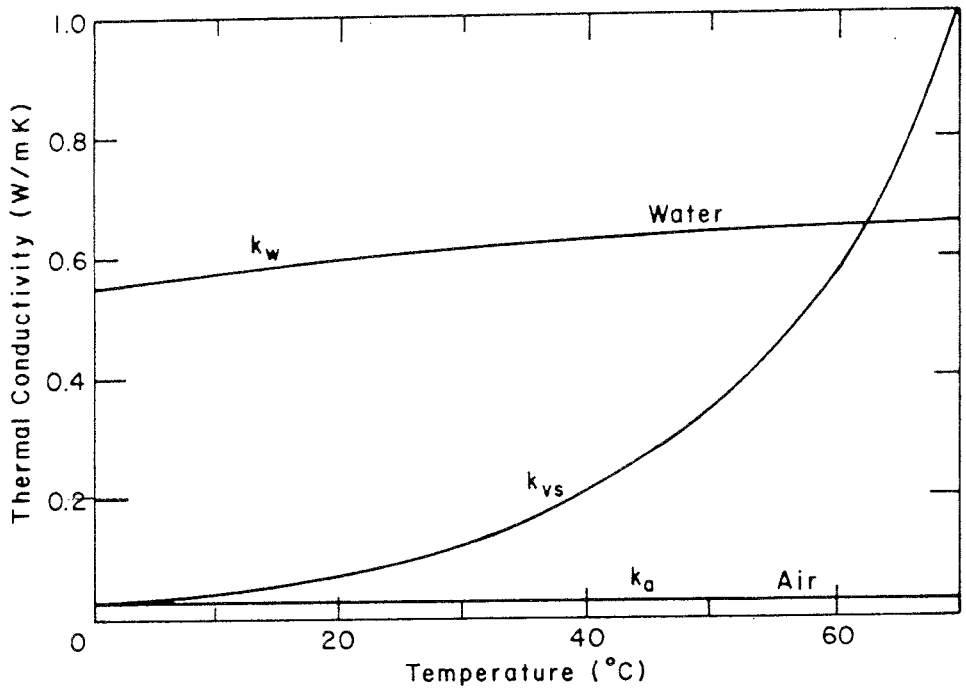

Figure 5-7. *Apparent thermal conductivity of the pore air k_{vs} due to vapour flow at 1 bar as a function of temperature (/3-7/ and /5-3/).*

where
- λ_s = heat conductivity of solids
- λ_w = heat conductivity of water
- λ_a = heat conductivity of air
- n = porosity (pore volume divided to total volume)
- n = $e/(1+e)$
- S_r = degree of saturation

Using Eqn 5-5 and the relation between the apparent heat conductivity and the temperature in Fig 5-7, the heat conductivity can be corrected for vapour flow according to Eqn 5-6.

$$\lambda_{cv} = \lambda \left(\frac{\lambda_v^T}{\lambda_v^{T_{20}}} \right)^{\frac{e}{1+e}(1-S_r)} \qquad (5\text{-}6)$$

where

- λ_{cv} = apparent heat conductivity of the buffer material corrected for vapour flow
- λ =heat conductivity of the buffer material at T=20°C
- $\lambda_v^{T_{20}}$ =heat conductivity of pore air at T=20°C
- λ_v^T =apparent heat conductivity of pore air at any temperature T

λ_{cv} can thus be calculated from Eqns 5-6 and 5-4 as a function of void ratio, degree of saturation and temperature. The influence of the void ratio is small in the limited range of the test, and it is estimated that the initial value e=0.7 can be used. The variation of λ_{cv} with S_r and T used in the calculation is shown in Table 5-4.

Table 5-4. The apparent heat conductivity of the buffer material λ_v (W/m,K) corrected for vapour flow as a function of the temperature and the degree of saturation.

	S_r=0.2	S_r=0.4	S_r=0.6	S_r=0.8	S_r=1.0
T=20°C	0.67	0.96	1.26	1.55	1.84
T=40°C	0.94	1.24	1.50	1.69	1.84
T=60°C	1.33	1.60	1.77	1.84	1.84

The specific heat c and bulk density ρ has been assumed to be constant because of the very small influence these parameters have on the temperature. The following values were used in the calculations:

c=1533 Ws/kg,K
ρ=1940 kg/m^3

5.3.4 Mechanical material model

The material model for the mechanical properties of the buffer material includes the properties of the *structure*, the properties of the *water* in the saturated and unsaturated stages, and the properties of the *particles*. The input data are given as parameter values for most models. For more information see /3-3/.

Structure

Porous elastic

The mechanical parameters required for the material model are not known and should be determined by laboratory testing. In this report, the parameters have been estimated from recalculation of the given data and from the author's experience from laboratory testing of similar materials.

κ=0.10 (=Porous bulk modulus)
ν=0.4 (=Poisson's ratio)

Drucker Prager

β=50	(="friction angle" in the *q-p* plane)
ψ=5	(=dilation angle)
K=1.0	(=influence of the intermediate principal stress)

The yield function, which corresponds to the relation between the stress and the plastic strain in the plastic zone, is defined as the plastic strain ε_y for a stress path that corresponds to uniaxial compression test without confining pressure. The total strain is the sum of the elastic and plastic strains.

Table 5-5. Yield function

q (kPa)	ε_y
13	0
38	0.005
63	0.02
88	0.04
113	0.1

"Moisture swelling", which is also a structural parameter is given in the part describing the water properties.

ρ=	1940 t/m^3	(bulk density used for the geostatic calculation of the effect of the gravitation)

Particles

B_s=2.1E8 kPa	(Bulk modulus of solid grains)
α_s=0	(Coefficient of thermal expansion)
ρ_s=2750 kg/m^3	(Density of solids)

Water

B_w=2.1E6 kPa	(Bulk modulus of water)
α_w=3.0E-4	(Coefficient of thermal expansion)
ρ_s=1000 kg/m^3	(Density of water)

The suction pressure s_w of the buffer material has been given in the specifications only for very dry material (S_r<30%) and it was proposed in the specifications that a logarithmic relation to a suction close to 0 at 100% saturation should be used. Lacking other information, the data in Table 5-6 between the suction and the degree of saturation was used. The same relation has been used for adsorption and exsorption. The relation implies a logarithmic decrease in suction with increasing degree of saturation starting

from an average of the given values. The values are taken from Eqns 5-7 and 5-8.

$$s_w = -Ae^{-Bw} \quad (5\text{-}7)$$

$$w = eS_r \frac{\rho_w}{\rho_s} \quad (5\text{-}8)$$

A=5.0E5 kPa
B=36.7

These two equations thus describe the suction potential at all combinations of void ratio and degree of saturation.

Table 5-6 also shows the moisture suction input data. These data were derived from the drying tests (Fig 5-1)

Table 5-6. Input data for the suction s_w and the moisture swelling for $e = 0.7$

Degree of saturation S_r	Suction kPa	Moisture swelling
0.01	500000	
0.05	314995	
0.10	198444	0.111
0.15	125018	
0.20	78760	0.111
0.25	49618	
0.30	31259	0.105
0.35	19693	
0.40	12406	0.085
0.45	7816	
0.50	4924	0.059
0.55	3102	
0.60	1954	0.025
0.65	1231	
0.70	775.6	0.000
0.75	448.6	
0.80	307.8	-0.017
0.85	193.9	
0.90	122.2	-0.035
0.95	77.0	
1.00	48.5	-0.052

The values of the suction pressure of the pore water and the corresponding values of the moisture swelling are essential for the whole calculation. These values are not accurately known for S_r>40%, which correspond to the test situation. This calls for more laboratory testing.

5.3.5 Water flux model

The water flux is controlled by the hydraulic conductivity of saturated soil k and the thermally driven water vapour diffusivity D_{Tv}. The value given was k=4.0E-13 m/s, which is assumed to be valid at room temperature. Calculations of the water uptake tests showed, however, that the rate of water uptake was too slow if this value was used. A good agreement was achieved when k=8.0E-13 m/s was used and it was decided that this value should be used in the calculations although the slow water uptake might as well be used by too low suction values.

The hydraulic conductivity of buffer materials increases with increasing temperature in proportion to the decreased water viscosity /5-5/. An increased temperature from 20°C to 50°C results in a decrease in viscosity by a factor 2, and thus an increase in hydraulic conductivity also by a factor 2.

For these two reasons the following input data for the hydraulic conductivity were used (linear interpolation):

k(20°C)=8.0E-13 m/s
k(50°C)=16.0E-13 m/s

The thermal water vapour diffusivity D_{Tv} was evaluated from the moisture redistribution tests by calibration calculations. It was brought to vary with the degree of saturation for taking into account the difference in air-filled connections in the buffer and the difference in bonds between the clay particles and the water. The following relation was found to yield accurate results (see Fig 5-8):

$$D_{Tvb}=8.0\text{E-}11\ \text{m}^2/\text{s,K} \qquad 0.3\le S_r\le 0.7$$

$$D_{Tv} = D_{Tvb}\cdot\cos^6\left(\frac{S_r-0.7}{0.3}\cdot\frac{\pi}{2}\right) \qquad S_r\ge 0.7$$

$$D_{Tv} = D_{Tvb}\cdot\sin^6\left(\frac{S_r}{0.3}\cdot\frac{\pi}{2}\right) \qquad S_r\le 0.3$$

The diffusivity is thus constant with a basic value D_{Tvb} between 30% and 70% saturation, which decreases strongly to D_{Tv}=0 at 0% and 100% saturation.

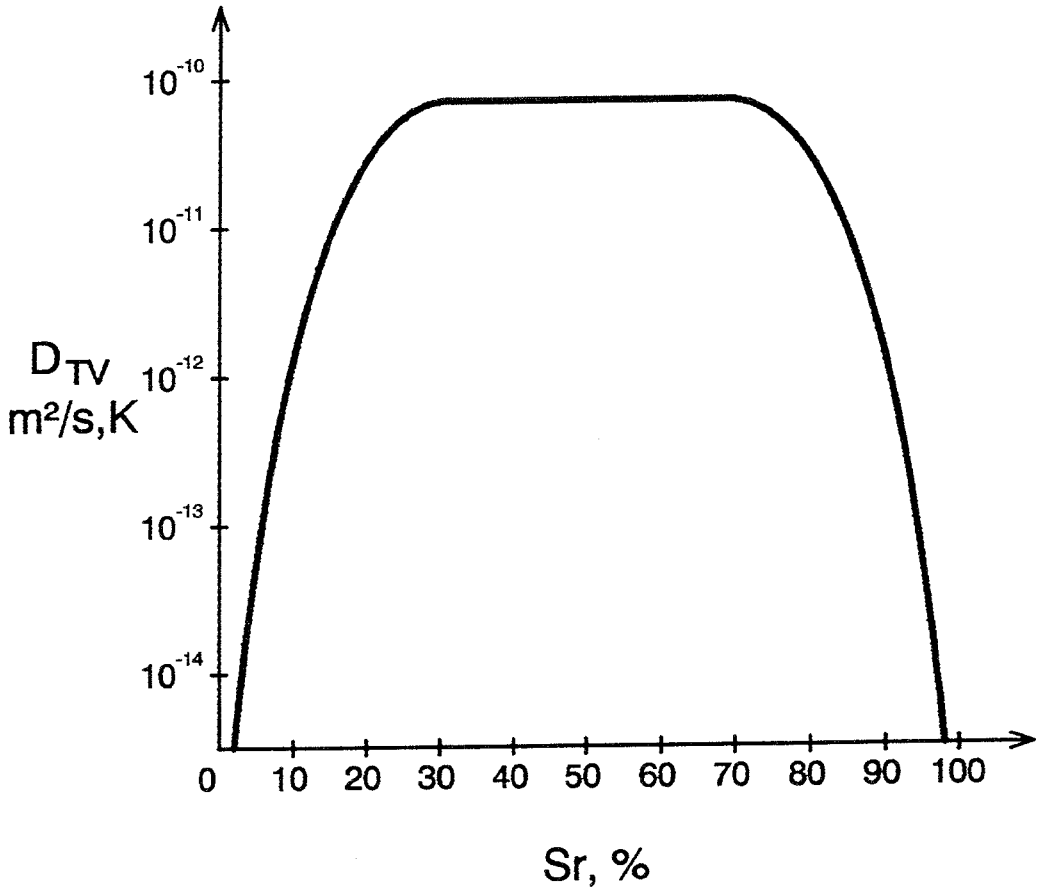

Figure 5-8. *Thermal vapour diffusivity D_{Tv} as a function of the degree of saturation S_r. This relation was used in the calculation.*

5.3.6 Initial conditions

The initial state of all variables in the material model needs to be defined. These values correspond to the conditions in the buffer material just after emplacement in the deposition hole.

e= 0.7
S_r= 0.65
p= 800 kPa (effective average stress)
s_w= -1231 kPa
T= 15°C

These input data yields the following values:

w= 16.6%
ρ_d= 1620 kg/m^3 (dry density)
p_{tot}= $p+s_w S_r$=0 (total average stress before applying the gravity)

The buffer material is thus initially assumed to be in equilibrium with no total stress acting on the rock or canister except for the own weight of the material.

6 MODEL CALIBRATION AND VERIFICATION

6.1 GENERAL

The three laboratory test series were simulated by applying the extended ABAQUS code and the new procedure for vapour flow in order to calibrate and verify the code and the material models. Numerous calculations have been made but only those with the material models and parameters described in chapters 5.3.3 to 5.3.5 will be shown here.

6.2 DRYING TESTS

The effect of wetting and drying of an unconfined sample is simulated by a simple 5 element mesh as shown in Fig 6-1. At first, water is added to the sample uniformly at a constant rate and then water is taken from the sample until the sample is almost dry. Fig 6-1 also shows how the void ratio changes with time. It increases at wetting until the time 1.5E5 and then decreases due to drying. Time is only fictive in this calculation. Fig 6-2 shows the change in average effective stress p and pore pressure s_w. P increases and s_w decreases very much at the end of the calculation due to the strong decrease in degree of water saturation, but the total stress defined by Eqns 2-2 and 2-3 is always p_{tot}=0.

Fig 6-3 shows results that can be compared to the measurements. The void ratio e is plotted as a function of the water ratio w and the degree of saturation S_r. The calculation starts at e=0.7, S_r=0.65, and w=16.6%. S_r and w increases until e=0.82, where the sample gets water saturated at w=30% and then follows the e-w line that corresponds to completely saturated soil. At drying, the same paths are followed since s_w has been equally defined for adsorption and exsorption. At very low water ratio w<2%, the behaviour is not relevant.

If the calculated results in Fig 6-3 are compared to the measurements in Fig 5-1 it can be seen that the inclination of the curves in the unsaturated parts are about the same although the level of the void ratio from the measurements is lower than the calculated ones. The difference is caused by different starting points. The samples in the laboratory had lower initial void ratios than the simulated sample. The relation is obviously dependent on the start conditions, but it is concluded that the modelled behaviour at drying is acceptable.

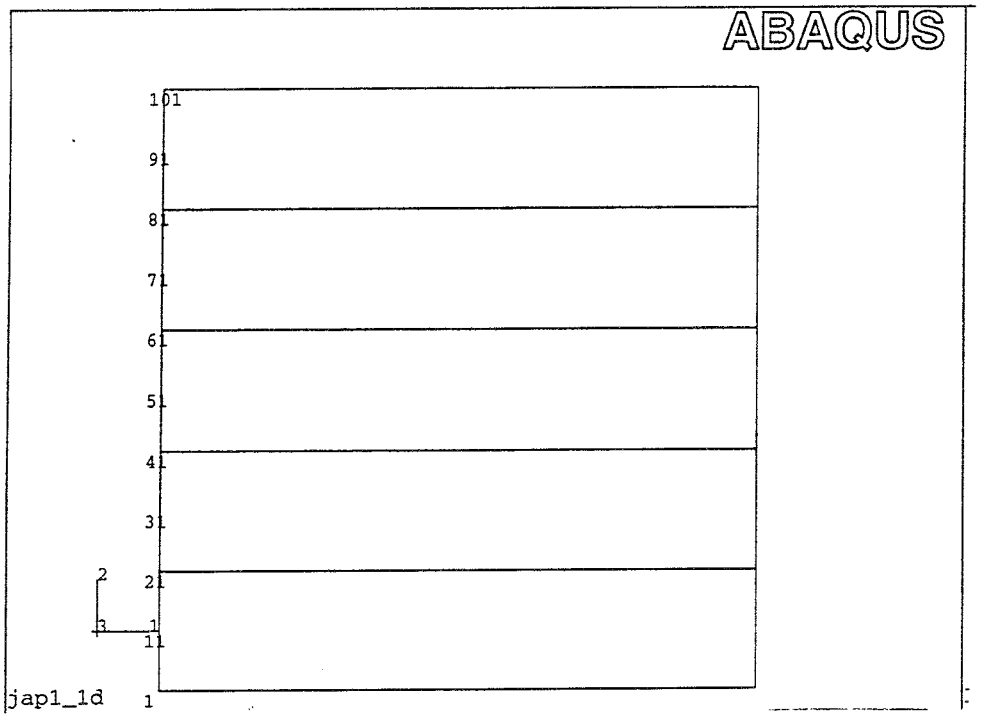

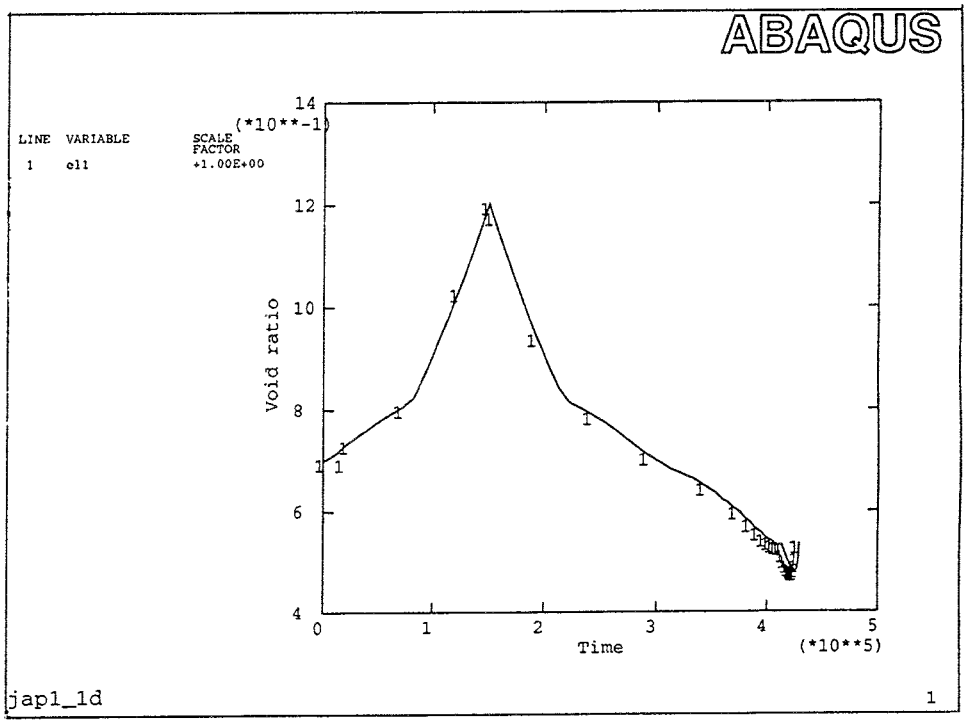

Figure 6-1. *Calculation of the drying test. Element mesh (upper) and the change in void ratio due to wetting until the time 1.5E5 and then drying.*

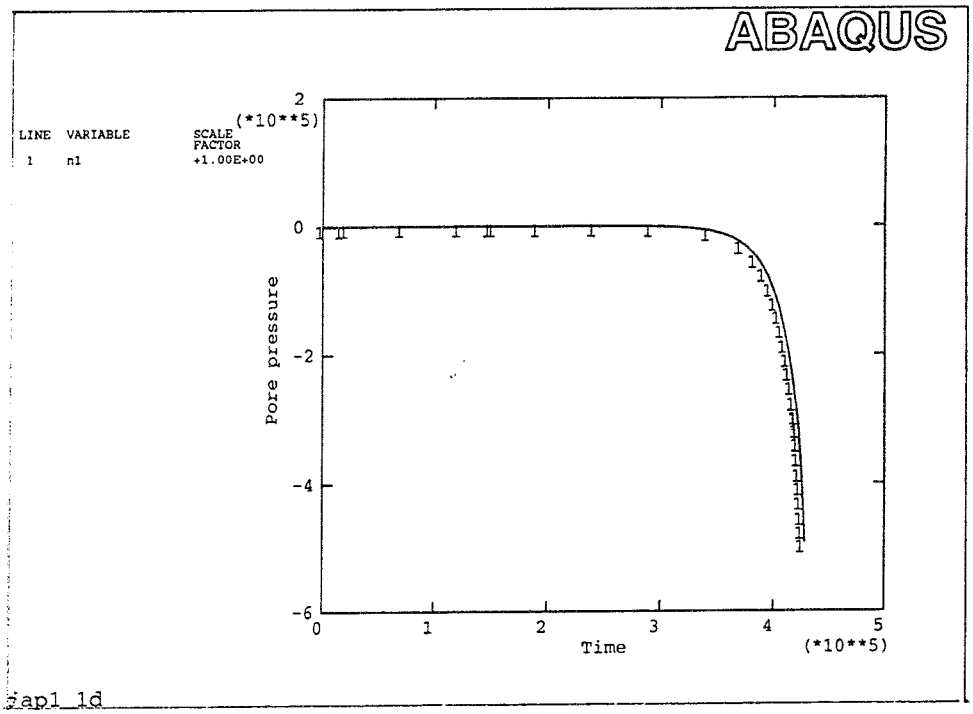

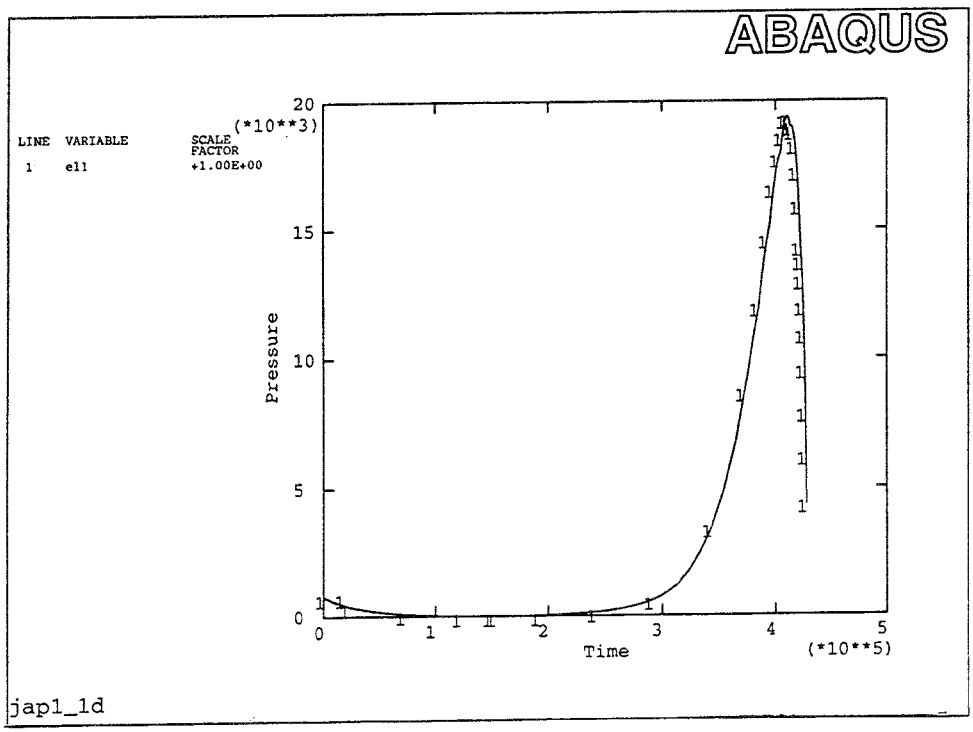

Figure 6-2. *Calculation of the drying test. The change in s_w (upper) and p with time due to wetting and drying.*

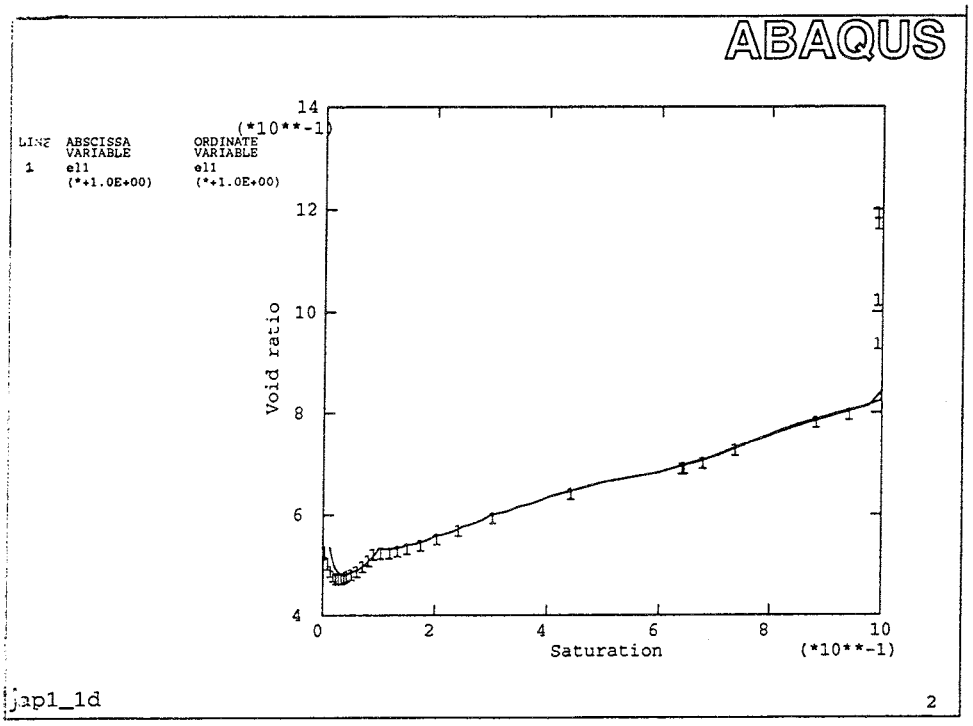

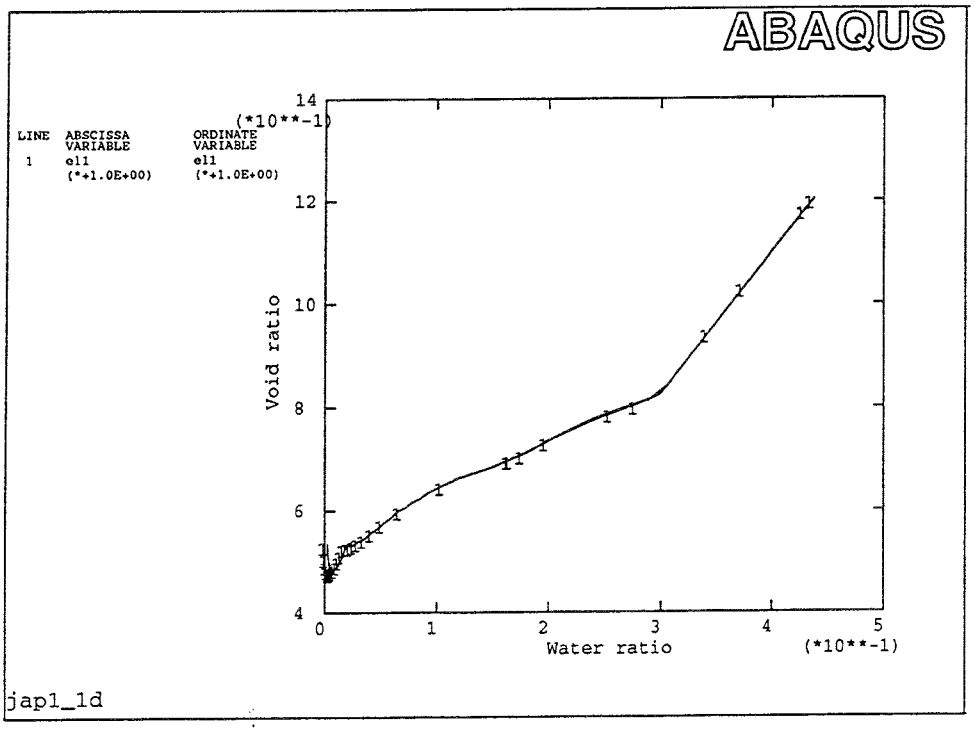

Figure 6-3. *Calculation of the drying test. Relation between the water ratio, the degree of saturation and the void ratio.*

6.3 WATER UPTAKE TESTS

The water uptake tests were simulated by using the element mesh shown in Fig 6-4. The element height decreases close to the bottom where unlimited access to water was assumed to prevail. The mechanical boundary was infinitely stiff but the simulated sample was allowed to deform freely inside the boundaries, meaning that there was no friction between the sample and the walls.

Fig 6-4 also shows the calculated reaction force at the top boundary (kN/m). Since the width of the simulated sample was 5 cm, the force can be transformed to pressure by dividing by 0.05 m. This yields a swelling pressure that approaches 400 kPa at the end of the test which is close to the value given in the specifications /1-1/. The test was simulated for 5E6 seconds which correspond to 58 days. Comparing Fig 6-4 from start to 1.7E6 s. with the measured swelling pressure in Fig 5-6 it is obvious that the shape of the curves agree but the measured swelling pressure after 20 days was only 210 kPa which is lower than the calculated 330 kPa. A somewhat too high void ratio in the laboratory sample may partly explain the difference.

Fig 6-5 shows the change in void ratio and degree of saturation as a function of time for all 20 elements. The lower curves represent the upper element at the dry end of the sample in both figures. The figures show that the void ratio is strongly changed during the test, with a large swelling of the elements close to the water inlet, and compression of the elements at the dry end at the beginning of the test. However, at the end of the test the sample is homogenised and the difference very small. This is a trend that has been observed in laboratory tests although with smaller swelling than predicted by the calculations.

Figs 6-6 - 6-8 show w, S_r, and e as a function of the distance from the water inlet after 5 and 20 days corresponding to the times for termination of the two laboratory tests. Comparing the calculated water ratios in Fig 6-6 with the measured one in Fig 5-5 it can be concluded that the agreement is good, with very high values close to the water inlet and no increase at the dry end after 5 days. After 20 days the water ratio has decreased to about 26% at the wet end and increased to about 18% at the dry end in both the calculated and measured samples. It is difficult to compare the void ratios and also the values of degree of saturation, since the measurements are not accurate enough but the trends of the calculations and of the laboratory tests are similar.

The conclusion from these laboratory tests and corresponding calculations are that the combination of the applied values of k and s_w are relevant for unsaturated water flow in spite of the uncertainty of s_w.

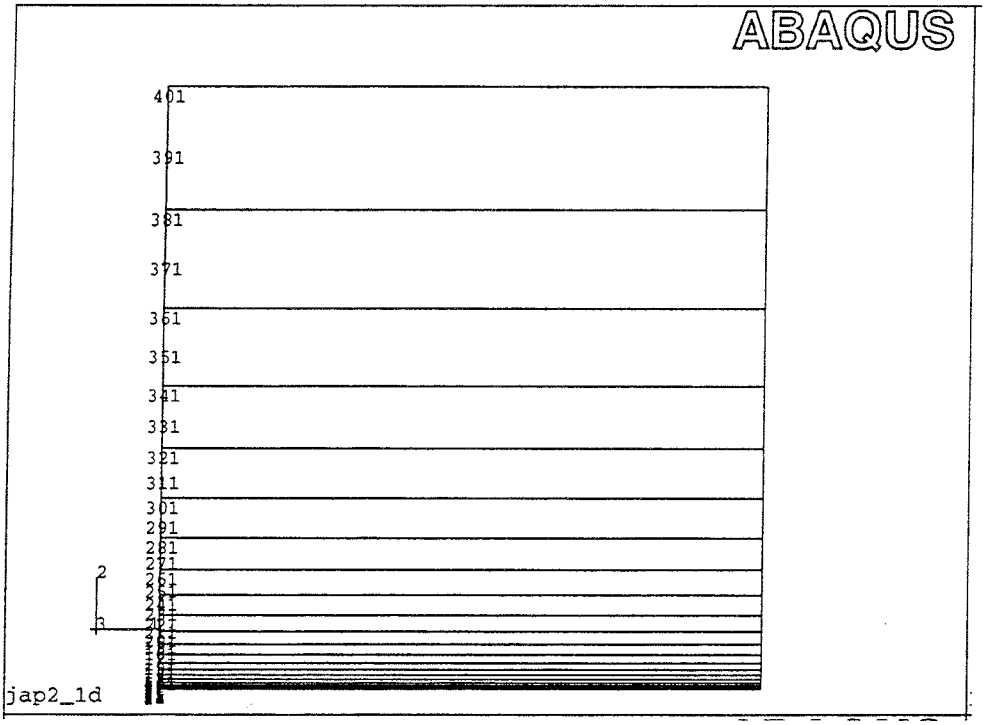

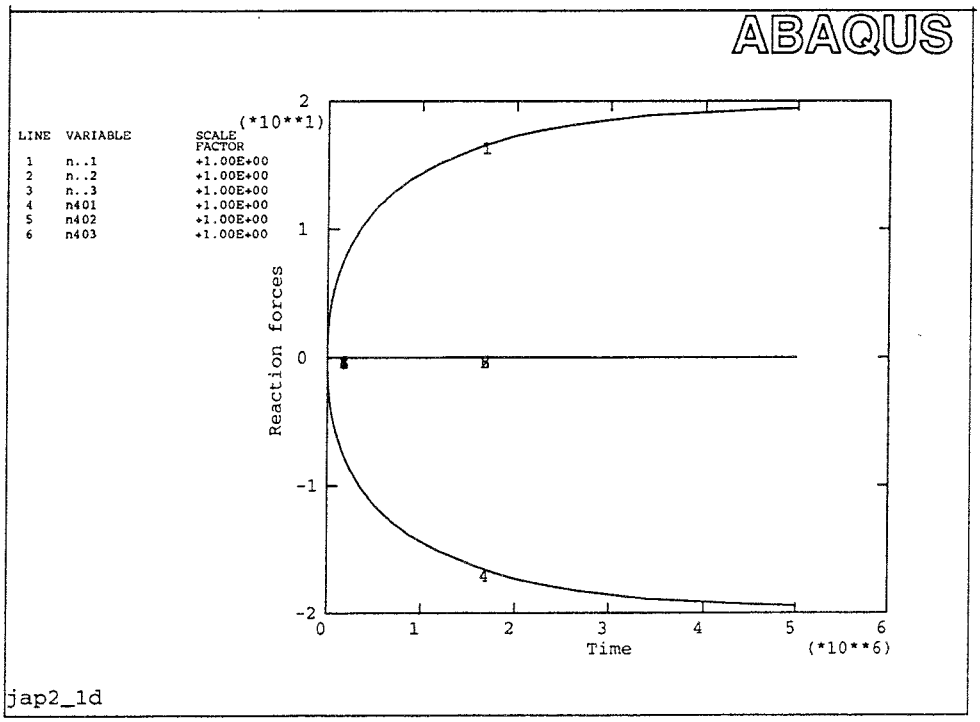

Figure 6-4. *Calculation of the water uptake test. The element mesh and the development of the reaction force (kN) as a function of time (s) are shown. Swelling pressure p_s (kPa) can be calculated by multiplying the reaction force with 20.*

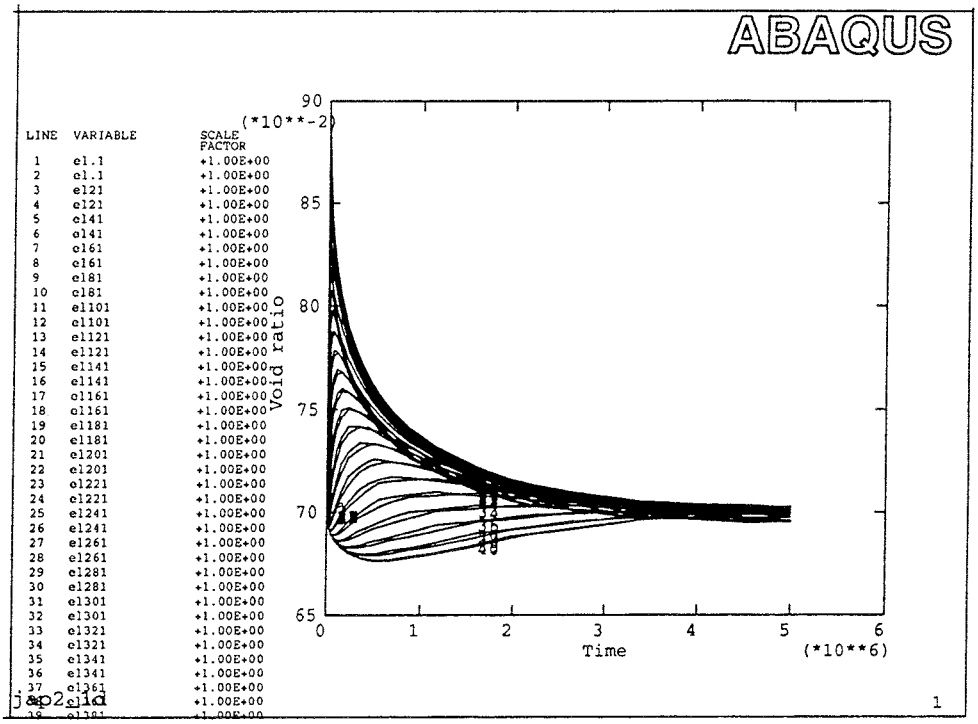

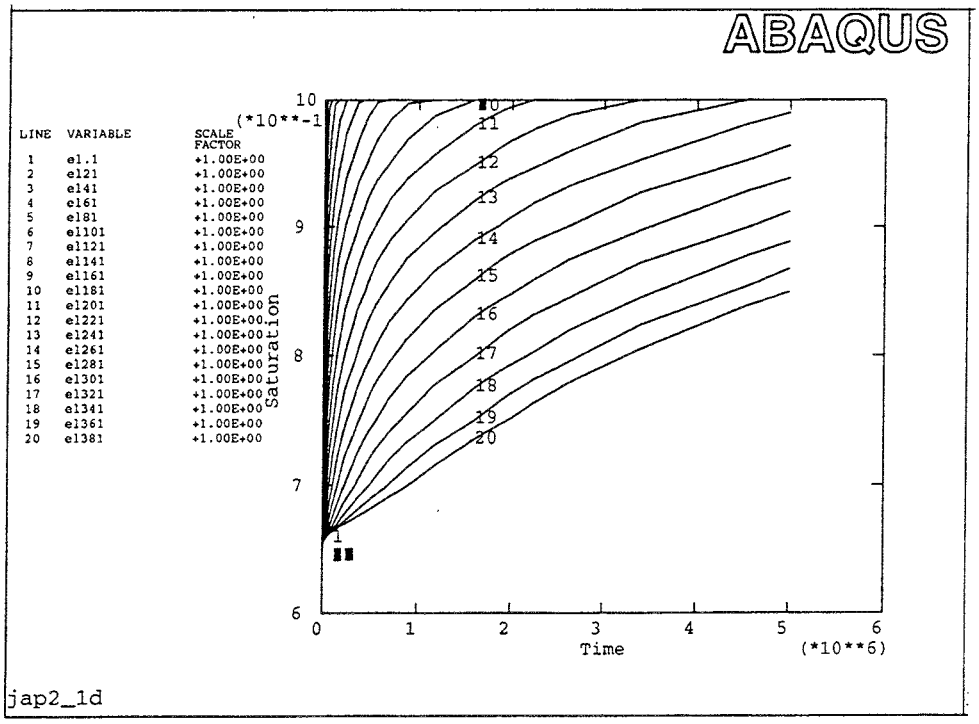

Figure 6-5. *Calculation of the water uptake test. The change in void ratio (upper) and degree of saturation as a function of time (s).*

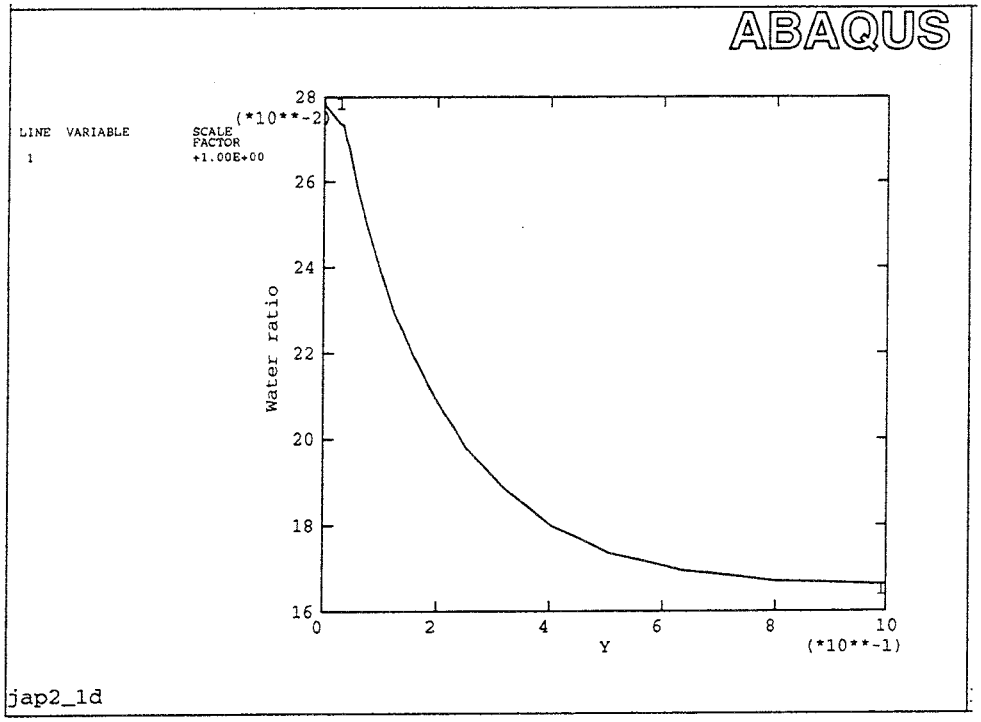

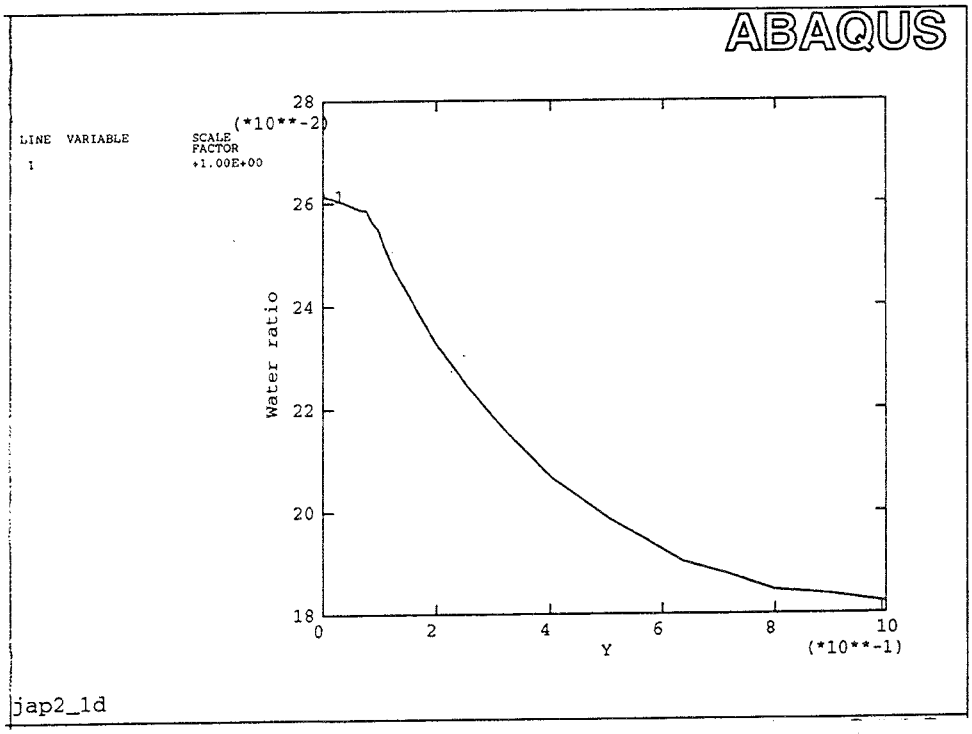

Figure 6-6. *Calculation of the water uptake test. The water ratio is plotted as a function of the distance from the water inlet after 5 days (upper) and 20 days. Y=0.2 corresponds to 1 cm.*

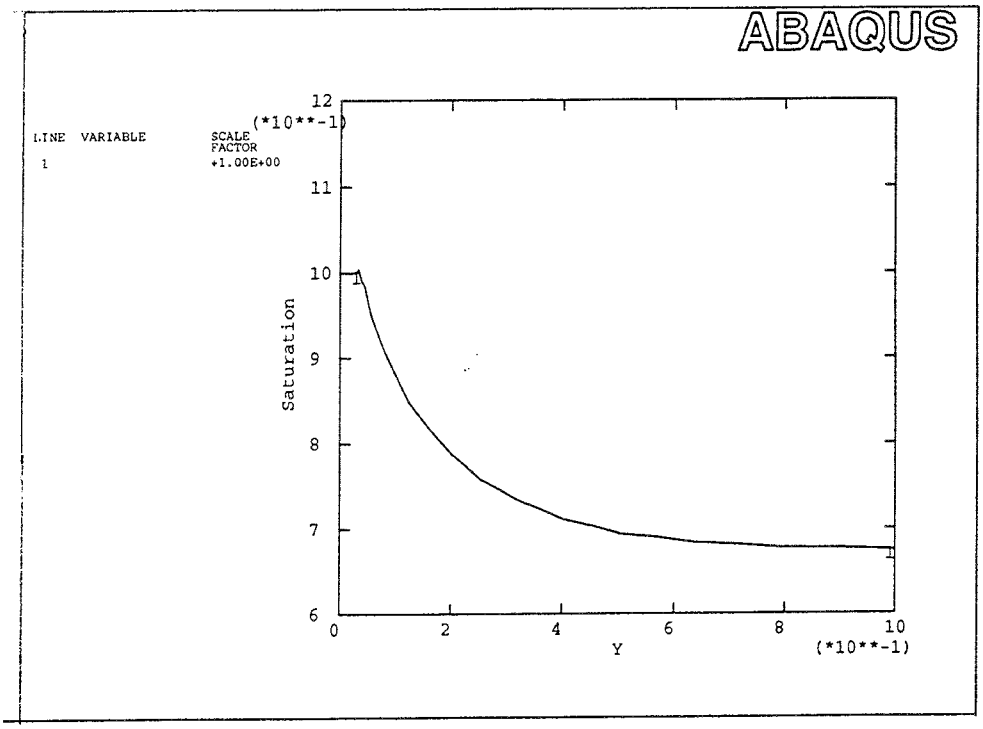

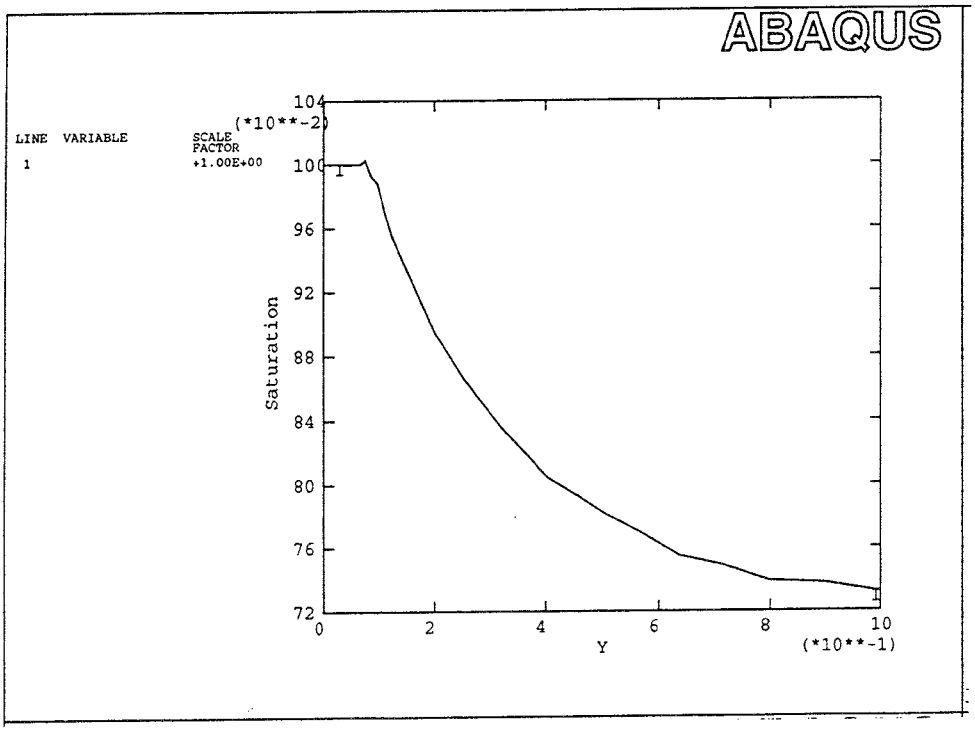

Figure 6-7. *Calculation of the water uptake test. The degree of saturation is plotted as a function of the distance from the water inlet after 5 days (upper) and 20 days. Y=0.2 corresponds to 1 cm.*

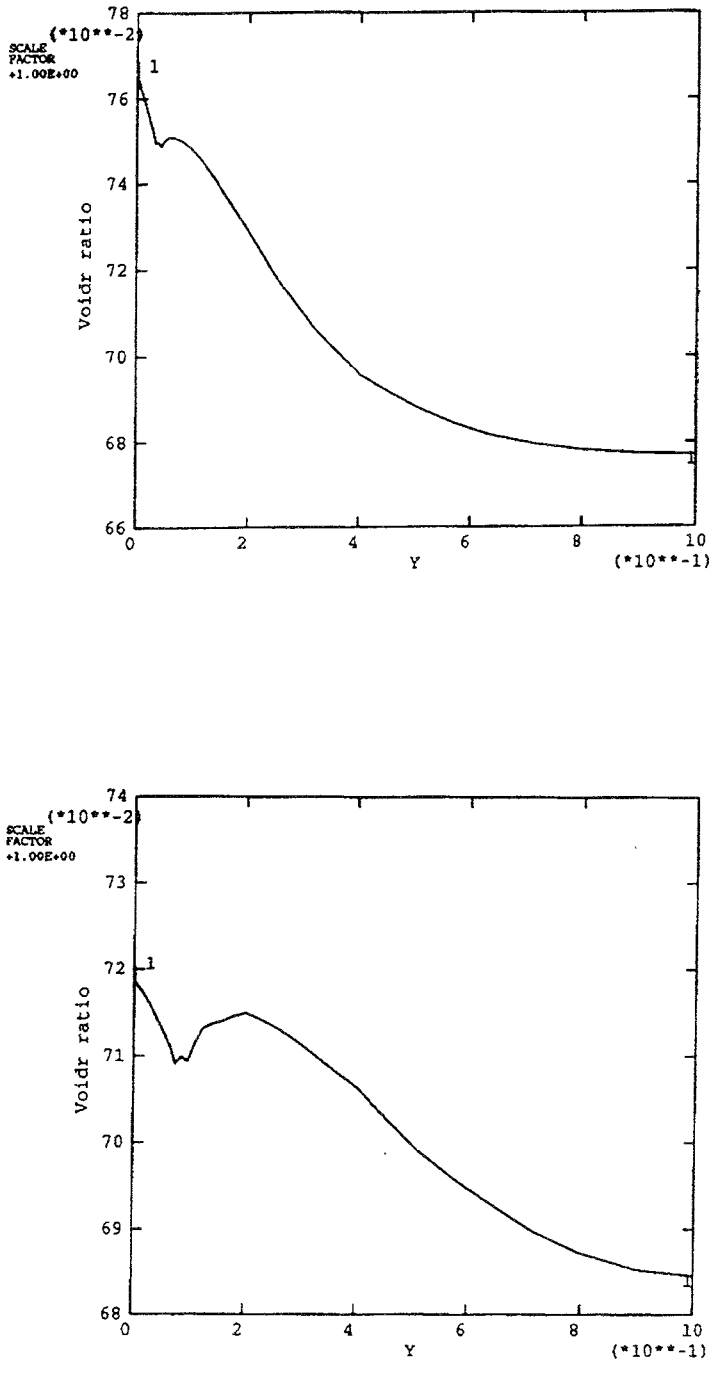

Figure 6-8. *Calculation of the water uptake. The void ratio is plotted as a function of the distance from the water inlet after 5 days (upper) and 20 days. Y=0.2 corresponds to 1 cm.*

6.4 MOISTURE REDISTRIBUTION TESTS

These tests were simulated with the same element mesh as the water uptake tests (Fig 6-4). A temperature gradient was applied across the sample with the highest temperature at the top of the sample (at the largest element) and the lowest temperature at the bottom (at the smallest element). All boundaries were completely water tight. Two calculations will be shown. The first one corresponds to test 1 with a temperature difference of 65% between the top and the bottom of the 5 cm high sample. The second corresponds to test 2 with a temperature difference of 10°C.

Test 1

Results from the simulation of test 1 are shown in Figs 6-9 and 6-10. Fig 6-9 shows the change in degree of saturation and void ratio with time from start. These diagrams show that the change is very large and goes very fast. Equilibrium in degree of saturation is established already after about 1E5 seconds, i.e. a little more than one day. The diagrams also show that something strange is happening in one element with a very strong swelling that is reduced after some time. This is an irrelevant behaviour caused by problems when the element reaches 100% saturation. There is obviously some problem with the material models when the material changes from being unsaturated to become completely saturated.

Fig 6-10 shows S_r, e and w as functions of the distance from the hot end after 4 days. The effect of the irrelevant behaviour, seen as the peak, has not completely disappeared yet. The calculated results agree very well with the measurements shown in Fig 5-2. A high water ratio with a degree of saturation close to 90% in about 2/5 of the sample at the cold end and a strong decrease to a water ratio of only a few per cent at the hot end can be seen in both the calculation and the test. The rate of redistribution also seems to agree, since the test had not reached equilibrium after 6 hours but was close to equilibrium after 1 day. The only parameter that does not agree very well is the void ratio that has changed very much in the calculation but very little in the measurements. However, the measurements are very uncertain and the tests should be repeated. Also, a more relevant technique for measuring the void ratio should be developed.

Test 2

Results from the simulation of test 2 are shown in Figs 6-11 and 6-12. Fig 6-11 shows the change in degree of saturation and void ratio with time from start. These diagrams show that the change is smaller and slower than in test 1. Equilibrium in degree of saturation is established after 4E5 seconds or about five days. No irrelevant behaviour appears in this calculation.

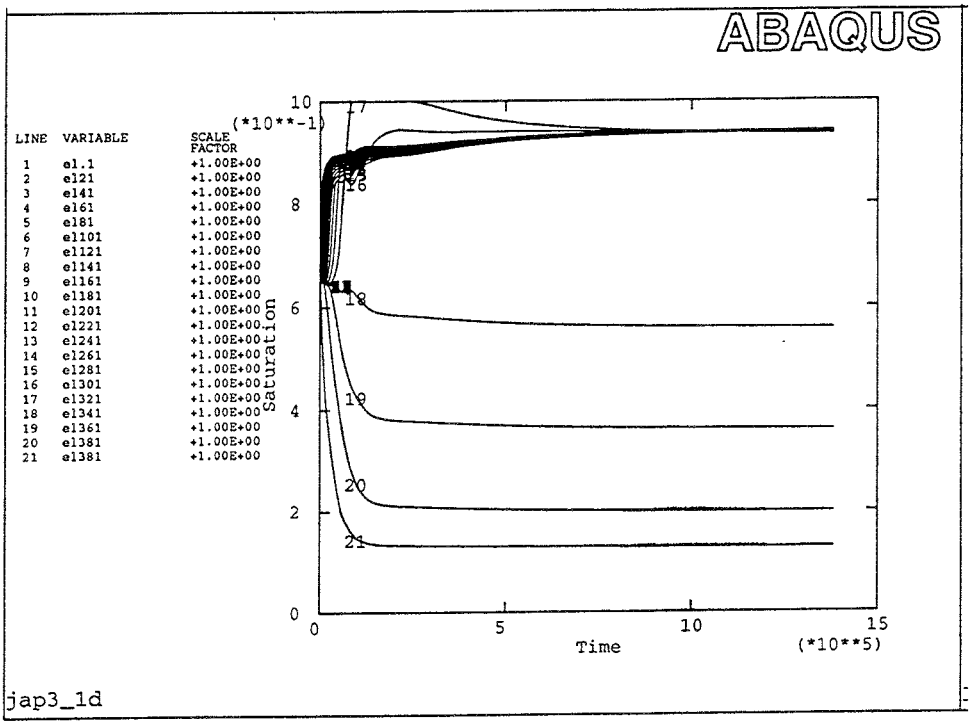

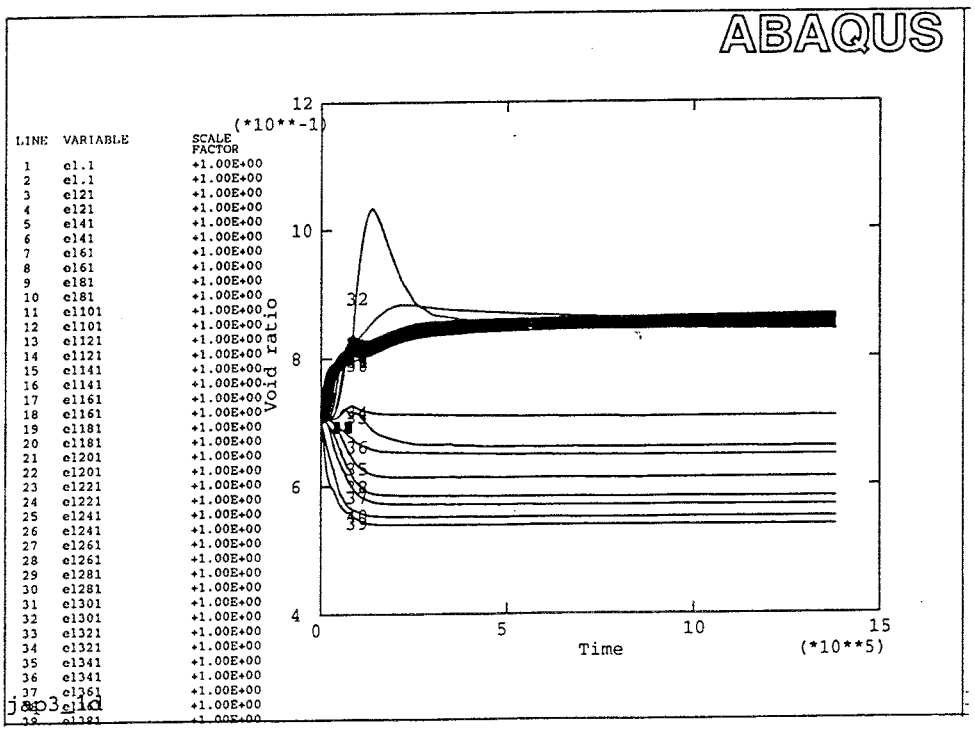

Figure 6-9. *Calculation of the water redistribution test (ΔT=65°C). Degree of saturation and void ratio are plotted as functions of time (s) for all elements.*

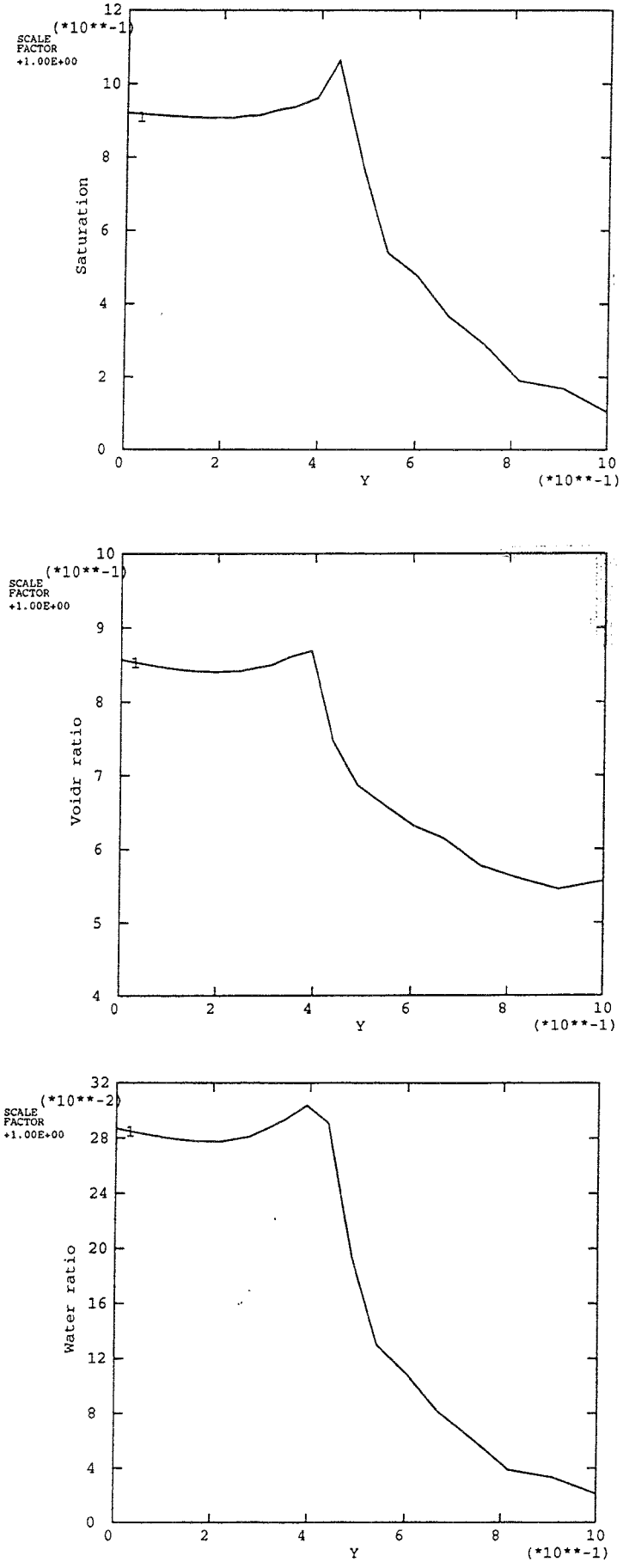

Figure 6-10. *Calculation of the water redistribution test (ΔT=65°C). Degree of saturation, void ratio, and water ratio are plotted as functions of the distance from the cold end after 4 days. Y=0.2 corresponds to 1 cm.*

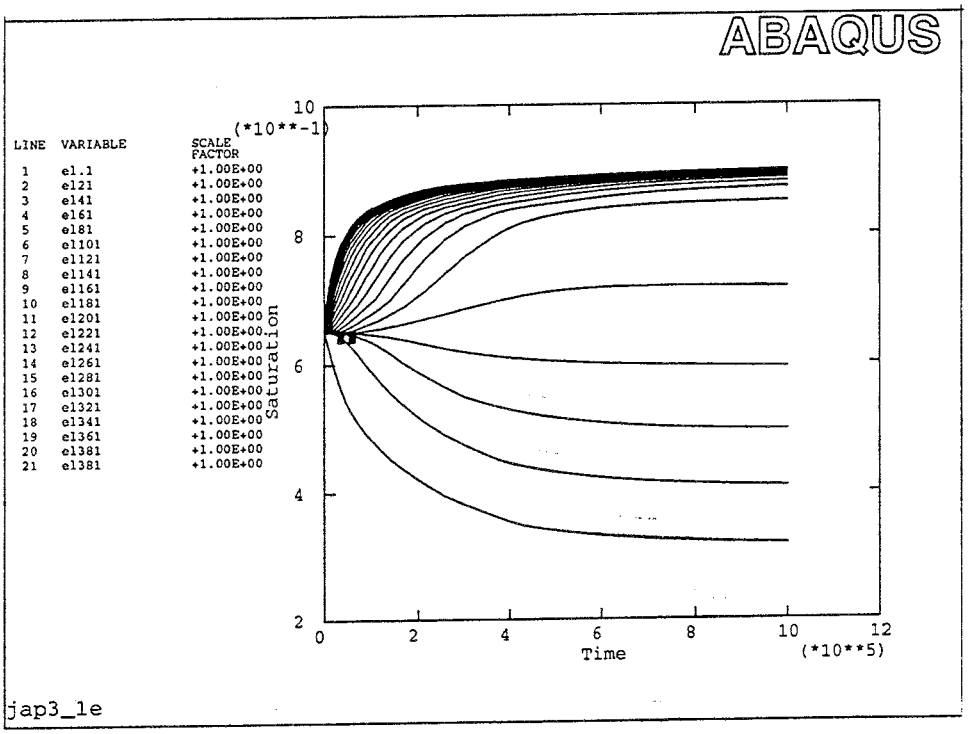

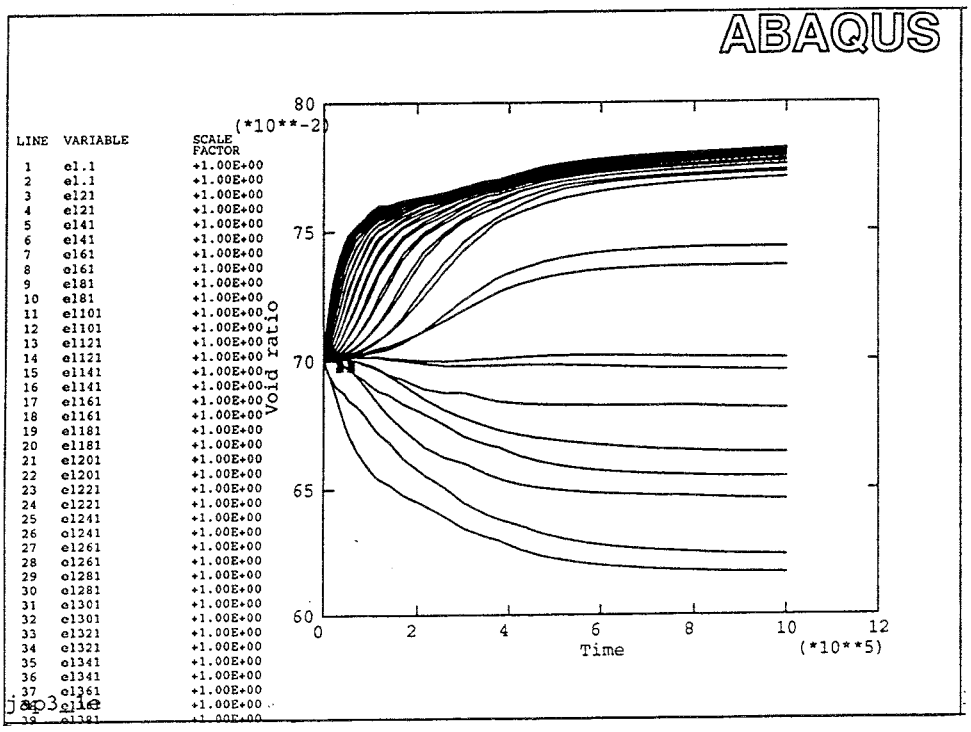

Figure 6-11. *Calculation of the water redistribution test (ΔT=10°C). Degree of saturation and void ratio are plotted as functions of time (s) for all elements.*

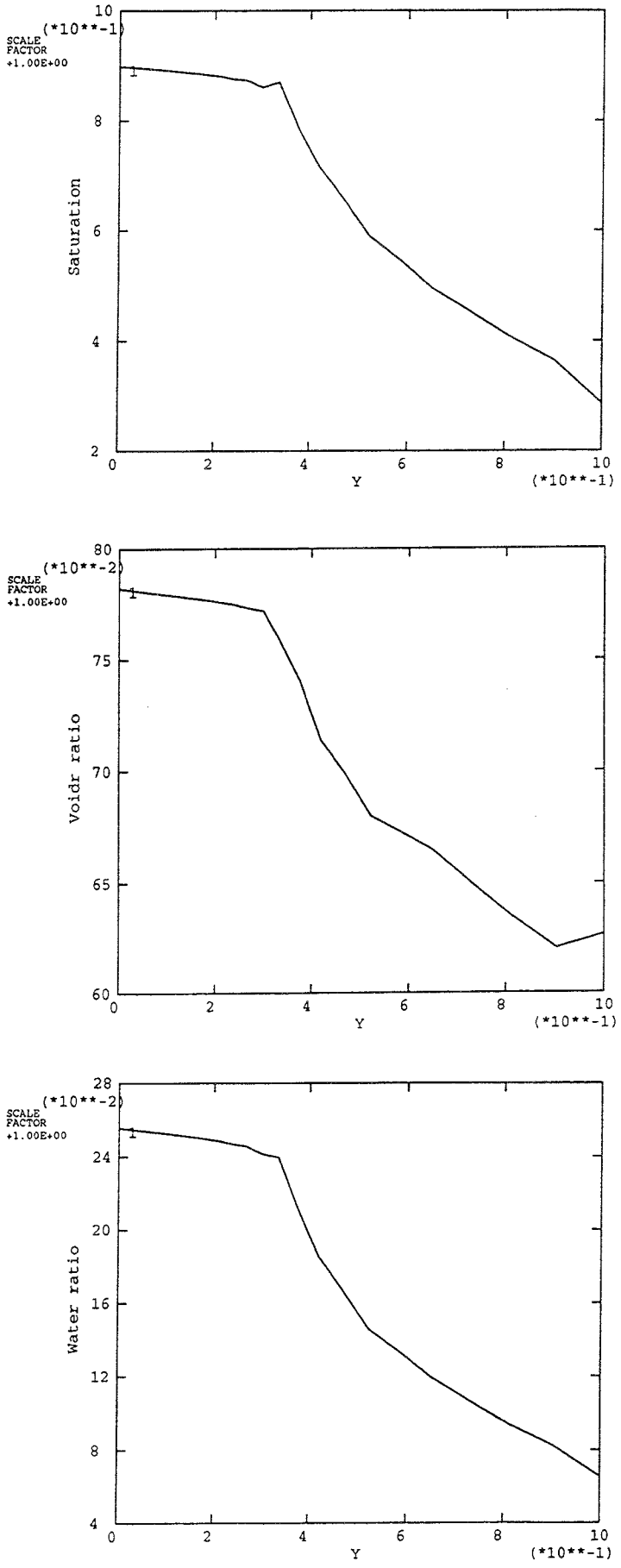

Figure 6-12. *Calculation of the water redistribution tests (ΔT=10°C). Degree of saturation, void ratio and water ratio are plotted as functions of the distance from the cold end after 4 days. Y=0.2 corresponds to 1 cm.*

Fig 6-12 shows S_r, e, and w as functions of the distance from the hot end after 12 days. The calculated results agree fairly well with the measurements shown in Fig 5-3 although the calculation seems to exaggerate the change in void ratio and water ratio a little. The calculated and recorded rates of redistribution also seem to agree, since the laboratory test had not reached equilibrium after 4 days.

The conclusion from these calculations and the corresponding laboratory tests are that the value of D_{Tv} according to chapter 5.3.5 is properly chosen in combination with the applied values of k and s_w.

7 CALCULATION OF THE BIG-BEN TEST

7.1 GENERAL

The hydro-mechanical calculation was completely coupled. The temperature calculation was semi-coupled by an iterative procedure. The temperature and hydro-mechanical calculations were repeated until no change in results between two iterations was obtained.

7.2 ELEMENT MESH AND BOUNDARY CONDITIONS

The element mesh of the Big-Ben calculation is shown in Fig 7-1. The mesh is axially symmetric around the left boundary. The height of the model is 5 m and the radius 3 m. The geometry and the location of the different materials are as shown in Figs 2-1 and 2-2. The properties of the different materials are described in chapter 5.

Only the heat calculation was made with the entire element mesh. The boundary conditions for the heat calculation were taken to be the following:

- Upper boundary: Heat transfer coefficient α_t=0.5 W/m^2,K
- Right boundary: α_t=0.5 W/m^2,K
- Lower boundary: α_t=1.0 W/m^2,K

These data were not known initially and had to be derived from calibration calculations.

Fig 7-1 also shows the location of the spots for which the calculated temperatures are plotted as functions of time.

The element model for the hydro-mechanical calculation only included the buffer material and the sand layers confining the buffer material, since test calculations showed that the canister and rock had a negligible influence on the buffer material in comparison with the effect of changing the unknown properties of the sand slots as noted earlier. Fig 7-2 shows a close up of the element mesh of the buffer material. The 9 spots for which the calculated results were requested are also shown in Fig 7-2.

The boundary conditions for the hydro-mechanical calculation were the following:

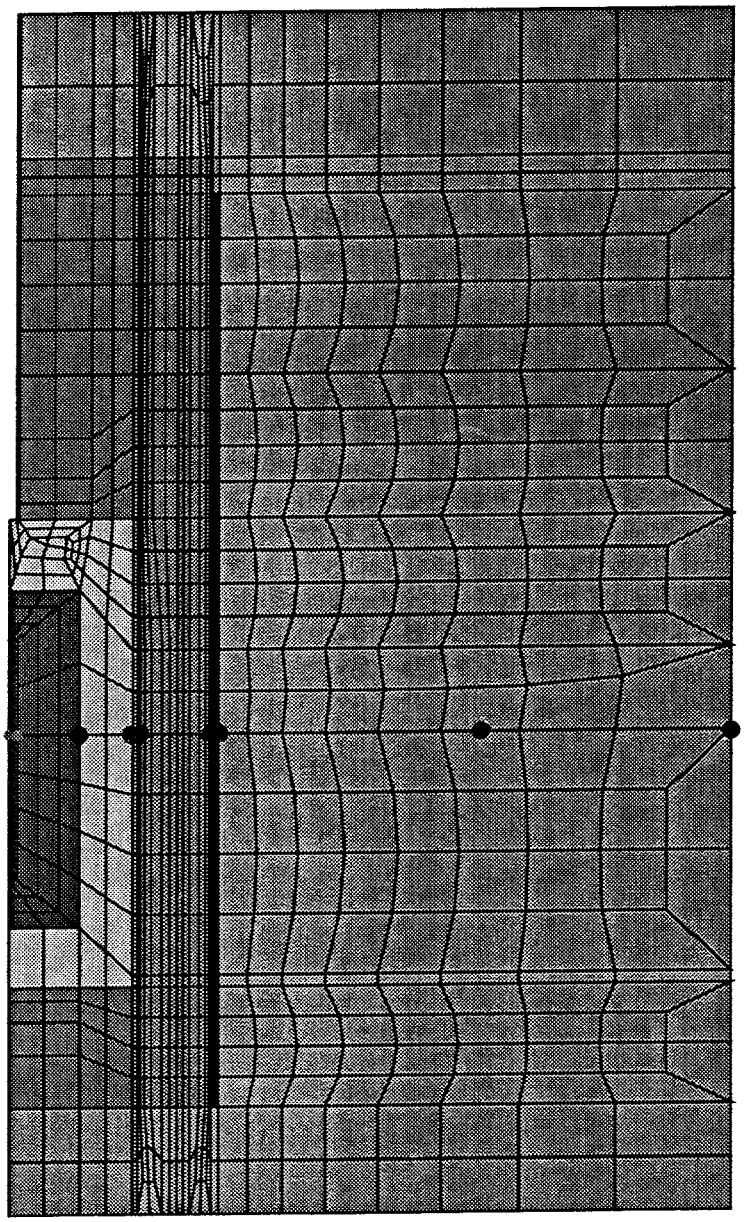

Figure 7-1. *Element mesh of the Big-Ben calculation. The mesh is axial symmetric around the left boundary. The light-coloured part corresponds to the steel canister.*

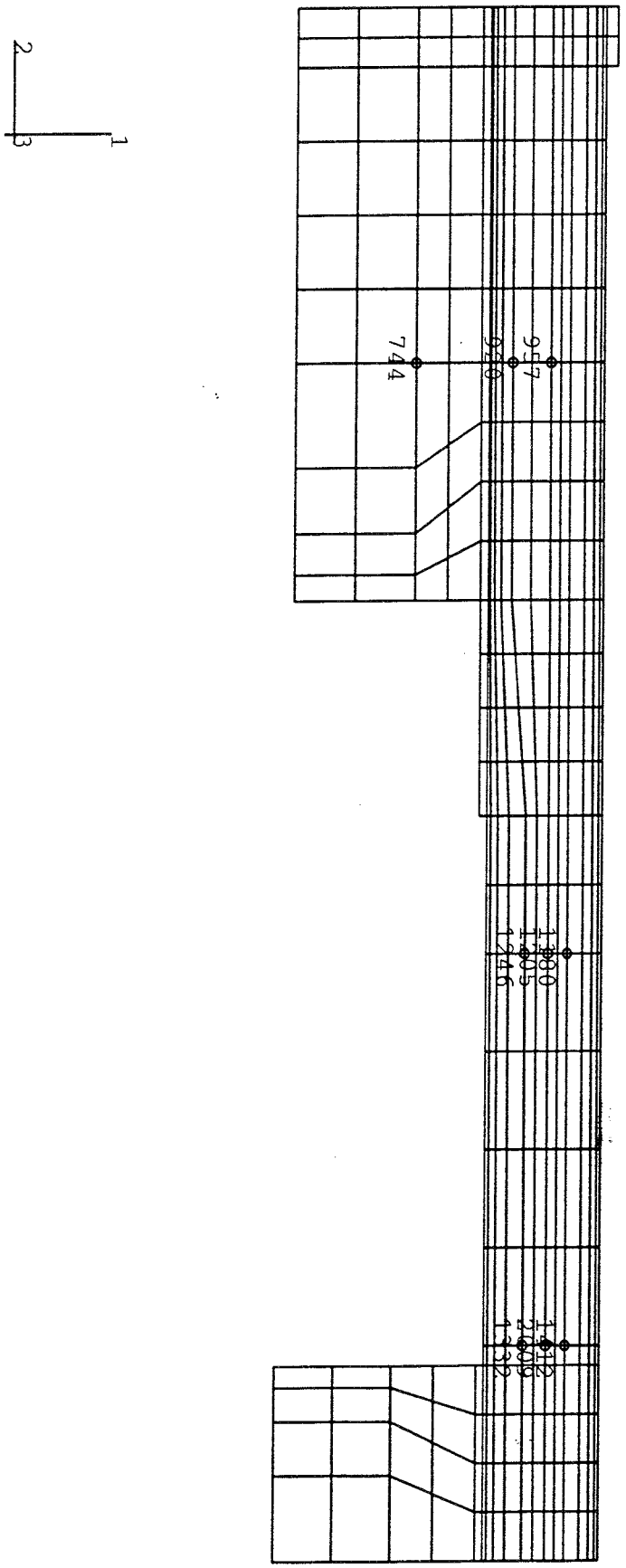

Figure 7-2. *Element mesh of the buffer material in the Big-Ben calculation.*

- The mechanical boundary was infinitely stiff.

- The hydraulic boundaries of the buffer material were the following: completely water-tight confinement of the buffer material except for the boundary to the outer sand layer which was exposed to a hydrostatic pressure with a water level 2 m above the top of the sand layer.

7.3 TEMPERATURE RESULTS

The results of the temperature calculations are shown in Figs 7-3 to 7-7. Fig 7-3 shows the temperature distribution in the entire model after 5 months and Fig 7-4 the temperature in the buffer at the same time.

Fig 7-5 shows the temperature in the buffer as a function of the distance from the inner sand layer in a horizontal plane through the centre of the heater after 1 month and 5 months, respectively.

Time-history plots of the temperature development are shown in Figs 7-6 and 7-7. The temperature in the spots along the horizontal centre line with the locations shown in Fig 7-1 are plotted in Fig 7-6, while the temperature in the specified 9 points A1 to C3 are shown in Fig 7-7.

The results agree fairly well with the measurements /1-1/ although the calculated temperature of the central part of the buffer material is about 2°C too high after 1 month and 1°C too high after 5 months. The temperature drop over the buffer material agrees very well.

7.4 HYDRO-MECHANICAL RESULTS

7.4.1 General

The results are presented in the following three types of diagrams:

- Time-history plots which show the development of the different parameters as a function of time for selected spots.

- Contour plots which show contour lines of the parameter values in the whole structure at selected times.

- Function plots which show the parameter values as functions of the distance from the boundaries.

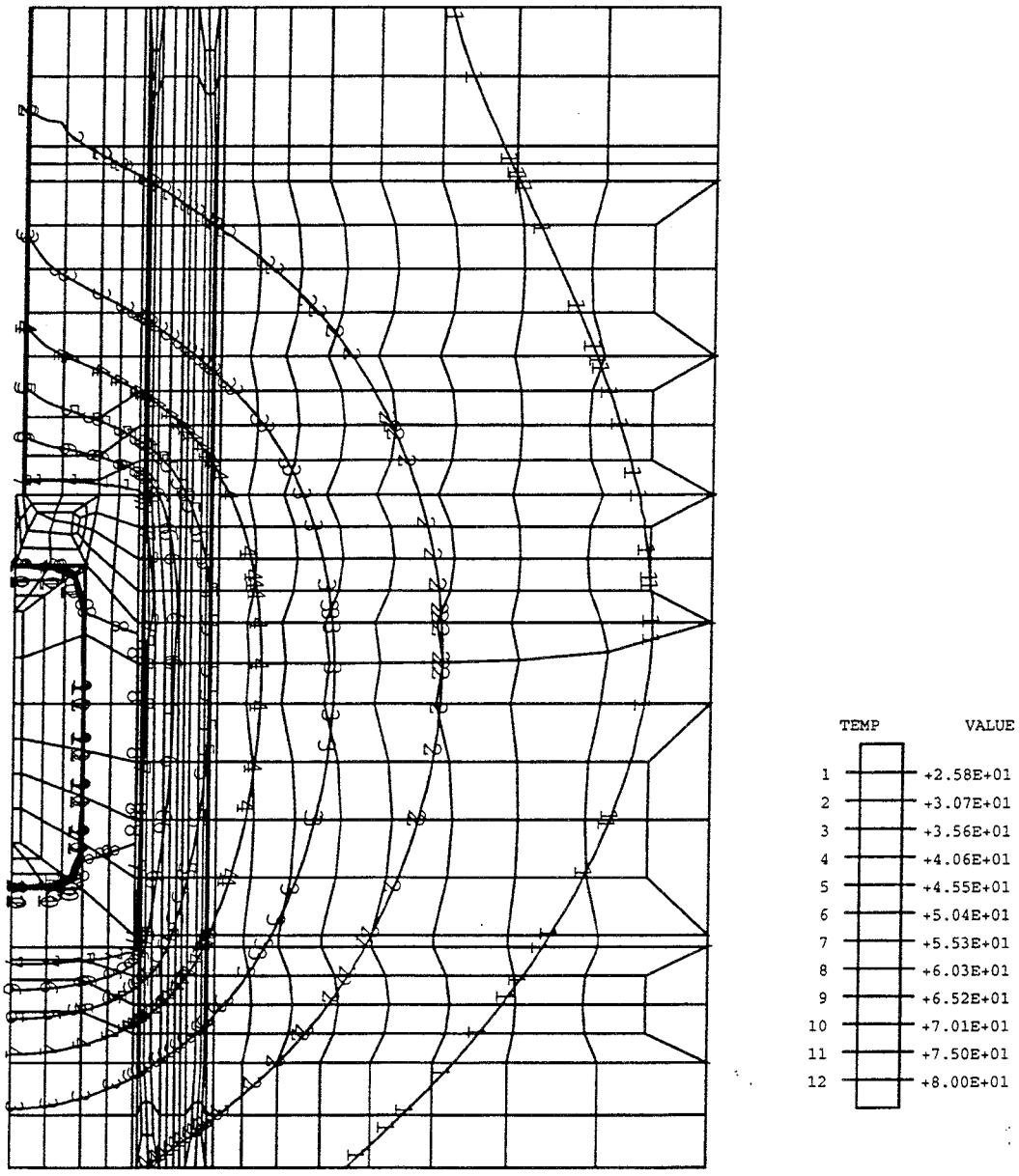

Figure 7-3. Temperature distribution in the model after 5 months (°C).

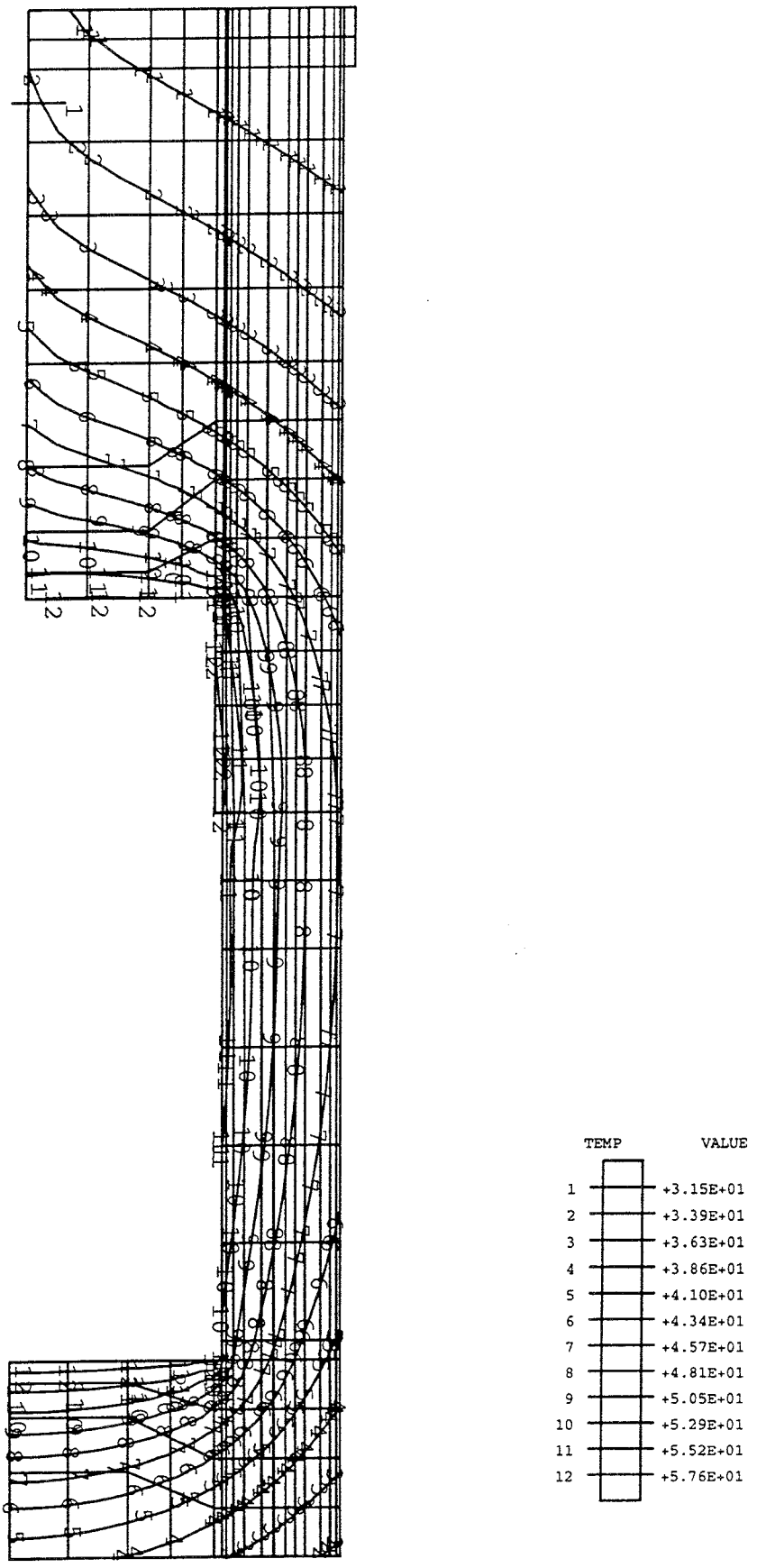

Figure 7-4. *Temperature distribution in the buffer after 5 months (°C).*

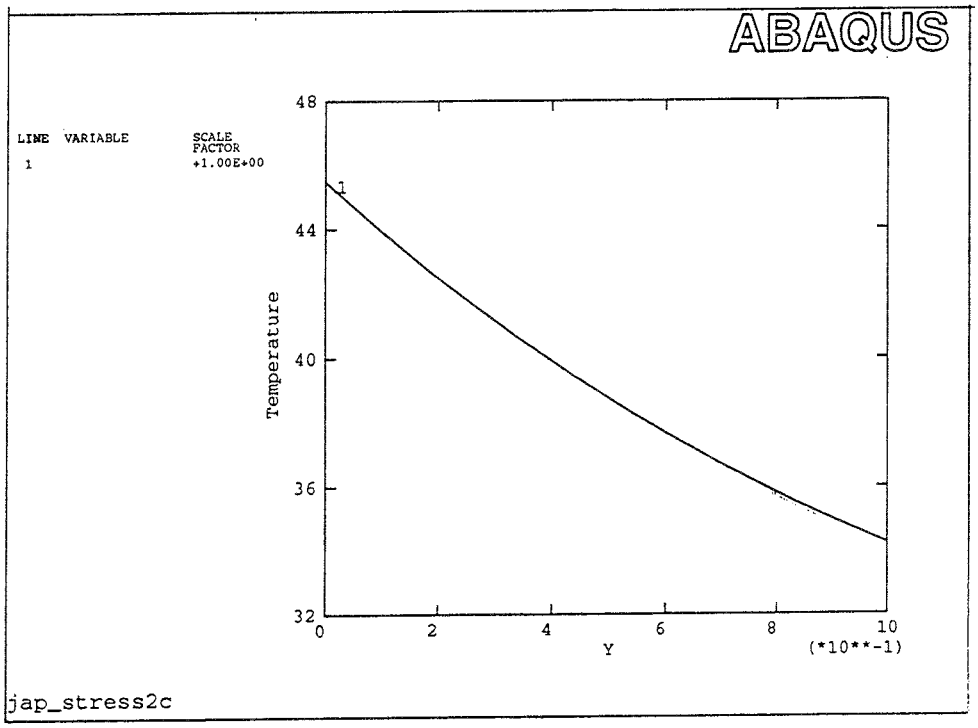

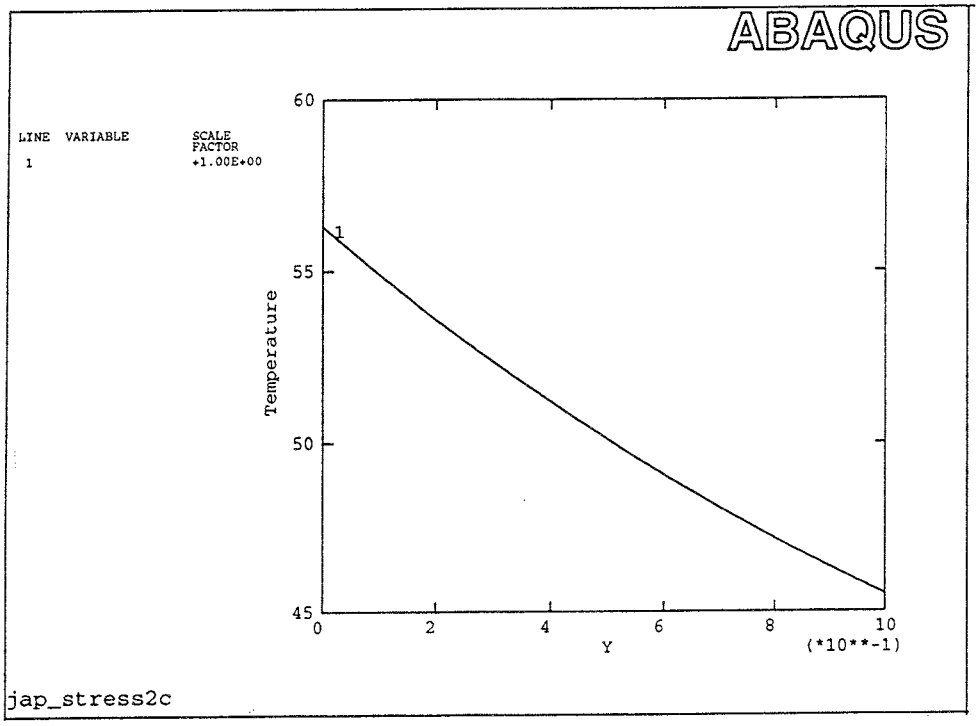

Figure 7-5. *Temperature (°C) in the buffer as a function of the distance from the inner sand slot in the horizontal plane through the centre of the heater after 1 month (upper) and after 5 months. Y=0.1 corresponds to the distance 3 cm.*

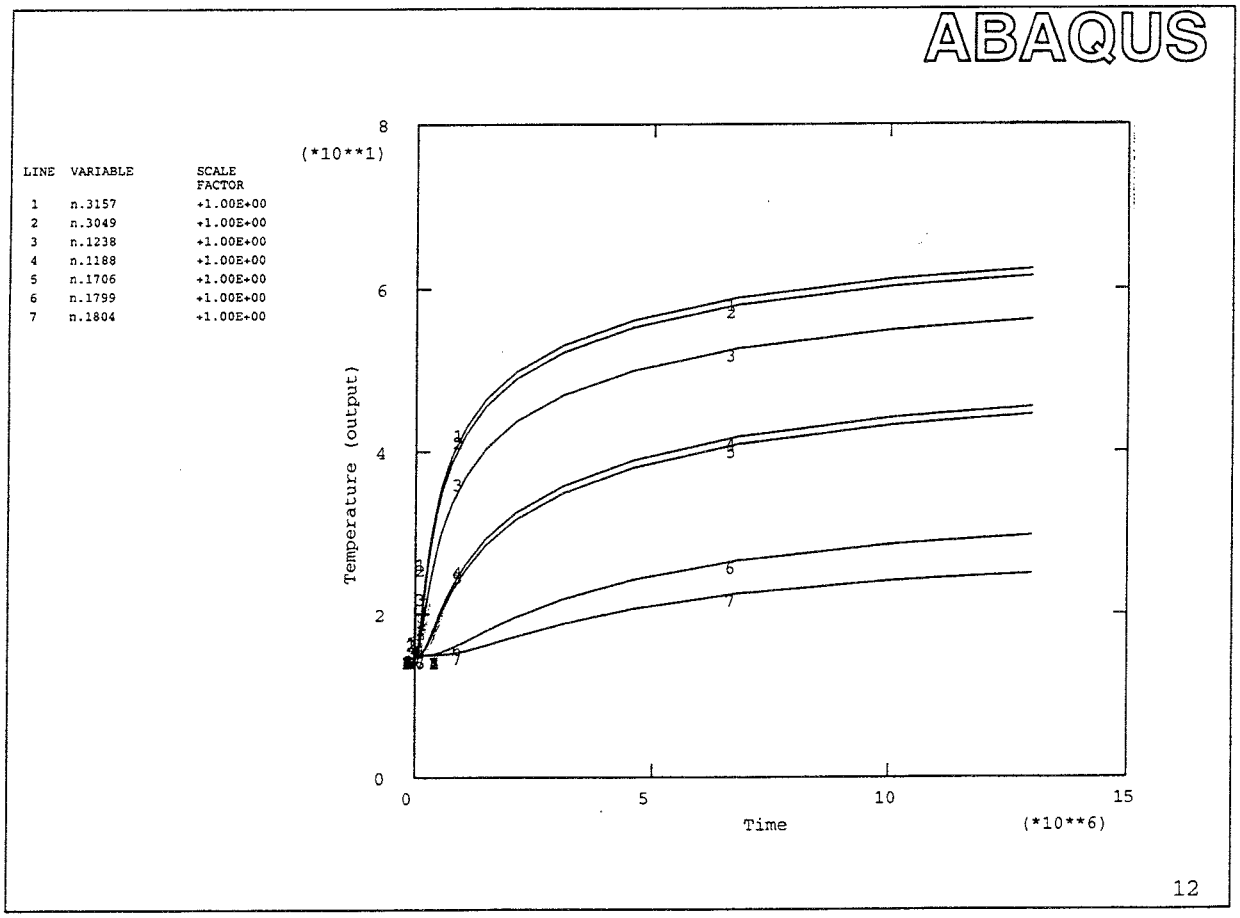

Figure 7-6. *Temperature (°) plotted as a function of time (s) in the 7 points along the horizontal centre line (see Fig 7-1)*

1 Inner canister surface
2 Outer canister surface
3 Inner bentonite surface
4 Outer bentonite surface
5 Inner rock surface
7 Outer rock surface

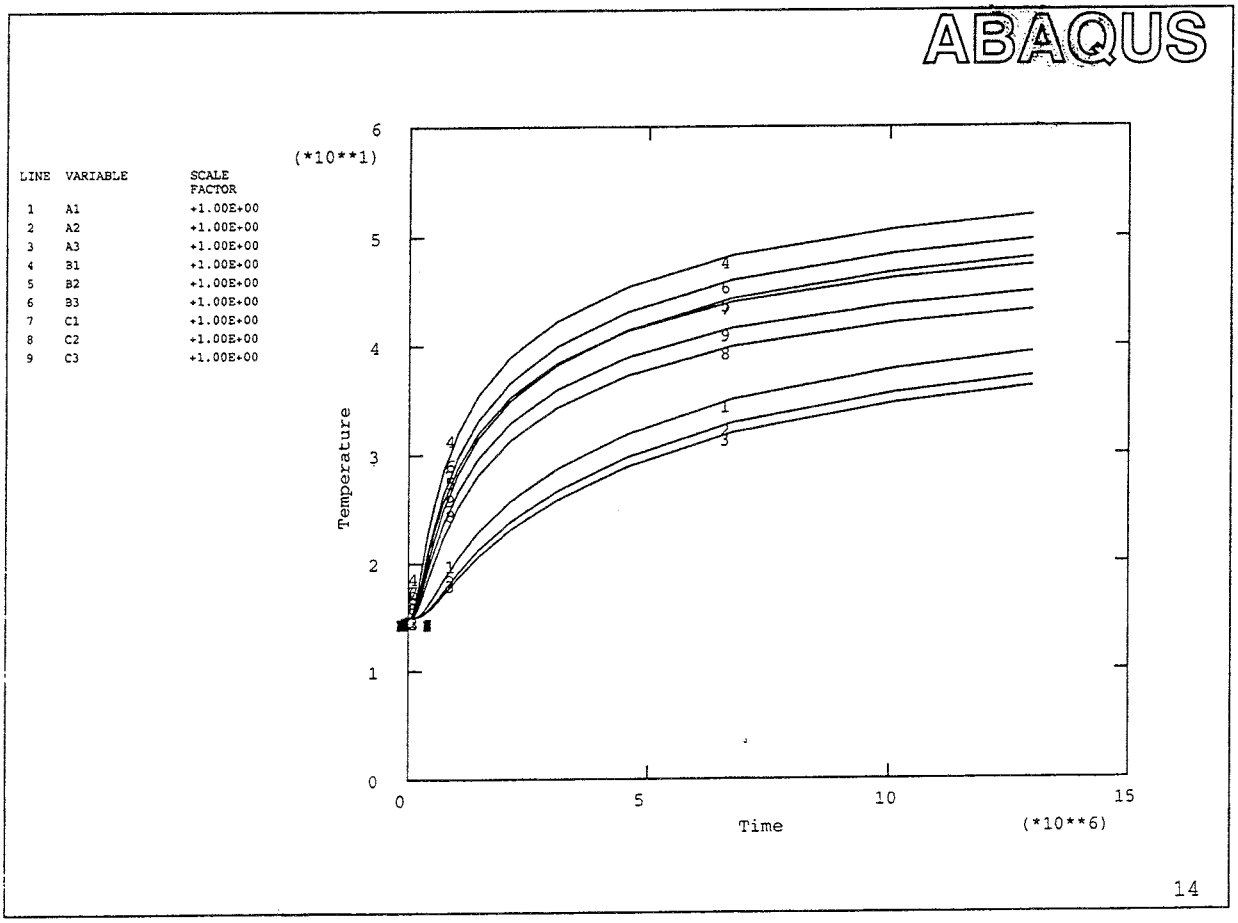

Figure 7-7. *Temperature (°C) plotted as a function of time (s) in Points A1 to C3 according to the specification.*

7.4.2 Time-history plots

Time-history plots will be shown for all nodes in the horizontal centre line and for the 9 specified spots.

Spots at the horizontal central line

The degree of saturation and the void ratio are plotted in Fig 7-8 and the water ratio in Fig 7-9. The diagrams show that there is a substantial redistribution of water and pore volume in the buffer. There is also a slow increase in water ratio with time in the outer nodes due to the water uptake from the outer sand layer. The diagrams also show that irrelevant conditions prevail when the outer element gets water saturated as in the calculation of one of the laboratory tests.

The total axial and radial stresses are plotted in Fig 7-10. These stresses are calculated as the sum of the pore pressure multiplied with the degree of saturation and the effective stress (Eqn 3.2). At a low degree of saturation this means that the total stress is represented by the difference between two high numbers and it is therefore not very accurate.

9 specified points

The results for the 9 specified points are shown in Figs 7-11 - 7-13. Fig 7-11 shows the degree of saturation and the void ratio, Fig 7-12 shows the water ratio, and Fig 7-13 shows the total radial and axial stresses.

7.4.3 Contour plots

After 1 month

Contour plots of void ratio, degree of saturation and water ratio after 1 month are shown in Figs 7-14 to 7-16. The buffer geometry has been scaled different in the axial and radial directions in order to have a better radial resolution.

After 5 months

Contour plots of void ratio, degree of saturation and water ratio after 5 months are shown in Figs 7-17 to 7-19.

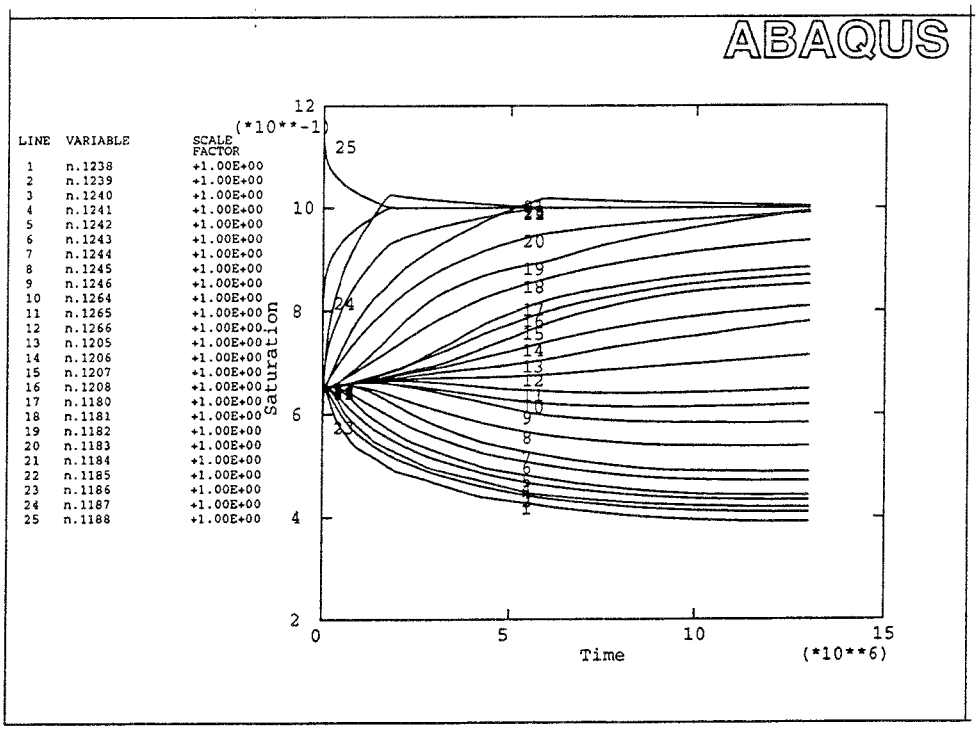

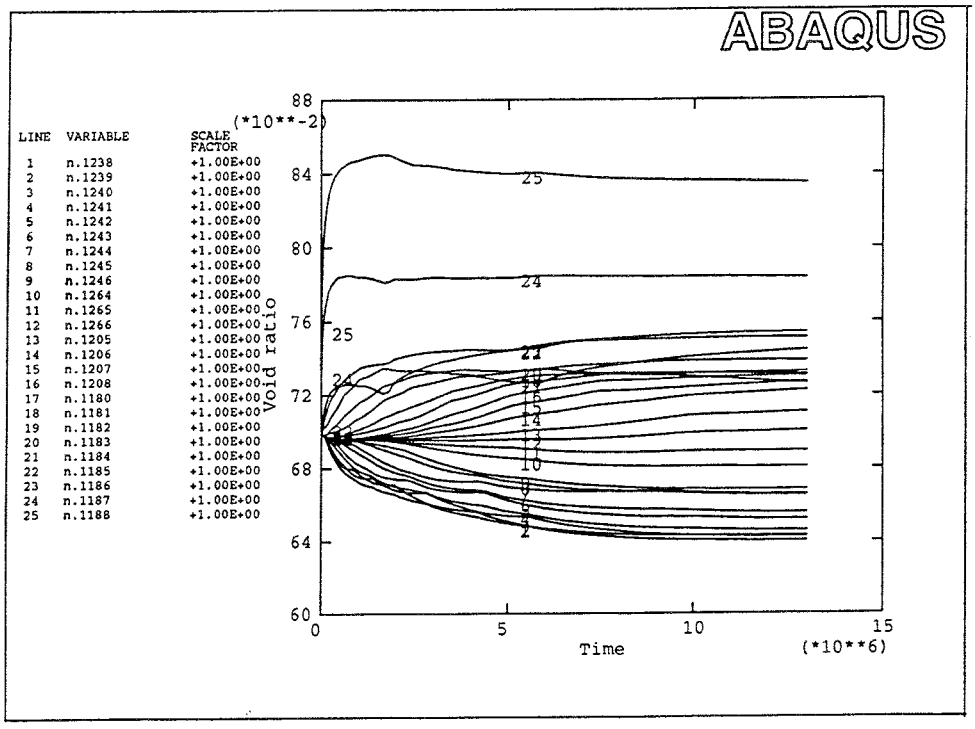

Figure 7-8. *Degree of saturation and void ratio as functions of time (s) plotted for all nodes in the horizontal centre line in the buffer. The points are numbered from 1 at the inner boundary to 25 at the outer boundary.*

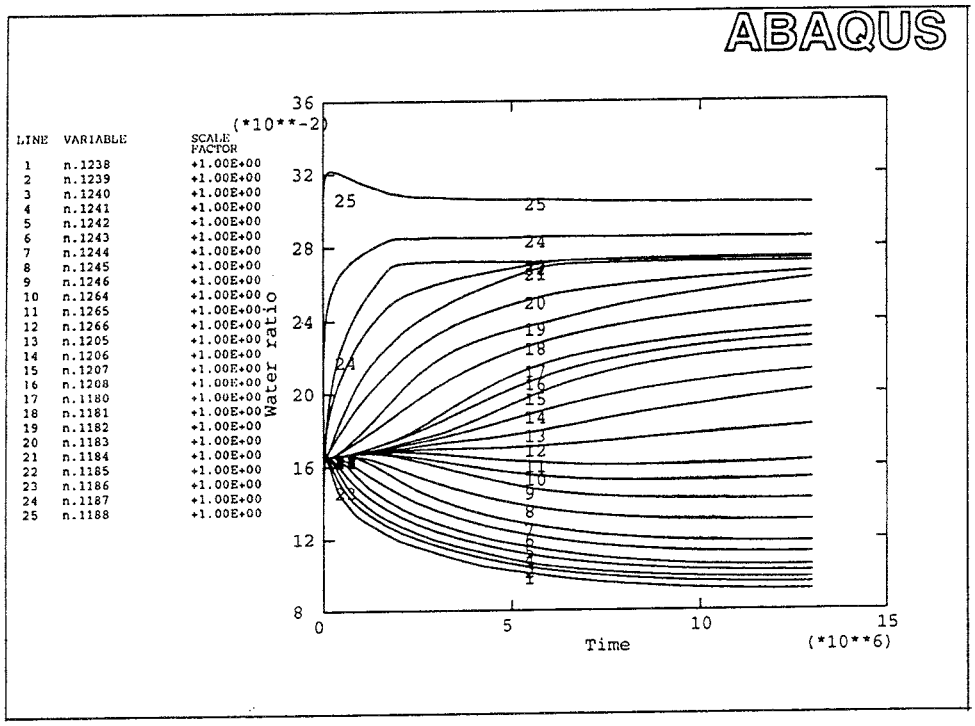

Figure 7-9. *Water ratio as a function of time (s) plotted for all nodes in the horizontal centre line in the buffer. The points are numbered from 1 at the inner boundary to 25 at the outer boundary.*

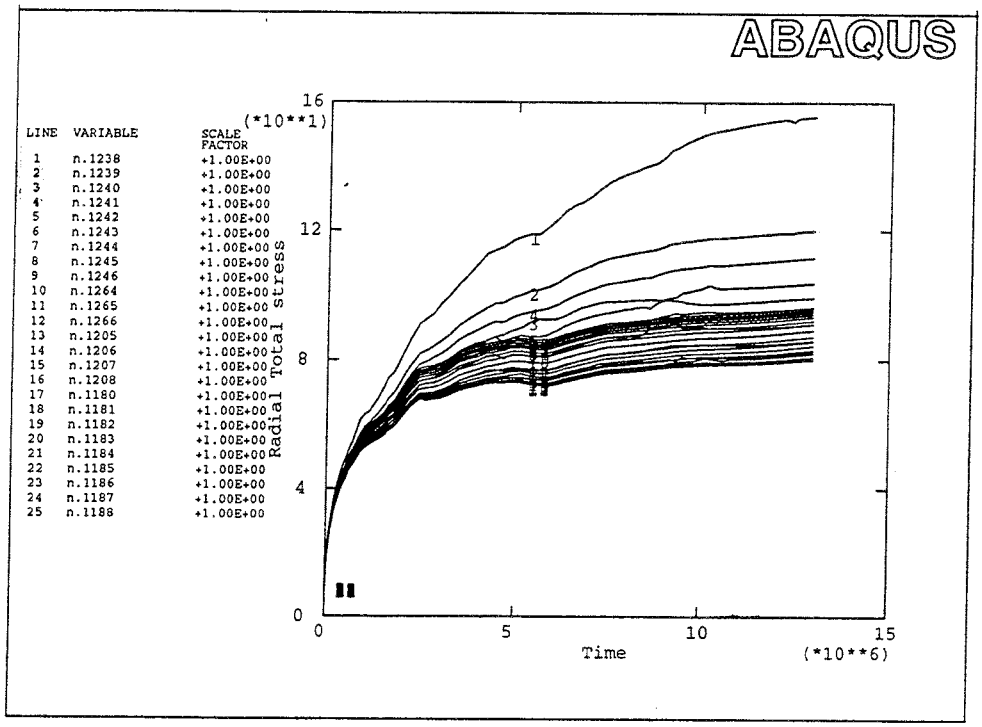

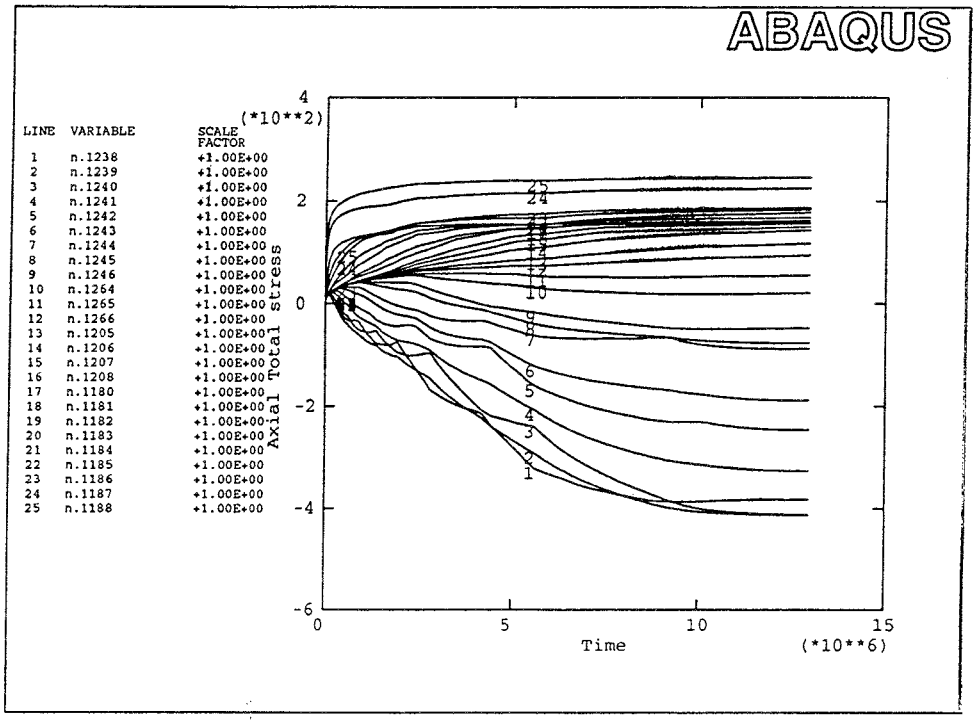

Figure 7-10. *Radial and axial total stress as functions of time (s) plotted for all nodes in the horizontal centre line in the buffer. The points are numbered from 1 at the inner boundary to 25 at the outer boundary.*

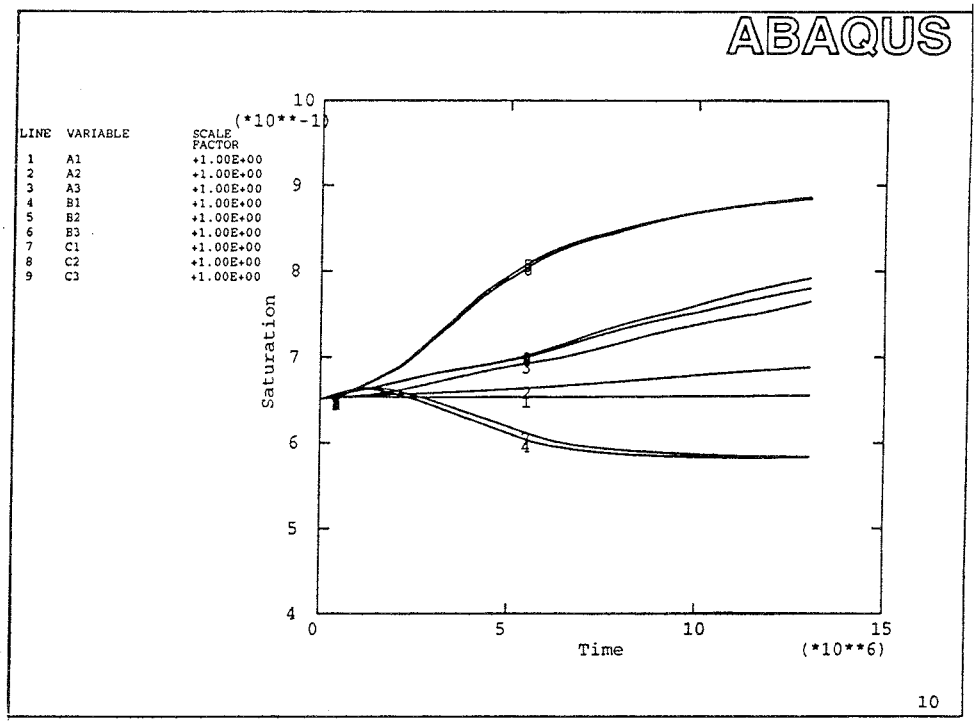

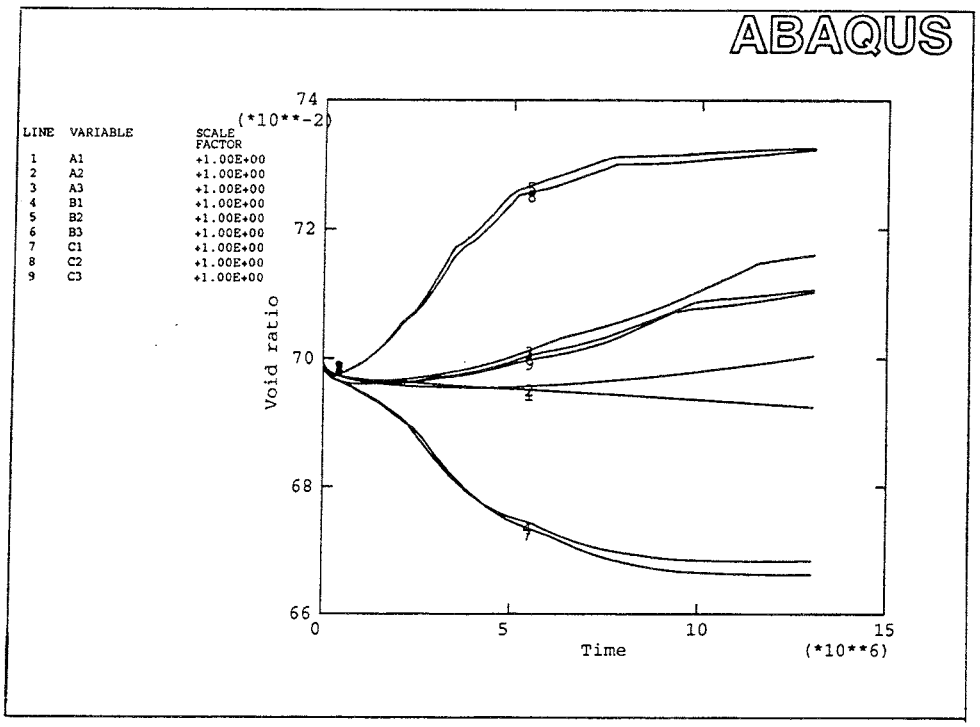

Figure 7-11. *Degree of saturation and void ratio as functions of time (s) plotted for the specified points A1 to C3 (see Fig 7-2) in the buffer.*

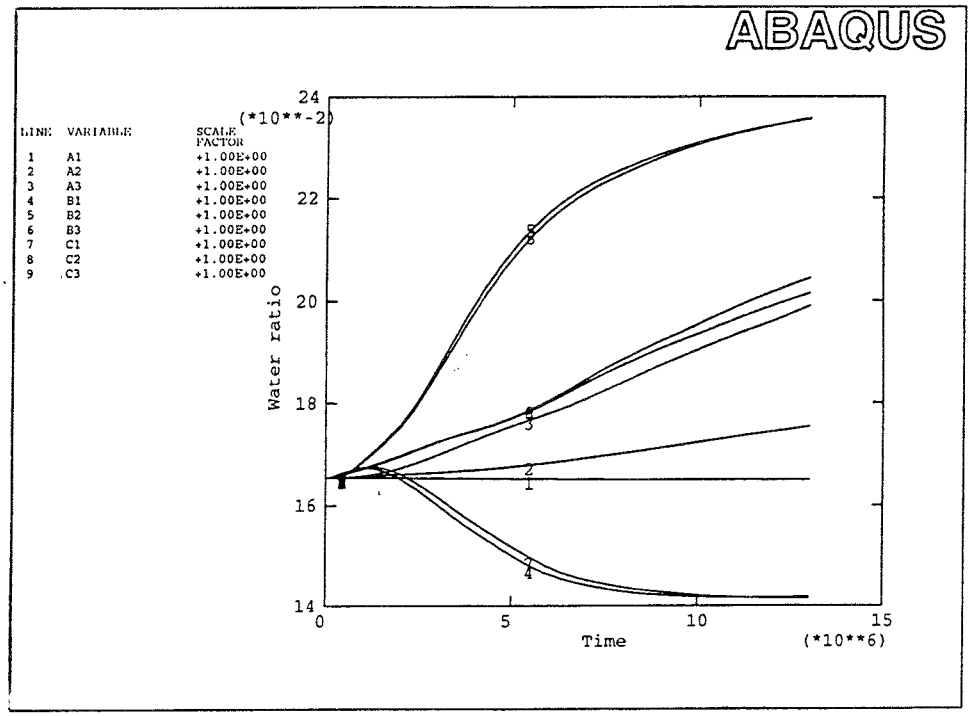

Figure 7-12. *Water ratio as a function of time (s) plotted for the specified points A1 to C3 (see Fig 7-2) in the buffer.*

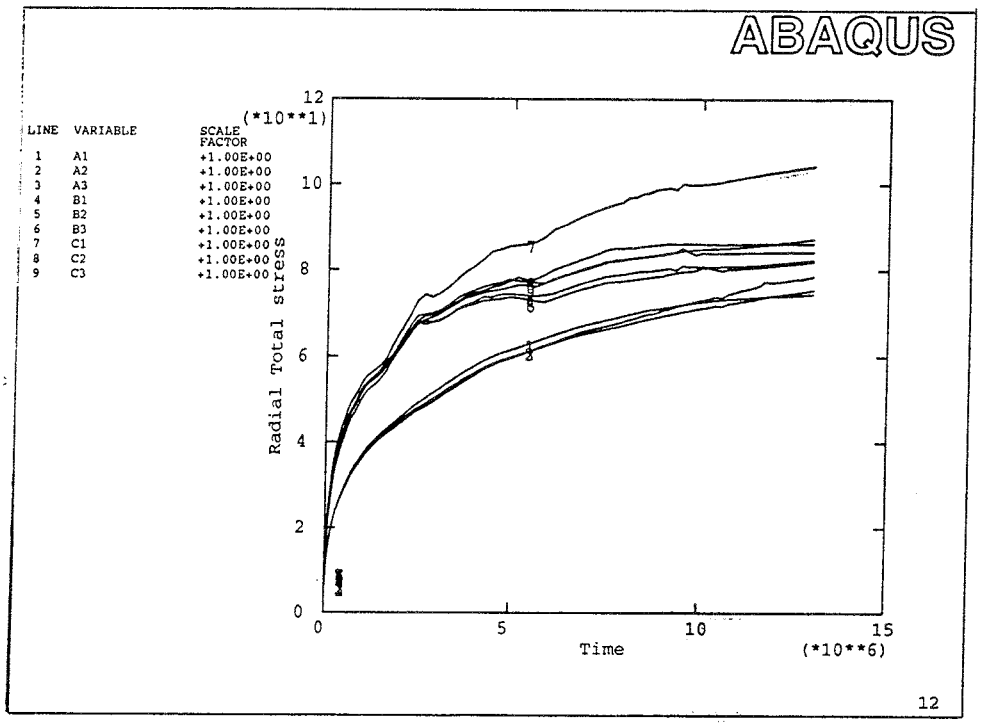

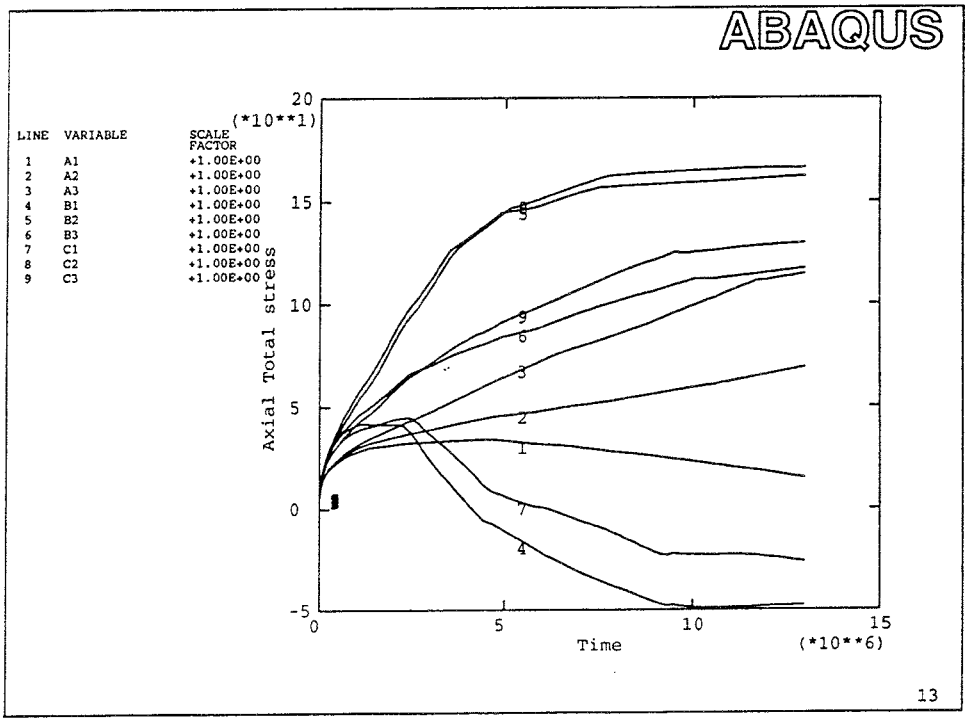

Figure 7-13. *Radial and axial total stress as functions of time (s) plotted for the specified points A1 to C3 (see Fig 7-2) in the buffer.*

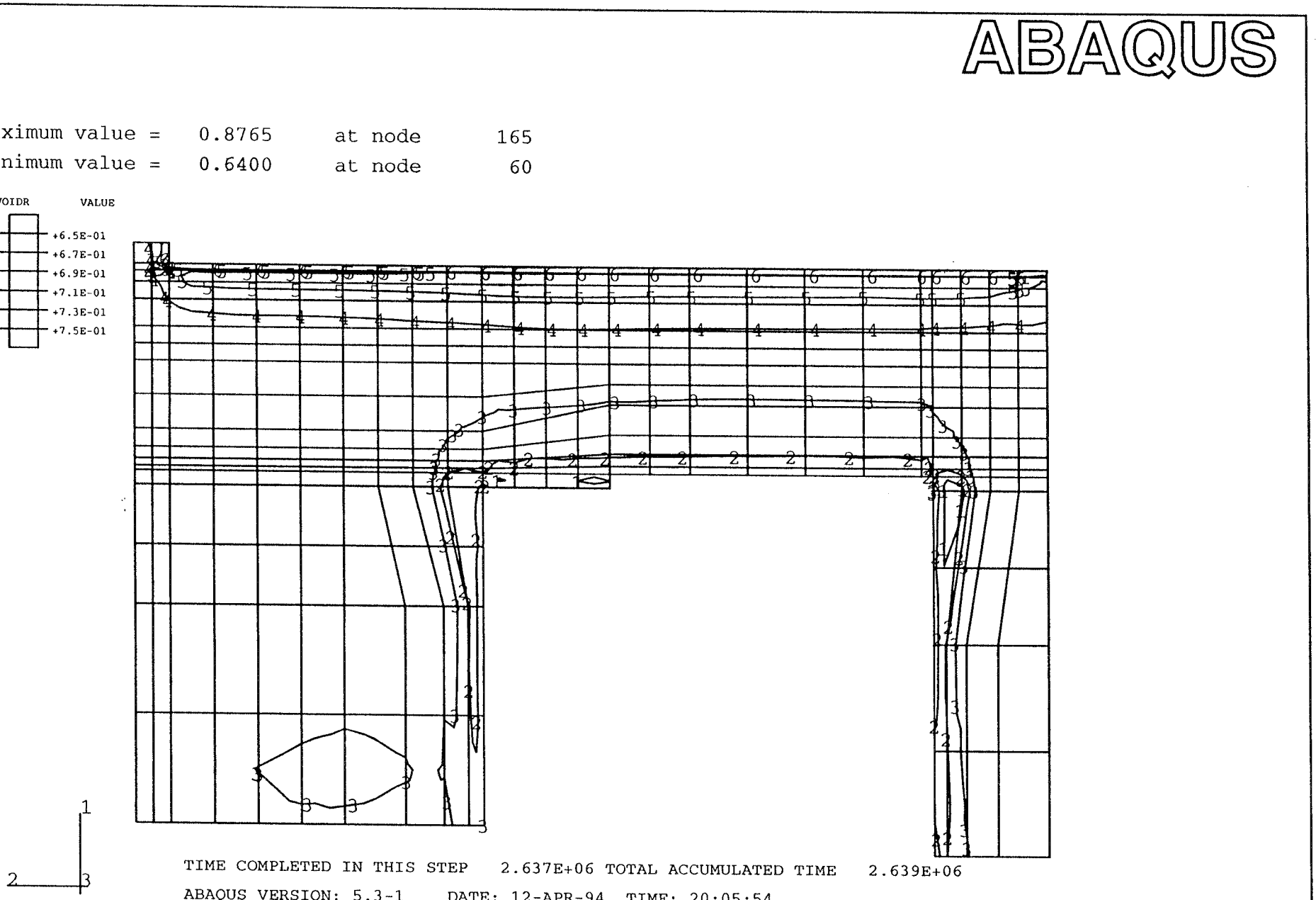

Figure 7-14. Contour plot of void ratio after 1 month.

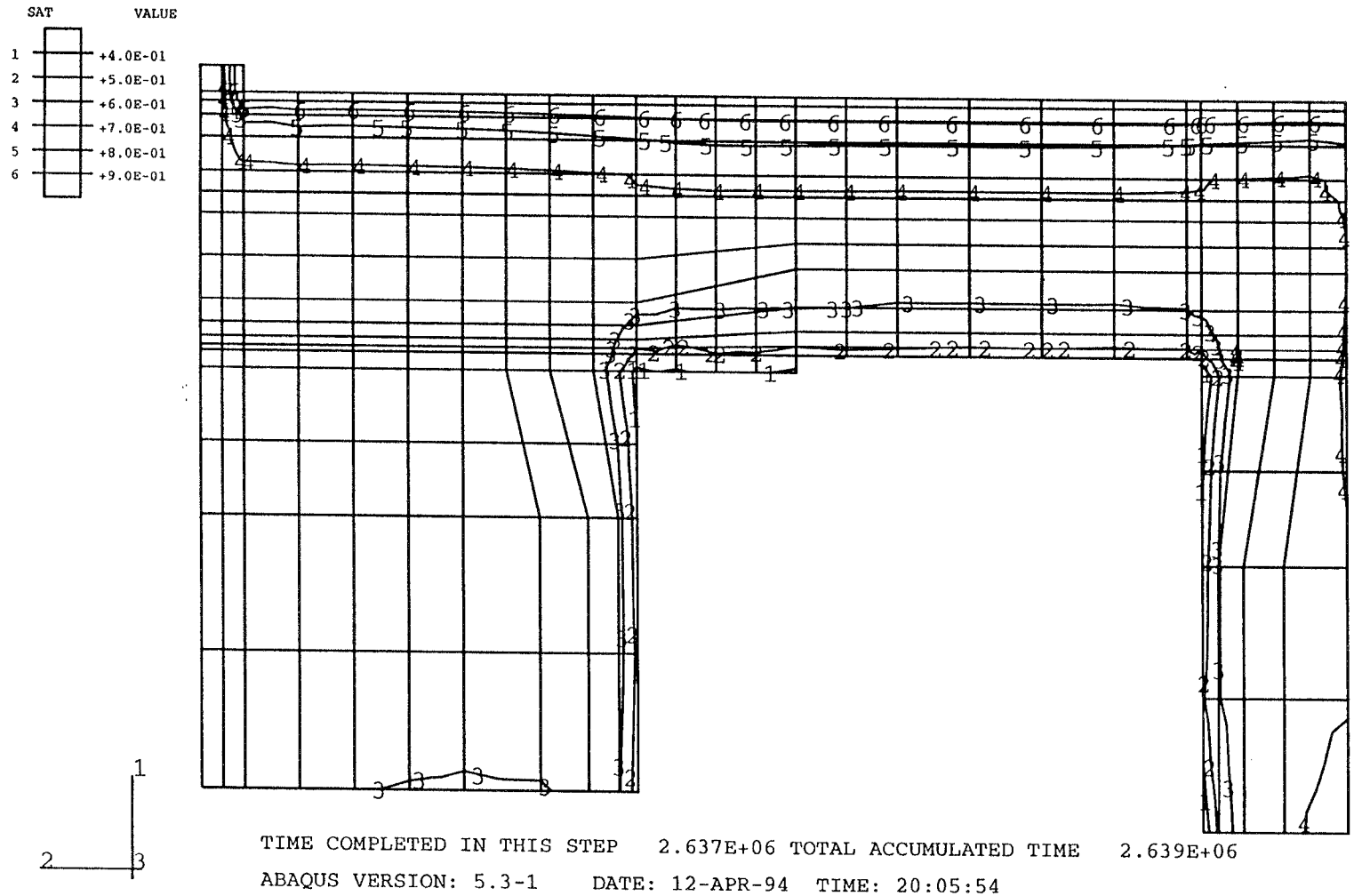

Figure 7-15. Contour plot of degree of saturation after 1 month.

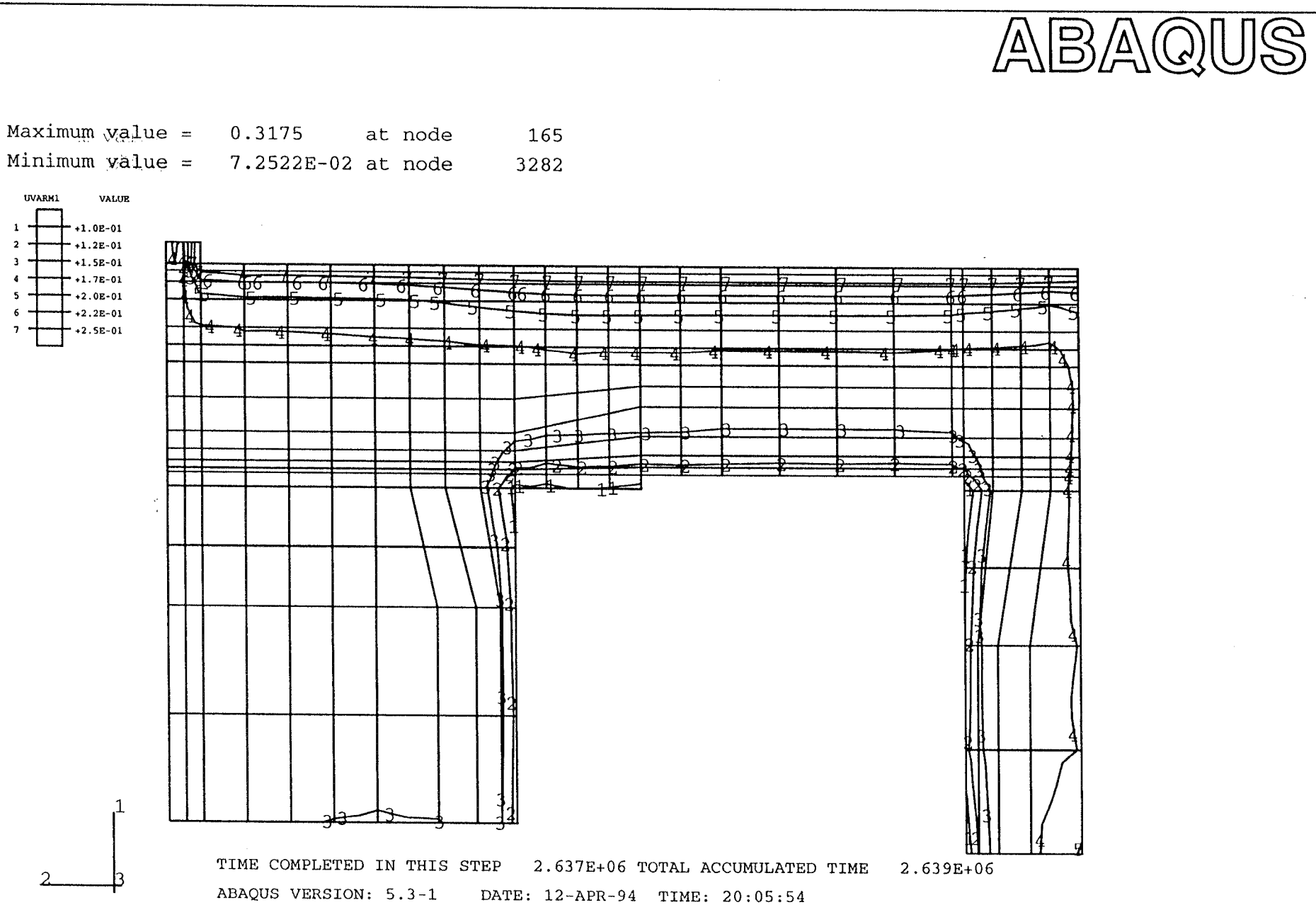

Figure 7-16. Contour plot of water ratio after 1 month (called uvarm1).

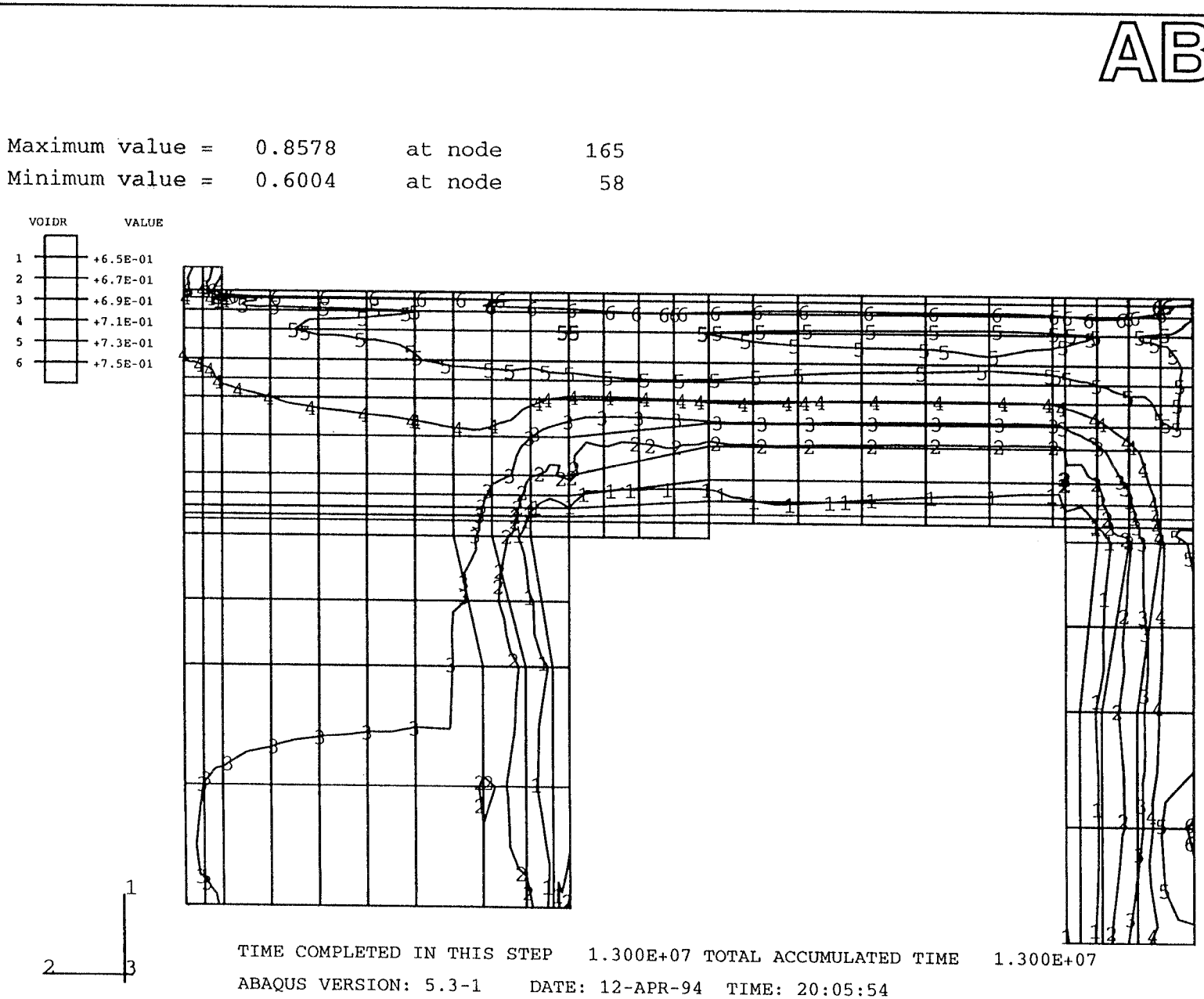

Figure 7-17. Contour plot of void ratio after 5 months.

ABAQUS

Maximum value = 1.202 at node 3338
Minimum value = 0.1520 at node 3282

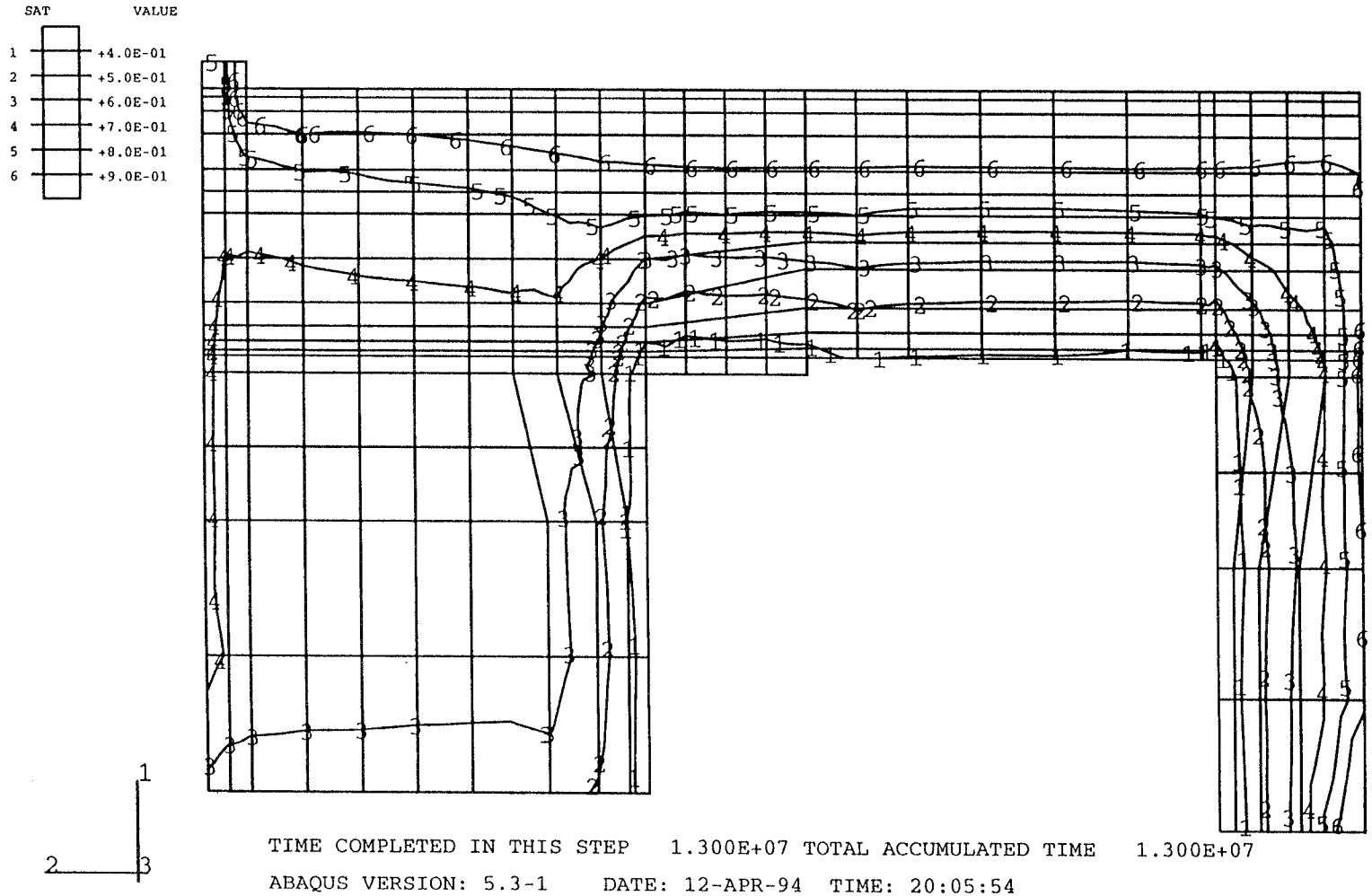

TIME COMPLETED IN THIS STEP 1.300E+07 TOTAL ACCUMULATED TIME 1.300E+07
ABAQUS VERSION: 5.3-1 DATE: 12-APR-94 TIME: 20:05:54
STEP 5 INCREMENT 95

Figure 7-18. Contour plot of degree of saturation after 5 months.

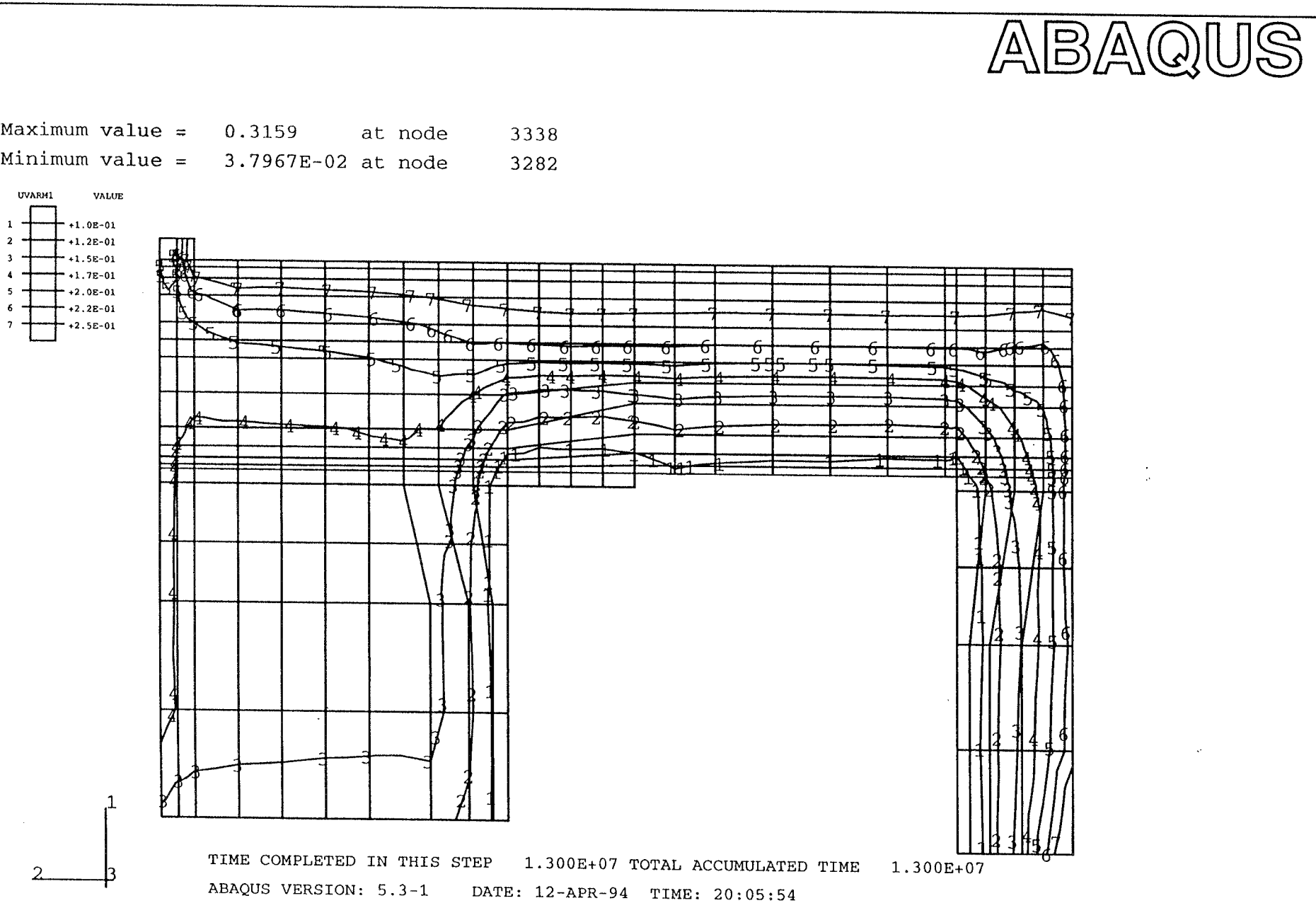

Figure 7-19. Contour plot of water ratio after 5 months (called uvarm1).

7.4.4 Function plots

Function plots are shown with the parameter value as a function of the distance from the inner buffer boundary in the central horizontal plane. This corresponds to the same location as for the time-history plots in Figs 7-8 - 7-10.

- Fig 7-20 shows the pore pressure and the degree of saturation after 1 month.
- Fig 7-21 shows the void ratio and the water ratio after 1 month.
- Fig 7-22 shows the pore pressure and the degree of saturation after 5 months.
- Fig 7-23 shows the void ratio and the water ratio after 5 months.

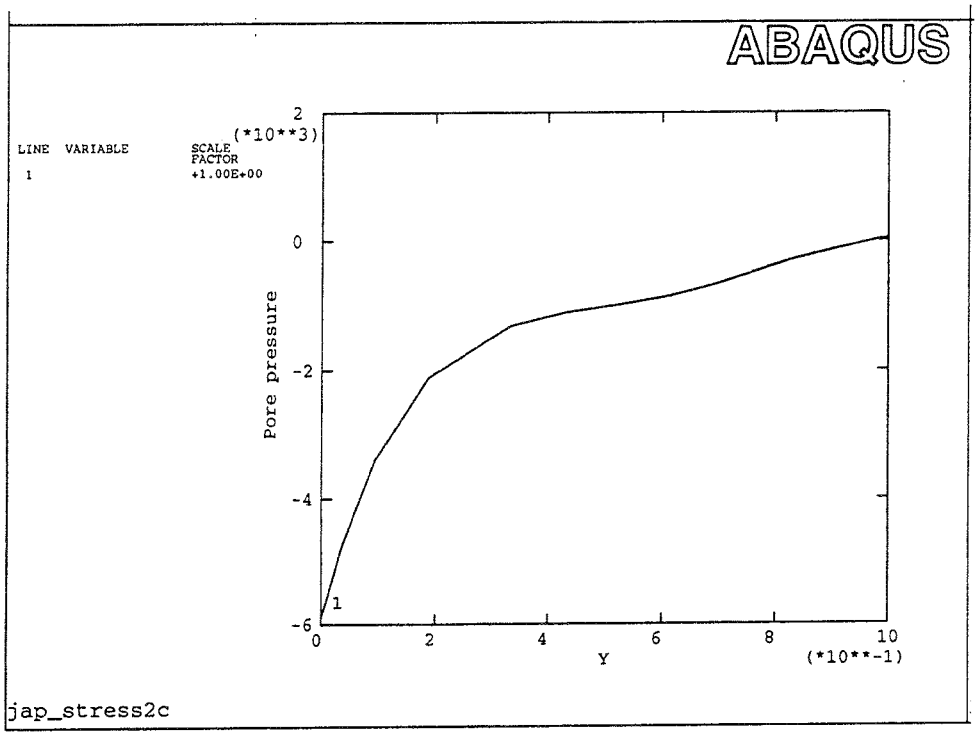

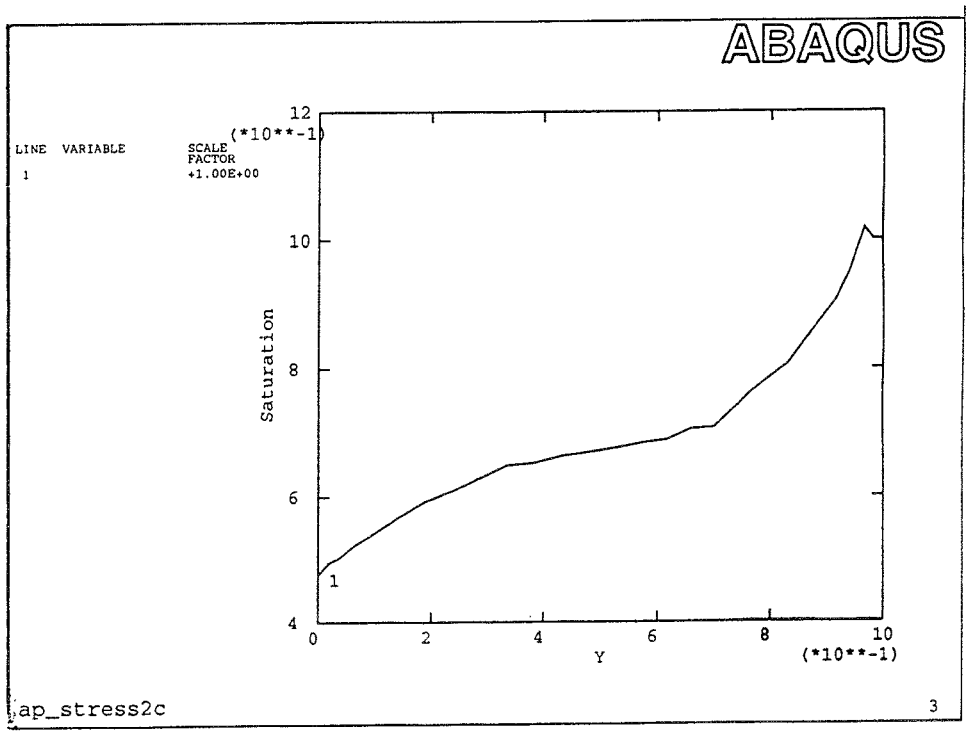

Figure 7-20. *Pore pressure and degree of saturation after 1 month as a function of the distance from the inner sand slot in a horizontal plane through the centre of the heater. Y=0.1 corresponds to the distance 3 cm.*

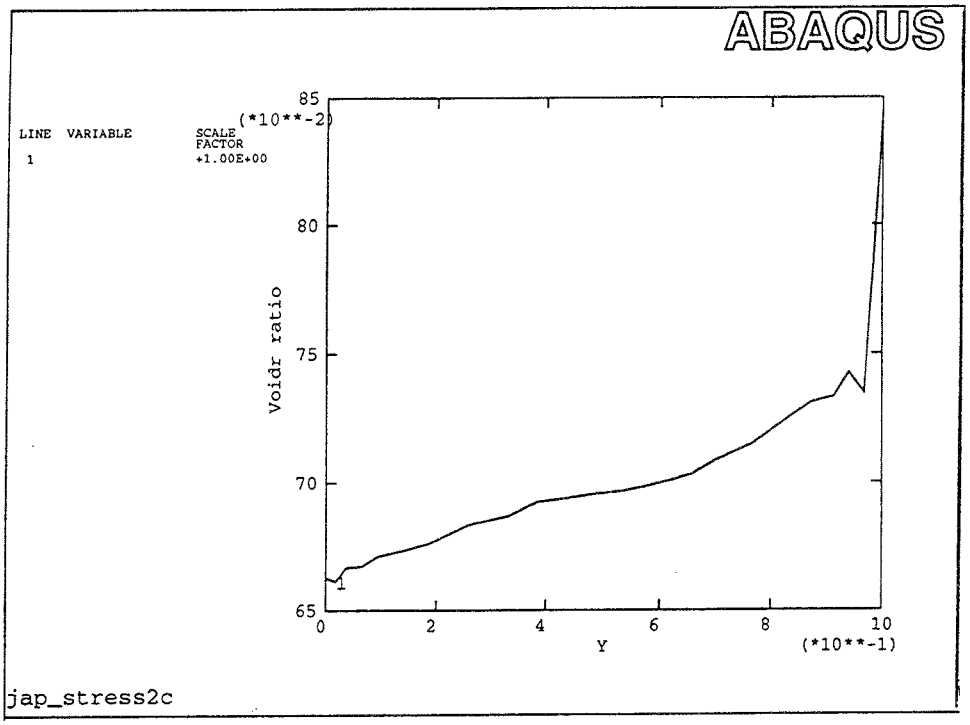

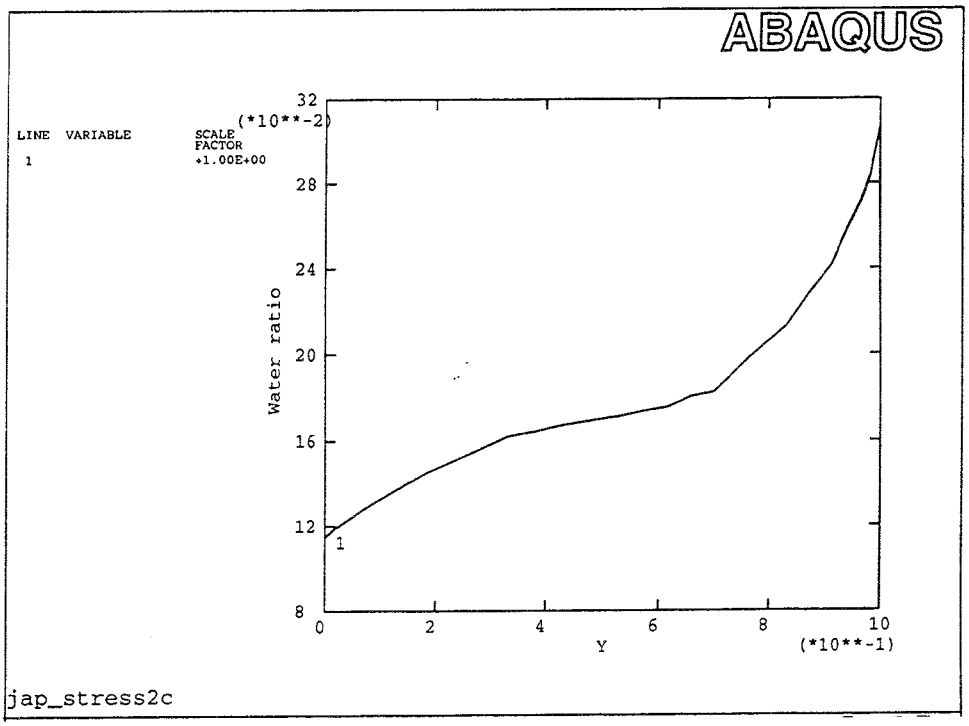

Figure 7-21. *Void ratio and water ratio after 1 month as a function of the distance from the inner sand slot in a horizontal plane through the centre of the heater. Y=0.1 corresponds to the distance 3 cm.*

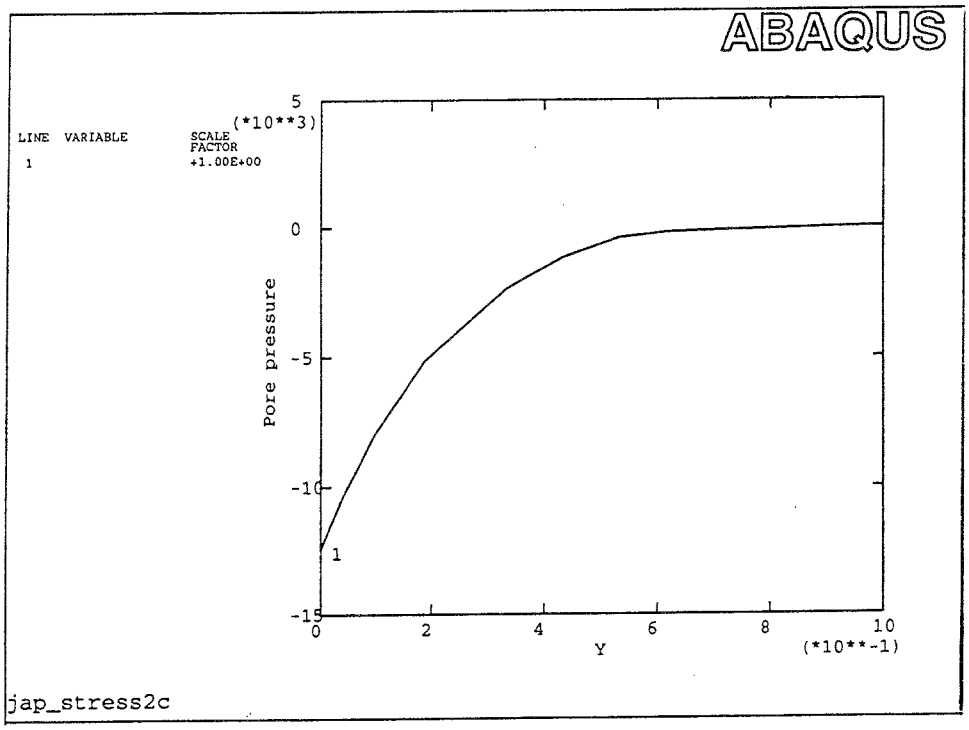

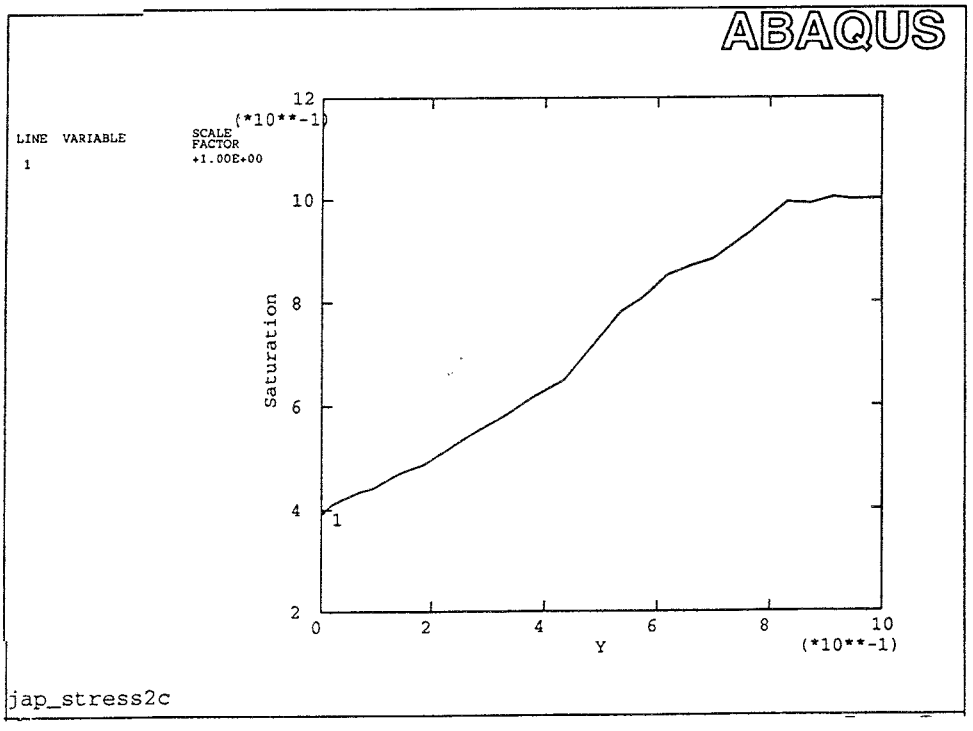

Figure 7-22. *Pore pressure and degree of saturation after 5 months as a function of the distance from the inner sand slot in a horizontal plane through the centre of the heater. Y=0.1 corresponds to the distance 3 cm.*

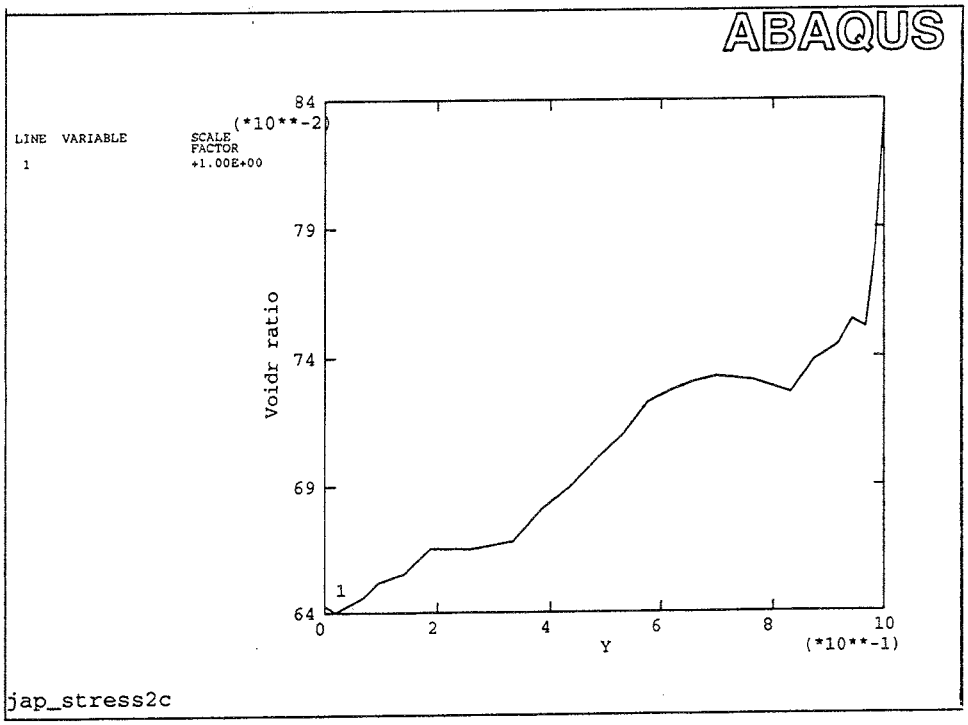

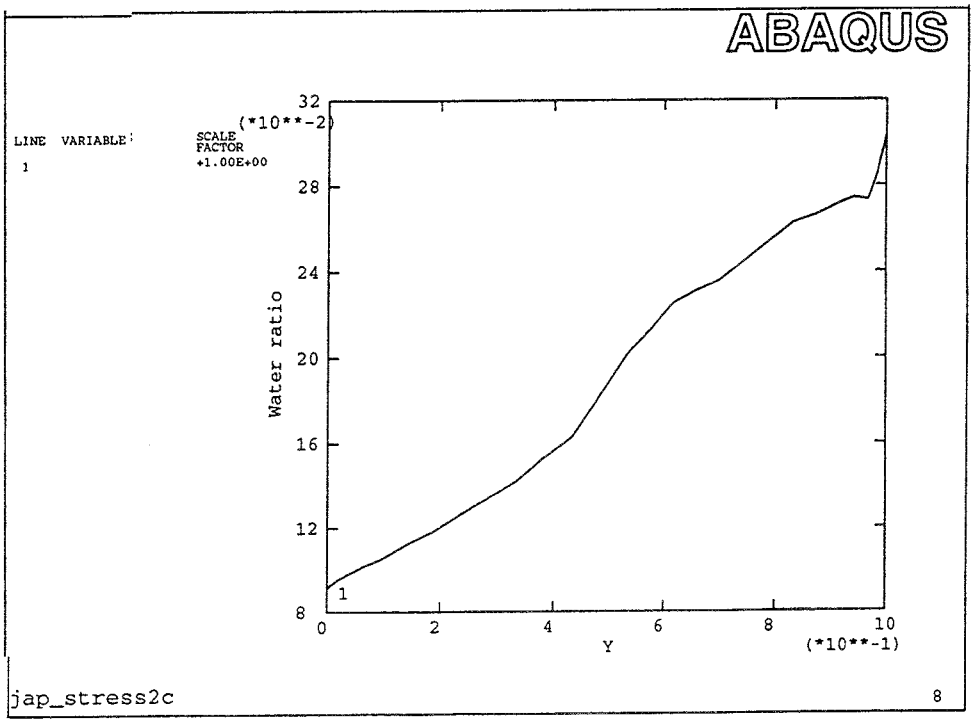

Figure 7-23. *Void ratio and water ratio after 5 months as a function of the distance from the inner sand slot in a horizontal plane through the centre of the heater. Y=0.1 corresponds to the distance 3 cm.*

8 SPECIFIED RESULTS

The results are specified in Tables 8-1 and 8-2 in 9 points A1 to C3 according to the requirements. Fig 8-1 shows the location of the points /1-1/. See also Fig 7-2.

Table 8-1 Results in the specified points after 1 month

Point	Temperature °C	Water ratio $w^{1)}$ %	Total axial stress MPa	Total radial stress MPa
A1	27.1	16.5	0.033	0.050
A2	25.1	16.6	0.038	0.048
A3	24.3	16.9	0.045	0.048
B1	40.5	16.2	0.033	0.069
B2	36.4	18.1	0.103	0.069
B3	38.3	17.2	0.068	0.069
C1	36.8	16.4	0.043	0.074
C2	32.7	18.1	0.099	0.069
C3	34.3	17.2	0.066	0.069

1) Water ratio defined as weight of water divided to weight of dry material

Table 8-2 Results in the specified points after 5 months

Point	Temperature °C	Water ratio $w^{1)}$ %	Total axial stress MPa	Total radial stress MPa
A1	39.3	16.5	0.015	0.074
A2	37.1	17.5	0.069	0.075
A3	36.1	19.9	0.115	0.078
B1	51.9	14.2	-0.048	0.082
B2	48.0	23.6	0.163	0.085
B3	49.7	20.1	0.118	0.082
C1	47.2	14.1	-0.027	0.104
C2	43.1	23.6	0.167	0.085
C3	44.8	20.4	0.130	0.085

1) Water ratio defined as weight of water divided to weight of dry material

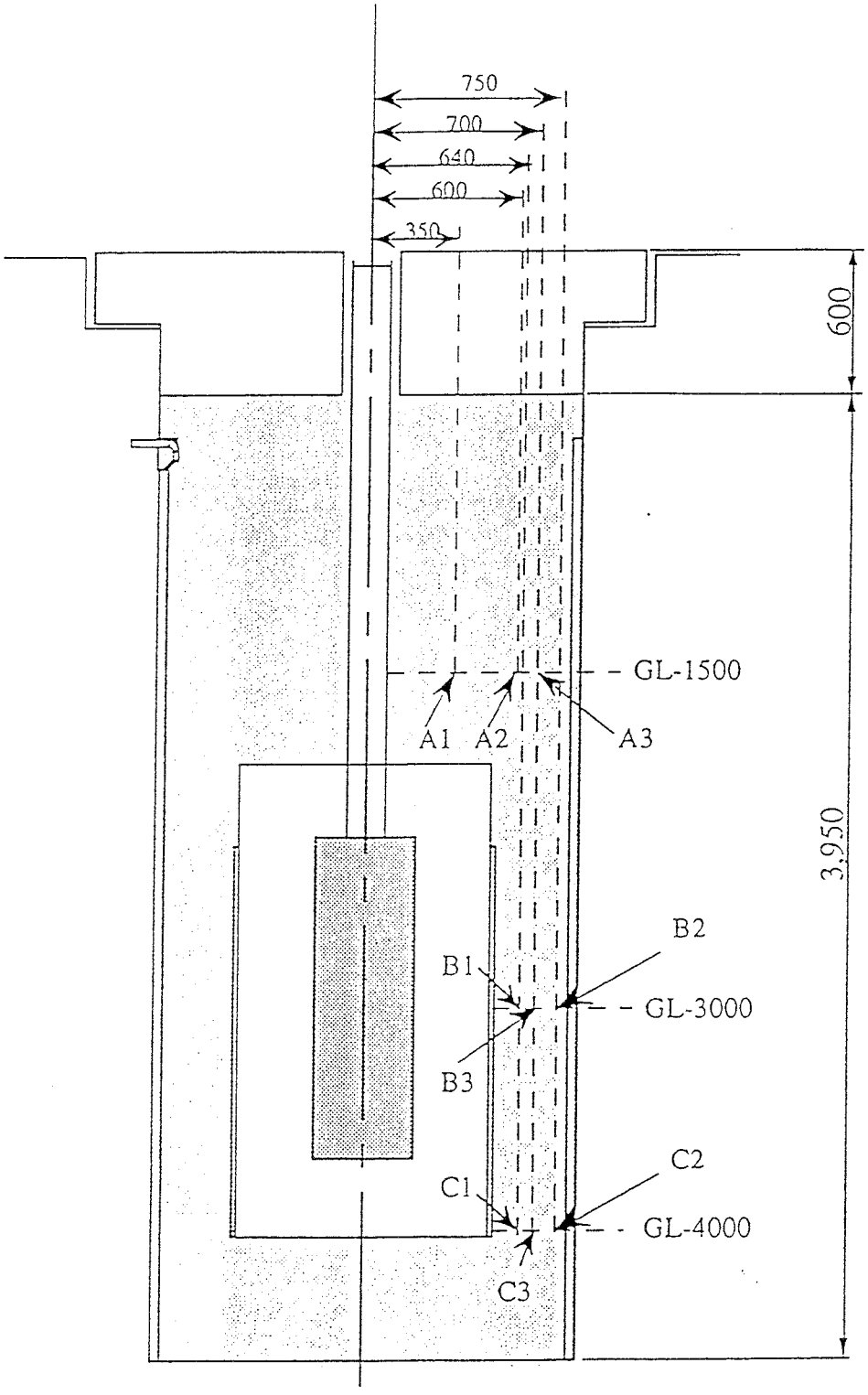

Figure 8-1. *Monitoring points for the result specifications /1-1/.*

9 CONCLUSIONS

The calculations show that the inner half of the buffer material close to the canister will dry and shrink. The drying will decrease the water ratio from 16.6% to 10% at the inner buffer boundary. The volumetric shrinkage will be 3.5% at the inner buffer boundary, which corresponds to a decrease in void ratio from 0.7 to 0.64. The calculations also show that that there will be tension total stresses close to the inner boundary in the axial and tangential directions as shown in Fig 9-1. Although the strength and failure behaviour of the unsaturated buffer material is not known, cracking close to the canister is a possibility that cannot be ruled out.

A comparison with the available measured test results shows that the measured and calculated temperatures agree very well. Also the changes in water ratio agree quite well. The radial total pressure measured at the outer bentonite boundary were generally higher than the calculated values. Unfortunately, the void ratio was not measured after the test, so no comparison with the calculated shrinkage can be made.

The results show that it is possible to make complete coupled calculations of the complicated thermo-hydro-mechanical processes in water unsaturated buffer materials with the developed calculation technique, although improvements of models and data are needed. It is highly recommended that the calculation is followed up with more accurate determination of required parameters and new calculations.

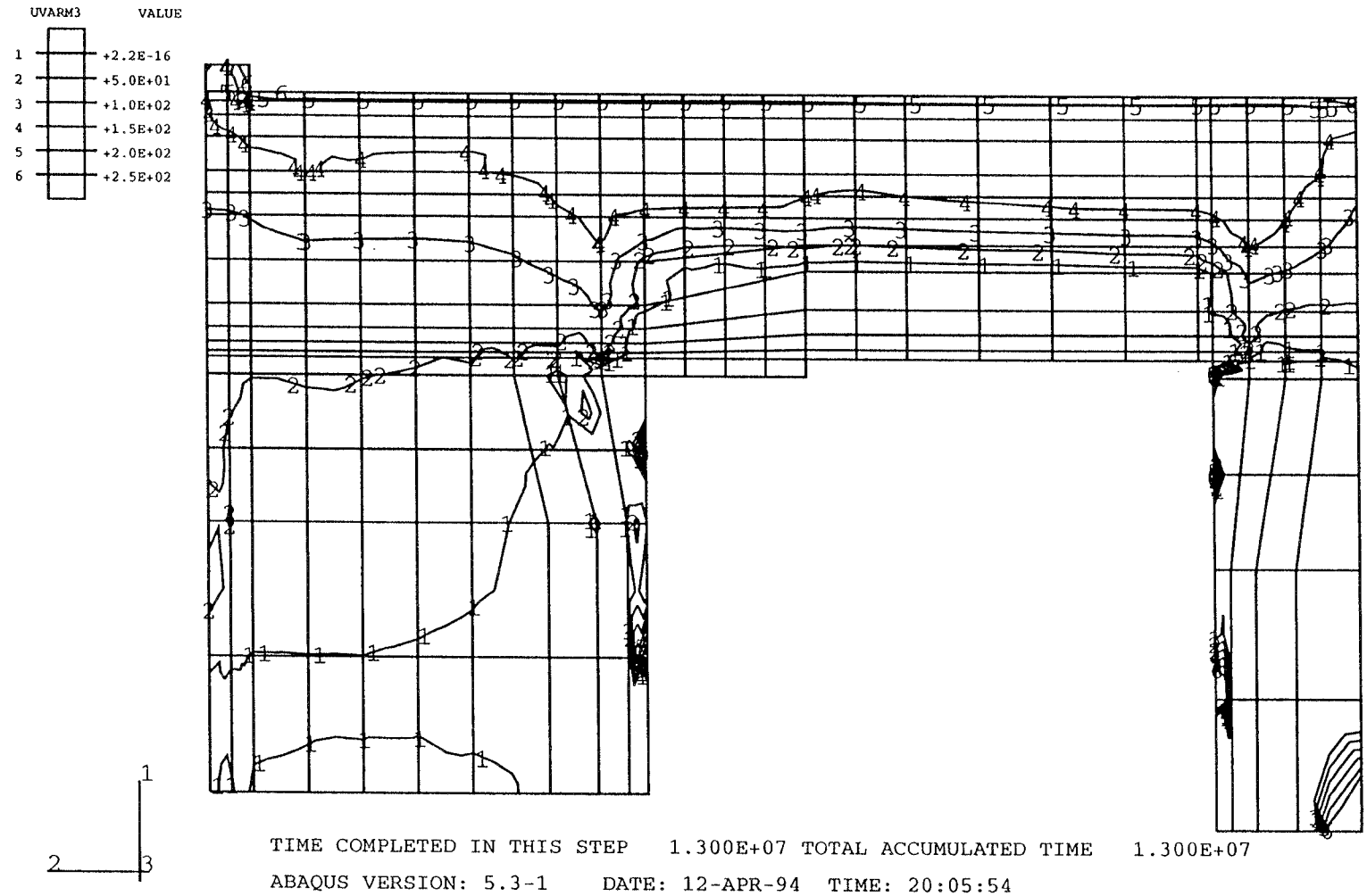

Figure 9-1. *Contour plot of the calculated total radial stress (called uvarm3) in the buffer material after 5 months. Tension stresses appear between the inner boundary and line 1.*

REFERENCES

1-1 **Fujita T., Moro Y., Hara K., Kobayashi A., and Ohnishi Y. (1993)** - DECOVALEX - Specifications for test-case 3 - BIG-BEN experiment. PNC, Japan.

3-1 **Börgesson L. (1990)** - Interim report on the laboratory and theoretical work in modelling the drained and undrained behaviour of buffer materials. SKB Technical Report 90-45.

3-2 **Börgesson L. (1993)** - Modelling of the physical behaviour of water saturated clay barriers. SKB Arbetsrapport 93-49

3-3 **Hibbitt, Karlsson, and Sorensen (1993)** - ABAQUS manuals, version 5.3. Hibbitt, Karlsson, & Sorensen, Inc.

3-4 **Farouki O.T. (1986)** - Thermal properties of soils. Trans Tech Publications

3-5 **Brooks R.H., and Corey A.T. (1964)** - Hydraulic properties of porous media. Colorado State Univ. Hydrol. Paper, No. 3, Mar. 1964

3-6 **Philip, J. R. and DeVries, D. A. (1957)** - Moisture movement in porous materials under temperature gradients. American Geophysical Union Transaction, Vol. 38, No. 3, April 1957.

3-7 **Cameron J. T. (1986)** - A numerical model for coupled heat and moisture flow through porous media. Doctor's thesis, University of California, Berkely.

5-1 Swedish Geotechnical Society - Laboratory Manual part 7.

5-2 **Börgesson L., Hökmark H., and Karnland O. (1988)** - Rheological properties of sodium smectite clay. SKB Technical Report 88-30.

5-3 **De Vries, D.A. (1974)** - Heat tranfer in soils. In *Heat and Mass Transfer in the Biosphere. 1. Transfer Processes in Plant Environment* (D.A. De Vries and N.H. Afghan, Eds.) New York: John Wiley & Sons Inc.

5-4 **Woodside W. and Messmer J.M. (1961)** - Thermal conductivity of porous media. Journal of Applied Physics, vol. 32, No. 9.

5-5 **Karnland O., Pusch R., and Sandén T. (1992)** - Elektrolytens betydelse för de fysikaliska egenskaperna hos Mx-80 bentonit. SKB Arbetsrapport 92-35.

List of SKB reports

Annual Reports

1977-78
TR 121
KBS Technical Reports 1 – 120
Summaries
Stockholm, May 1979

1979
TR 79-28
The KBS Annual Report 1979
KBS Technical Reports 79-01 – 79-27
Summaries
Stockholm, March 1980

1980
TR 80-26
The KBS Annual Report 1980
KBS Technical Reports 80-01 – 80-25
Summaries
Stockholm, March 1981

1981
TR 81-17
The KBS Annual Report 1981
KBS Technical Reports 81-01 – 81-16
Summaries
Stockholm, April 1982

1982
TR 82-28
The KBS Annual Report 1982
KBS Technical Reports 82-01 – 82-27
Summaries
Stockholm, July 1983

1983
TR 83-77
The KBS Annual Report 1983
KBS Technical Reports 83-01 – 83-76
Summaries
Stockholm, June 1984

1984
TR 85-01
Annual Research and Development Report 1984
Including Summaries of Technical Reports Issued during 1984. (Technical Reports 84-01 – 84-19)
Stockholm, June 1985

1985
TR 85-20
Annual Research and Development Report 1985
Including Summaries of Technical Reports Issued during 1985. (Technical Reports 85-01 – 85-19)
Stockholm, May 1986

1986
TR 86-31
SKB Annual Report 1986
Including Summaries of Technical Reports Issued during 1986
Stockholm, May 1987

1987
TR 87-33
SKB Annual Report 1987
Including Summaries of Technical Reports Issued during 1987
Stockholm, May 1988

1988
TR 88-32
SKB Annual Report 1988
Including Summaries of Technical Reports Issued during 1988
Stockholm, May 1989

1989
TR 89-40
SKB Annual Report 1989
Including Summaries of Technical Reports Issued during 1989
Stockholm, May 1990

1990
TR 90-46
SKB Annual Report 1990
Including Summaries of Technical Reports Issued during 1990
Stockholm, May 1991

1991
TR 91-64
SKB Annual Report 1991
Including Summaries of Technical Reports Issued during 1991
Stockholm, April 1992

1992
TR 92-46
SKB Annual Report 1992
Including Summaries of Technical Reports Issued during 1992
Stockholm, May 1993

1993
TR 93-34
SKB Annual Report 1993
Including Summaries of Technical Reports Issued during 1993
Stockholm, May 1994

1994

TR 94-33

SKB Annual Report 1994

Including Summaries of Technical Reports Issued during 1994.
Stockholm, May 1995

List of SKB Technical Reports 1995

TR 95-01

Biotite and chlorite weathering at 25°C. The dependence of pH and (bi) carbonate on weathering kinetics, dissolution stoichiometry, and solubility; and the relation to redox conditions in granitic aquifers

Maria Malmström[1], Steven Banwart[1], Lara Duro[2], Paul Wersin[3], Jordi Bruno[3]
[1] Royal Institute of Technology, Department of Inorganic Chemistry, Stockholm, Sweden
[2] Universidad Politécnica de Cataluña, Departmento de Inginería Química, Barcelona, Spain
[3] MBT Tecnología Ambiental, Cerdanyola, Spain
January 1995

TR 95-02

Copper canister with cast inner component. Amendment to project on Alternative Systems Study (PASS), SKB TR 93-04

Lars Werme, Joachim Eriksson
Swedish Nuclear Fuel and Waste Management Co, Stockholm, Sweden
March 1995

TR 95-03

Prestudy of final disposal of long-lived low and intermediate level waste

Marie Wiborgh (ed.)
Kemakta Konsult AB, Stockholm, Sweden
January 1995

TR 95-04

Spent nuclear fuel corrosion: The application of ICP-MS to direct actinide analysis

R S Forsyth[1], U-B Eklund[2]
[1] Caledon-Consult AB, Nyköping, Sweden
[2] Studsvik Nuclear AB, Nyköping, Sweden
March 1995

TR 95-06

Palaeohydrological implications in the Baltic area and its relation to the groundwater at Äspö, south-eastern Sweden – A literature study

Bill Wallin
Geokema AB, Lidingö, Sweden
March, 1995

TR 95-07

Äspö Hard Rock Laboratory Annual Report 1994

SKB
April 1995

TR 95-08

Feasibility study for siting of a deep repository within the Storuman municipality

Swedish Nuclear Fuel and Waste Management Co., Stockholm
January 1995

TR 95-09

A thermodynamic data base for Tc to calculate equilibrium solubilities at temperatures up to 300°C

Ignasi Puigdomènech[1], Jordi Bruno[2]
[1] Studsvik AB, Nyköping, Sweden
[2] Intera Information Technologies SL, Cerdanyola, Spain
April 1995

TR 95-10

Investigations of subterranean microorganisms. Their importance for performance assessment of radioactive waste disposal

Karsten Pedersen[1], Fred Karlsson[2]
[1] Göteborg University, General and Marine Microbiology, The Lundberg Institute, Göteborg, Sweden
[2] Swedish Nuclear Fuel and Waste Management Co., Stockholm, Sweden
June 1995

TR 95-11

Solute transport in fractured media – The important mechanisms for performance assessment

Luis Moreno, Björn Gylling, Ivars Neretnieks
Department of Chemical Engineering and Technology, Royal Institute of Technology, Stockholm, Sweden
June 1995

TR 95-12
Literature survey of matrix diffusion theory and of experiments and data including natural analogues
Yvonne Ohlsson, Ivars Neretnieks
Department of Chemical Engineering and Technology, Royal Institute of Technology, Stockholm, Sweden
August 1995

TR 95-13
Interactions of trace elements with fracture filling minerals from the Äspö Hard Rock Laboratory
Ove Landström[1], Eva-Lena Tullborg[2]
[1] Studsvik Eco & Safety AB
[2] Terralogica AB
June 1995

TR 95-14
Consequences of using crushed crystalline rock as ballast in KBS-3 tunnels instead of rounded quartz particles
Roland Pusch
Clay Technology AB
February 1995

TR 95-15
Estimation of effective block conductivities based on discrete network analyses using data from the Äspö site
Paul R La Pointe[1], Peter Wallmann[1], Sven Follin[2]
[1] Golder Associates Inc., Seattle, WA, USA
[2] Golder Associates AB, Lund, Sweden
September 1995

TR 95-16
Temperature conditions in the SKB study sites
Kaj Ahlbom[1], Olle Olsson[1], Stefan Sehlstedt[2]
[1] Conterra AB
[2] MRM Konsult AB
June 1995

TR 95-17
Measurements of colloid concentrations in the fracture zone, Äspö Hard Rock Laboratory, Sweden
Anna Ledin, Anders Düker, Stefan Karlsson, Bert Allard
Department of Water and Environmental Studies,Linköping University, Linköping, Sweden
June 1995

TR 95-18
Thermal evidence of caledonide foreland, molasse sedimentation in Fennoscandia
Eva-Lena Tullborg[1], Sven Åke Larsson[1], Lennart Björklund[1], Lennart Samuelsson[2], Jimmy Stigh[1]
[1] Department of Geology, Earth Sciences Centre, Göteborg University, Göteborg, Sweden
[2] Geological Survey of Sweden, Earth Sciences Centre, Göteborg, Sweden
November 1995

TR 95-19
Compaction of bentonite blocks. Development of technique for industrial production of blocks which are manageable by man
Lars-Erik Johannesson, Lennart Börgesson, Torbjörn Sandén
Clay Technology AB, Lund, Sweden
April 1995

TR 95-20
Modelling of the physical behaviour of water saturated clay barriers. Laboratory tests, material models and finite element application
Lennart Börgesson[1], Lars-Erik Johannesson[1], Torbjörn Sandén[1], Jan Hernelind[2]
[1] Clay Technology AB, Lund, Sweden
[2] FEM-Tech AB, Västerås, Sweden
September 1995

TR 95-21
Conceptual model for concrete long time degradation in a deep nuclear waste repository
Björn Lagerblad, Jan Trägårdh
Swedish Cement and Concrete Research Institute
February 1994

TR 95-22
The use of interaction matrices for identification, structuring and ranking of FEPs in a repository system. Application on the far-field of a deep geological repository for spent fuel
Kristina Skagius[1], Anders Ström[2], Marie Wiborgh[1]
[1] Kemakta, Stockholm, Sweden
[2] Swedish Nuclear Fuel and Waste Management Co, Stockholm, Sweden
November 1995

TR 95-23
Spent nuclear fuel. A review of properties of possible relevance to corrosion processes
Roy Forsyth
Caledon Consult AB
April 1995

TR 95-24
Studies of colloids and their importance for repository performance assessment
Marcus Laaksoharju[1], Claude Degueldre[2], Christina Skårman[1]
[1] GeoPoint AB, Sollentuna, Sweden
[2] University of Geneva, Switzerland
December 1995

TR 95-25
Sulphate reduction in the Äspö HRL tunnel
Marcus Laaksoharju (ed.)
GeoPoint AB, Sollentuna, Sweden
December 1995

TR 95-26
The Äspö redox investigations in block scale. Project summary and implications for repository performance assessment
Steven Banwart (ed.)
Dept. of Civil and Environmental Engineering, University of Bradford, UK
November 1995

TR 95-27
Survival of bacteria in nuclear waste buffer materials. The influence of nutrients, temperature and water activity
Karsten Pedersen[1], Mehrdad Motamedi[1], Ola Karnland[2]
[1] Department of General and Marine Microbiology, the Lundberg Institute, Göteborg University, Göteborg, Sweden
[2] Clay Technology AB, Lund, Sweden
December 1995

TR 95-28
DECOVALEX I – Test Case 2: Calculation of the Fanay-Augères THM Test – Thermomechanical modelling of a fractured rock volume
Lennart Börgesson[1], Jan Hernelind[2]
[1] Clay Technology AB, Lund, Sweden
[2] Fem-Tech AB, Västerås, Sweden
December 1995